OBSERVER BASED CONDITION MONITORING OF AN
ELECTROHYDRAULIC ACTUATION SYSTEM

A THESIS SUBMITTED TO
THE GRADUATE SCHOOL OF NATURAL AND APPLIED SCIENCES
OF
MIDDLE EAST TECHNICAL UNIVERSITY

BY

EMRE MURAT POYRAZ

IN PARTIAL FULFILLMENT OF THE REQUIREMENTS
FOR
THE DEGREE OF MASTER OF SCIENCE
IN
MECHANICAL ENGINEERING

DECEMBER 2019

Approval of the thesis:

OBSERVER BASED CONDITION MONITORING OF AN ELECTROHYDRAULIC ACTUATION SYSTEM

submitted by **EMRE MURAT POYRAZ** in partial fulfillment of the requirements for the degree of **Master of Science** in **Mechanical Engineering, Middle East Technical University** by,

Prof. Dr. Halil Kalıpçılar
Dean, Graduate School of **Natural and Applied Sciences**   _____

Prof. Dr. M. A. Sahir Arıkan
Head of the Department, **Mechanical Engineering**   _____

Assist. Prof. Dr. Ali Emre Turgut
Supervisor, **Mechanical Engineering, METU**   _____

Dr. Hakan Çalışkan
Co-Supervisor, **Mechanical Engineering, METU**   _____

Examining Committee Members:

Prof. Dr. R. Tuna Balkan
Mechanical Eng, METU   _____

Assist. Prof. Dr. Ali Emre Turgut
Mechanical Eng, METU   _____

Assist. Prof. Dr. Buğra Koku
Mechanical Eng, METU   _____

Assist. Prof. Dr. Selçuk Himmetoğlu
Mechanical Eng, Hacettepe University   _____

Assoc. Prof. Dr. Yiğit Taşçıoğlu
Mechanical Eng, TED University   _____

Date: 05.12.2019

I hereby declare that all information in this document has been obtained and presented in accordance with academic rules and ethical conduct. I also declare that, as required by these rules and conduct, I have fully cited and referenced all material and results that are not original to this work.

Name, Last name : Emre Murat Poyraz

Signature :

ABSTRACT

OBSERVER BASED CONDITION MONITORING OF AN ELECTROHYDRAULIC ACTUATION SYSTEM

Poyraz, Emre Murat
Master of Science, Mechanical Engineering
Supervisor: Assist. Prof. Dr. Ali Emre Turgut
Co-Supervisor: Dr. Hakan Çalışkan

December 2019, 123 pages

In this thesis study, jamming fault in an electrohydraulic actuation system which may be quite critical for aerospace applications are detected using model-based approaches.

A hydraulic test setup consisting of a connected motor controlled electro hydrostatic actuation (EHA) system and a servo Proportional valve controlled load simulator system is used for the verification of the proposed fault detection and diagnosis (FDD) algorithm. Based on the system dynamics of the equipment in the test bench, mathematical modelling of both EHA and the load simulator is to be performed for further model-based (FDD) techniques.

Several model-based approaches proposed for different kind of failure and fault cases are present in the literature. Among them, Kalman filtering and Observer based solutions are the most well-known and preferred model-based methods used in the residual generation step. However, there is no common procedure for the detection and the identification of 'a fault' as different failure conditions may result in distinct changes in the nominal behavior of the system or process.

Fault to be focused on this study is the jamming phenomena which could occur in an electro hydraulic actuator. This failure case might be severe and even lead to a catastrophic system safety failure.

In the scope of the thesis study a dedicated model based approach is developed for the detection and diagnosis of such faulty cases. State and disturbance observer techniques are applied for fault detection purposes. First, the disturbance load acting on an actuator is estimated by a disturbance observer. This observation is correlated with a faulty case and behaved as a residual. Once the residual, the rate of the disturbance estimation, exceeds a predefined value, the fault detection is triggered. The whole procedure is followed with the fault identification step where the moving average of the position tracking error is analyzed to diagnose jamming cases.

Keywords: Fault Detection and Diagnosis, Electro Hydraulic Actuation, Disturbance Observer, Model-Based FDD

ÖZ

BİR ELEKTRO HİROLİK EYLEYİCİ SİSTEMİN GÖZLEMCİ TABANLI DURUM DENETLENMESİ

Poyraz, Emre Murat
Yüksek Lisans, Makina Mühendisliği
Tez Yöneticisi: Dr. Öğr. Üyesi Ali Emre Turgut
Ortak Tez Yöneticisi: Dr. Hakan Çalışkan

Aralık 2019, 123 sayfa

Bu tez çalışması kapsamında, bir elektrohidrolik eyleyici sistem içindeki kitlenme gibi, havacılık uygulamarında oldukça kritik olabilecek bir hatanın farkedilip saptanması, model tabanlı yaklaşımlarla gerçekleştirilmiştir.

Hidrolik motor kontrollü bir elektrohidrostatik eyleyici (EHA) ve servo oransal valf kontrollü bir yük simülatörünün birleştirilmesiyle oluşan bir hidrolik test düzeneği, önerilen hata belirleme ve teşhisi algoritmasının gerçek zamanlı doğrulaması için kullanılmıştır. Test düzeneğindeki ekipmanların sistem dinamiğini temel alarak, model tabanlı hata belirleme metodlarını uygulamak için hem EHA hem de yük simülatörü sistemi için matematiksel modellenme yapılmıştır.

Literatürde, değişik hata senaryoları için önerilen birkaç model tabanlı yaklaşım mevcuttur. Bunların arasından en çok bilinen ve tercih edilen model tabanlı rezidüel (artık) oluşturma yöntemleri Kalman filtreleme ve gözlemci tabanlı çözümlerdir. Ancak, her özel hata durumu nominal sistem dinamiğinde kendine özel ayrı bir değişikliğe neden olabildiğinden herhangi bir hatanın gözlemlenmesi ve teşhisi için literatürde tanımlanmış ortak bir prosedür bulunmamaktadır.

Bu çalışmada odaklanılan temel hata durumu kitlenme (jamming) gibi bir elektro hidrolik eyleyici sistemde meydana gelebilecek senaryolardır. Bu durumlar, özellikle sistem emniyeti için çok şiddetli ve katastrofik sonuçlar doğurabilir.

Tez kapsamında bu tür hatalı durumların saptanması için özel bir model tabanlı yaklaşım metodu geliştirilmiştir. Sistem durumları ve bozucu etkileri için gözlemci teknikleri hata saptanması amacıyla uygulanmıştır. Öncelikle eyleyici sistem üzerine düşen bozucu yük, özel bir gözlemci tasarlanarak tahmin edilmiştir. Bu gözlem sonunda çıkan tahmin, hatalı bir durumla ilişkilendirilerek rezidüel (artık) bilgisi olarak değerlendirilmiştir. Bu rezidüel önceden tanımlanmış eşik değerini ki bu da sistemin, hata durumları için uygulayabileceği maksimum takat kuvvetine eşdeğerdir, geçtiği anda hata tespiti başlar. Prosedür daha sonra hata saptama adımıyla devam eder. Bu adımda eyleyicinin belli aralıklarla alınan konum bilgisi ve istenilen eyleyici konum bilgisi arasındaki fark analiz edilerek kitlenmenin gerçekleştiği doğrulanır.

Anahtar Kelimeler: Elektro Hidrolik Eyleyici, Durum Gözlemcisi, Bozuntu Gözlemcisi, Model Tabanlı Arıza Kestirimi

To ones who never give up and do struggle for going one step further…

ACKNOWLEDGMENTS

I would like to first express my deepest appreciation to my thesis supervisors, Dr. Hakan Çalışkan and Dr. Ali Emre Turgut, for their inspiration, encouragement, patience and countless support. I am really fortunate for having the opportunity to work with them having their support over the last three years.

Especially, I am really grateful to Dr. Çalışkan for his guidance and effort in studying the experimental test bench that he has developed. It was not an easy task to make such a comprehensive test system operational again. To simulate jamming failures was also a great challenge and risk within the scope of this study. With the help of Mr. Çalışkan, a lot of difficulties have been overcomed in a very tight schedule. I wish Dr. Çalışkan and Dr.Turgut great success in their Academic Careers.

And my dear family,

I would like to thank to my beloved mother Dilek Poyraz, father Mehmet Poyraz and my brother Cemre, for their endless support and patience. I could not be where I am today without them.

Last but not the least,

I would like to thank to all my colleagues and friends for their moral support.

TABLE OF CONTENTS

LIST OF TABLES

LIST OF FIGURES

FIGURES

LIST OF ABBREVIATIONS

ABBREVIATIONS

EHA: Electro Hydrostatic Actuator

EKF: Extended Kalman Filter

FDD: Fault Detection and Diagnosis

FTC: Fault Tolerant Control

LOE: Loss of Efficiency

LPV: Linear Parameter Varying

LSim: Load Simulator

OFC: Oscillatory Failure Case

UKF: Unscented Kalman Filter

LIST OF SYMBOLS

$\mathbf{A_{lsim}}$	State matrix of the valve controlled load simulator system
$\mathbf{A_{eha}}$	State matrix of the pump controlled EHA system
A_A	Piston side cross-sectional area
A_B	Rod side cross-sectional area of the valve controlled actuator
A_p	Piston side pressure area of the valve controlled actuator
$A_{P_{eha}}$	Piston side cross sectional area of the EHA system
$\mathbf{B_{lsim}}$	Input matrix of the valve controlled system
$\mathbf{B_{eha}}$	Input matrix of the pump controlled EHA system
C	Chamber capacitance of the valve controlled hydraulic actuator
C_a	Hydraulic capacitance of the EHA piston side chamber
C_b	Hydraulic capacitance of the EHA rod side chamber
C_d	Discharge coefficient
D_P	Displacement of the EHA hydraulic pump
F_d	Disturbance load

F_{d_obs}	Estimated disturbance load
F_f	Viscous friction force in the load simulator actuator
$F_{f_{eha}}$	Friction force within the EHA actuator
$G_v(s)$	Transfer function of the proportional valve
J_M	Inertia of the rotor of the electric motor
J_P	Inertia of the EHA hydraulic pump rotor
K_a	Steady state gain of the servo-proportional valve
K_c	Flow-pressure coefficient of the servo-proportional valve
K_{cA}	Flow-pressure coefficient corresponding to A port of the proportional valve
K_{cB}	Flow-pressure coefficient corresponding to B port of the proportional valve
K_{qA}	Flow gain corresponding to A port of the proportional valve
K_{qB}	Flow gain corresponding to B port of the proportional valve
K_q	Flow gain of the servo-proportional valve
K_v	Steady state flow gain of the servo-proportional valve

K_k	Kalman gain
L_{lsim}	Observer gain matrix for the valve-controlled load simulator system
L_1	Disturbance observer gain
P_a	Piston side chamber pressure of the EHA system
P_b	Rod side chamber pressure of the EHA system
P_o	Operating point around which the linearization of the proportional valve flow is performed
P_k	Posteriori error covariance estimate matrix
P_k^-	Priori error covariance estimate matrix
Q	Process noise covariance matrix
R	Measurement noise covariance matrix
T_v	Time constant of the valve actuator
V_A	Piston side volume of the valve-controlled hydraulic actuator
V_B	Rod side volume of the valve-controlled hydraulic actuator
V_{A0}	Initial piston side volume of the valve-controlled hydraulic actuator

V_{B0}	Initial rod side volume of the valve-controlled hydraulic actuator
b_M	Equivalent friction coefficient of the electric motor rotor bearings
b_p	Viscous friction coefficient for the valve-controlled actuator
b_{eha}	Viscous friction coefficient of the EHA actuator
$b_{p_{eha}}$	Viscous friction coefficient of the EHA hydraulic pump
e	Position tracking error of the EHA
k_s	Stiffness of the spring arrangement between two Actuator
k_T	Electric motor torque constant
m_p	Mass of the valve-controlled actuator piston
m_{eha}	Mass of the piston and rod of the EHA actuator
p_A	Piston side pressure of the valve-controlled hydraulic actuator
p_B	Rod side pressure of the valve-controlled hydraulic actuator
p_{Ao}	Steady state piston side pressure of the valve-controlled hydraulic actuator
p_{Bo}	Steady state rod side pressure of the valve-controlled hydraulic actuator

p_s	Supply pressure
p_r	Return (tank) pressure
p_L	Load pressure of the valve-controlled hydraulic actuator
p_{o_lsim}	Open loop poles of the valve-controlled load simulator system
p_{c_lsim}	Desired observer poles of the valve-controlled load simulator system
q	Flow rate
q_c	Flow through the hydraulic accumulator
q_{cA}	Control flow rate through A port of the proportional valve
q_{cB}	Control flow rate through A port of the proportional valve
q_{A0}	Steady state flow rate through A port of the proportional valve
q_{B0}	Steady state flow rate through A port of the proportional valve
u	Control input to the servo-proportional valve
u_M	Electric motor voltage input
ω_M	Angular speed of the electric motor

$\bar{x}$	Moving Average
x_p	Position of the valve controlled hydraulic actuator
$\dot{x}_p$	Velocity (rate) of the valve controlled hydraulic actuator
$\ddot{x}_p$	Acceleration of the valve controlled hydraulic actuator
y_A	EHA actuator piston position
$\dot{y}_A$	Velociy (rate) of the EHA piston
$\ddot{y}_A$	Acceleration of the EHA piston
t'	Sampling time
w	Peripheral width of the orifice
w_k	Process noise vector
a	Pressure area ratio of the valve controlled hydraulic cylinder
a_{eha}	Pressure area ratio of the EHA hydraulic cylinder
β	Bulk modulus of the hydraulic fluid in the load simulator
ρ	Density of the hydraulic fluid in the load simulator
ζ	Auxiliary variable in the disturbance observer

$\dot{\zeta}$	Dynamics of the auxiliary variable in the disturbance observer
i	Fault detection signal
τ	Fault detection threshold
τ	Fault identification threshold
σ	Signal variance

TERMINOLOGY

The terminology defined in [1] is organised and presented here.

Fault is an unpermitted deviation of at least one characteristic property or parameter of the system from the acceptable/usual/standard condition.

Failure: Permanent interruption of a systems ability to perform a required function under specified operating conditions.

Malfunction: A malfunction is an intermittent irregularity in the fulfillment of a system's desired function.

Reliability: Ability of a system to perform a required function under stated conditions, within a given scope, during a given period.

Safety: Ability of a system not to cause danger to persons or equipment or the environment.

Analytical redundancy: Use of more than one not necessarily identical ways to determine a variable, where one way uses a mathematical process model in analytical form.

Hardware redundancy: Use of more than single independent component or equipment to perform a required task.

Fault diagnosis: Determination of type, size, location, and time of occurrence of a fault. Includes fault detection and isolation.

Fault detection: Determination of faults present in a system and time of detection.

Model-Based fault detection: Use of relations between several measured variables to extract information on possible changes caused by faults.

Residual: Fault information carrying signals, based on deviation between measurements and model based computations.

Threshold: Limit value of a residual's deviation from zero, so if exceeded, a fault is declared as detected.

CHAPTER 1

INTRODUCTION

1.1   Background and Motivations

Hydraulic power technology has been preferred for many decades in a wide range of applications. Compared to any other types of power sources (electric, pneumatic, piezo, etc.) hydraulic systems generally offer the highest power to weight ratio and this leads to more compact and less weight solutions for most of the industrial applications today. From relatively simple applications like presses, extrusion molding machines, rolling mills and other [2] to quite complex engineering fields such as industrial robots, aerospace flight control and utility actuation [3], military, etc. hydraulic power technology is extensively used.

Besides its great power potential, hydraulic systems can also be utilized for applications where high precision and reliability is needed. Modern electronics and sensor technology together with the advances in manufacturing makes it possible to equip conventional hydraulic systems with feedback devices, control electronics and complex computing elements [4]. These integrated systems are often called as electro-hydraulic systems where inputs are usually electric signals and the desired output (force, torque, position, velocity, etc.) is generated hydraulically by using different components such as valves, pistons and hydraulic motors according to the application. Utilizing sensor technology can bring about the gathering information about system variables and transforming this data into electrical signals to be used in computing devices. Hence, hydraulic components can be precisely controlled in order to achieve better performance for more demanding requirements.

Among system requirements while designing a precise electro hydraulic control system, reliability and safety are one of the vital issues especially for critical applications like aircraft flight control System Actuation [5]. As electro hydraulic (or simply hydraulic) systems are getting more and more complex the demand for safer, more reliable and robust systems has risen for integrated system applications. Often, an anomaly, which may be treated as insignificant in the System, can cause considerable performance degredation and deteriorating effects or even worse it may end up with a catastrophic system failure. Due to increasing demand towards higher system reliability and safety, a great amount of research about fault detection, diagnosis and identification concepts is being carried out.

There are basically two main approach for detecting system anomalies independent of whether the system is hydraulic, electric or any other type: Prognostics and diagnostics approaches. Prognostics is the discipline which predicts when a system will not maintain performing the required task. It's related with the remaining useful life of a system, process or a machinery. Whereas diagnostics is more about the identification of errors and detection of faults whenever they are observed. Diagnostics allows complicated systems to take corrective actions on the instant of a failure. It also provides an insight into possible causes of faults and gives information about them to system users via designated interfaces. While it may be possible to estimate possible faults and the life of a system by performing extensive endurance and life tests, they are often quite expensive and time-consuming processes and test methods also rely on statistical results. For cost effective, precise and reliable system designs using prognostic and diagnostic methods in complex architectures are getting more common [6].

For safety critical systems, like aircraft, consequences of faults in a flight control system hardware or software can be extremely hazardous in terms of economical impact and human life. That is why, there are a number of aviation authorities that have stringent safety regulations.

In flight control applications, diagnosing the occurred faults in the system is vital. Faults should be detected and if possible recovered immediately while the aircraft is still operating. This is also the case for hydraulic flight control actuation in aircrafts. Flight control system is maybe the most important element in an A/C (aircraft) for the safety of flight and moslty they rely on electro hydraulic actuation technology for providing necessary power to control surfaces. There are quite a lot of studies on fault detection and diagnosis for aircraft flight control systems. Some of these studies focus on faults of which some them is discussed before in actuation systems as well.

Traditional approach to fault detection and diagnosis for aerospace applications is based on hardware redundancy methods where multiple sensors, actuators and computers are used. However, this approach generally complicates the system architecture and increase the weight. There is a growing tendency in modern aerospace systems towards the methods, which do not need additional hardware redundancy and only rely on the increasing level of computational power onboard the aircraft [7].

One of the trend topics in fault detection of aerospace hydraulic applications is about control surface jamming. **Jamming is a system failure where a control surface or a control effector is permenantly stuck at its current position.** This could have several consequences first of which is an undesirable aircraft motion. As flight control surfaces are responsible for the required manoeuvering, their loss of function in the event of jamming causes an asymmetry in aerodynamics balance of the aircraft. In order to compansate the aerodynamic asymmetry caused by the jamming of a control surface, other available control surfaces should be used further which eventually leads to an increase in the overall drag and fuel consumption.

There are various type of other faults investigated for flight control actuators as well. Servo valve failures in hydraulic actuators [8], incipient sensor failures [9], stall loads in control actuators [10] and control surface runaway [11], i.e. the unwanted surface motion which persists until the actuator runs the surface to the end of its travel, are some of the specific topics under research in FDD (fault detection and diagnosis) topics for flight control actuators.

1.2   Objective of the Thesis

The main objective of this thesis study is to develop a fault detection and diagnosis method for jamming cases that are critical for flight control actuation system applications in terms of safety of flight, fuel consumption and system integrity. In this point it should be noted that the jamming at deflections close to null (zero) deflection, corresponding to the mid-stroke point of an actuator, is a special case which leads to additional challanges regarding its idenfitication [31]. As all of faults within a flight control actuation system, except jamming, result in a non-zero variance on position measurement, usage of the position information for jamming (which might be the only available feedback for the actuation system) might not come up with a straightforward detection process. Therefore, the detection and identification of jamming faults is primary interesting at low deflection signals where the residual between the reference position input and the measured feedback is quite low. Whereas stall loads usually occur at extensive input maneuvers where the aerodynamic forces acting on the control surface are high [10]. After the development phase of the proposed fault detection and diagnosis method, it is aimed to evaluate the effectivity of fault detection of the proposed method by simulating permanent jamming with small input demands on an electro hydraulic actuation test bench.

4

In order to achieve this goal, model-based fault detection methods are applied. Firstly, the mathematical model of the actuation system is required to analyze system performance under faulty cases by checking specific system features. One of the key parameter to be observed for identifying jamming conditions may be presumed as the disturbance load acting against the movement of the piston in an electro hydraulic actuation system. The actuator is no longer able to generate motion in the case of jamming, this also means that it does not produce a net force even the given command into the control valve or servo motor is to be just the opposite. The jamming phenomena might be observed due to several reasons. Thus, it is possible to use the disturbance load information for the detection of jamming and cases. For this purpose, a disturbance observer is designed to estimate the force acting on the actuator.

Further information about system dynamics under faults is needed to detect two distinct failure conditions, i.e. jamming cases. For this purpose, available position information (sensor feedback) will be adressed. A successive methodolgy consisting the analyzing of the disturbance estimation and the tracking error, between the reference input position and the measured feedback, is to be followed.

Final step to complete the fault detection algorithm is to combine predefined two distinct methods. After simulating the faults to be of concern in the electro-hydraulic actuation test setup, developed FDD scheme will be analyzed and tuned to reduce the false alarm and to enhance the detection rate.

1.3   Thesis Outline

In the beginning chapter of the thesis, the main objective and the motivation behind this research are stated. Main faults to be investigated and why they should be focused on are discussed.

In the following Literature Review section, i.e. Chapter 2, critical faults in industrial and flight control actuation systems are introduced. Different types of failure cases which have been studied in the literature are represented. Then, some of the basic concepts of fault detection and diagnosis field are explained together with the methods used for FDD purposes including model and signal-based approaches. Furthermore, methodologies found in the literature which are used for the detection of different faults are discussed. FDD techniques are represented herein for both industrial and aerospace (especially in flight control actuation) applications. Model-based strategies for fault detection and diagnosis purposes are introduced in this chapter. Mainly, Observer and Kalman-based methods are focused. Further model-based methods for FDD are also referred. Then it is followed with the model-based linear parameter varying (LPV) techniques for detection of different failures in aerospace control systems. Especially the use of LPV methods for the detection jamming and stall cases are mentioned. Then,

Modelling of the electro hydraulic actuation system is performed in Chapter 3 in order to move on with the model-based FDD aproaches. This chapter mainly consists of the mathematical modelling of the proportional valve controlled system and the linear modelling of the EHA system, respectively.

Chapter 4 basically introduces the test setup and hardware used for the verification of the FDD technique to be developed. Details of the electro-hydraulic test bench system are given under two main parts. The first part describes the overall electro-hydraulic actuation system used as the experimental test up whereas the second part represents the components and the equipment in the setup in three sections. First section focuses on the components within the load simulator whereas

the second section represents the equipment of the electro hydraulic actuator (EHA) system. In the last part of this chapter, details of electronic hardware, which is responsible for control and monitoring of both systems are given.

Chapter 5 covers the proposed method for the detection and identification of jamming and stall cases. The method is introduced in section 5.1. In the beginning of the developed FDD system, a Luenberger state observer is designed to estimate unavailable state information for both valve and motor controlled actuator systems. Having known the state information with the available state feedbakcs, a disturbance observer is designed to estimate the load that the actuator is subjected. Disturbance and state observer models are validated with experimental results. In order to specifically detect the faulty cases and to distinguish the stall cases from the jamming an additional process, i.e. the fault identification, is described. In the identification step, variance of the actuator position measurement is compared with a threshold to identify the faults to be interested. The results for faulty jamming cases and nominal cases are presented at the end of this chapter.

Lastly in Chapter 6, the fault detection performance of the proposed method is evaluated, the investigated results are summerized and the conclusion is made based on these results.

CHAPTER 2

LITERATURE REVIEW

2.1 Faults in Industrial and Flight Control Hydraulic Actuation Systems

''A fault is an unpermitted deviation of at least one characteristic property (feature) of the system from the acceptable, usual, standard condition.'' [6]

In hydraulic actuation systems, a wide range of faults and failures may be observed. The most common faults in industrial applications are fluid contamination [12], supply pressure malfunction or loss [13], and internal and external leakage in the hydraulic actuator [14]. Somewhat more specific hydraulic actuator failures like jamming, hardover and loss of efficiency occur in aerospace applications. [15].

There are several types of common failures in flight control hydraulic actuators whose early detection and proper handling can significantly contribute to flight safety, excessive fuel consumption and increase the aircraft operational autonomy. The flight control actuator failures can be broadly divided into two categories: 1) failures which result in a total loss of effectiveness of control actuator and 2) failures that cause partial loss of effectiveness. First category may include lock-in-place (LIP, a.k.a 'Jamming'), float, and hard-over failure, while the other is referred as the loss-of-efficiency (LOE) type failures, which may be an internal or external leakage in the actuator, excessive seal friction on hydraulic piston, etc [16].
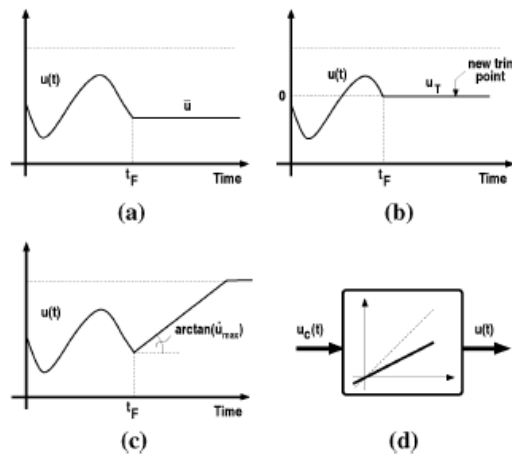
Figure 2.1. Types of control actuator failures (a) LIP (Jamming), (b) Float, (c) Hard-over, (d) LOE [17]

Lock-in-place type failure are also sometimes specified as jamming or jammed at a fixed position. Control surface actuator jamming can create an asymmetry in the nominal flight condition which should be compensated by appropriate amount of use of other surface actuators. One of the other impact of the jammed surface case is an increase in drag force that causes an increase in the overall fuel consumption if the control surface permanently stuck at a single position. The runaway is also an undesired or uncontrolled flight control surface motion that can continue until the surface reaches its stop. Depending on the significance of a control surface, the runaway might be catastrophic. If this fault occurs in a surface which does not directly affect flight path of an aircraft (also known as secondary flight control surfaces), aircraft structures can be exposed to additional loads. Else, runaway is observed in a surface which directly changes the trajectory of flight (primary control surfaces) result in an undesired manoeuver that may significantly increase the pilot workload. In any cases, the detection and diagnosis of such a failure must be achieved way before the related control surface is stuck at the full deflection.

Different faulty cases can be summerized under the loss of efficiency (LOE) type faults, as for example, speeding-up of the actuator dynamics which may be due to a mechanical disconnection (broken rod), and slowing-down of the actuator dynamics

due to a reduction of the actuator gain, or the inability to reach a commanded deflection (due to loss of power, hydraulic leakage or a sensor calibration error) [15]. The worst-case scenario for this type of fault is the case where the efficiency of the control surface goes to zero. The disconnection of the actuator as well as a damage on the control surface may lead to an increase in the bandwidth due to the reduced aerodynamic loads transferred to the actuator piston whereas leakage or excessive friction faults could cause decrease in bandwidth due to reduced available pressure [10]. Actuator stuck under the stall loads can also be considered as a special type of loss of efficiency (LOE) faults. Stall loads are intermittent saturations of the actuator, which occur when the aerodynamics loads temporarily exceed the maximum available actuator force produced by the hydraulic pressure difference in the system. Since stall loads are generally observed at large control amplitudes, their fast detection and identification might be important to distinguish them from other type of failures. Without explicitly diagnosis of stall loads, the detection of many additive LOE faults in the case of large control inputs becomes more difficult due to the need for using larger detection thresholds which limit the smallest amplitude of detectable faults.

A challenging case in fault detection is the jamming at small deflections (i.e. in null position) as it may remain undetected for a long period of time. For example, during a cruise phase this fault practically undetectable, due to the small control inputs. Therefore, the detection of actuator jamming in null position may be addressed for small actuator input demands. [18]

Another important type of failure in flight control systems is so-called Oscillatory Failure Case (OFC). Abnormal oscillations of a control surface are seen in this kind of failures. This phenomenon is caused by component malfunctions in flight control surface servo control loops and could excite aircraft structure amplifying structural loads. The major difficulty in the OFC is its nature of having unknown amplitude and frequency. [19]

11

2.2 Fault Detection and Diagnosis

Fault detection and diagnosis are fundementally based on measured variables by instrumental and observed variables and/or states by human observations. Processing and computation of measured states for fault detection purposes requires analytical knowledge and the evaluation of observed states needs heuristic knowledge. Hence, fault detection and diaognosis may be considered as a knowledge-based approach. [20] Below figure shows the overall layout of the knowledge-based fault detection and diagnosis.
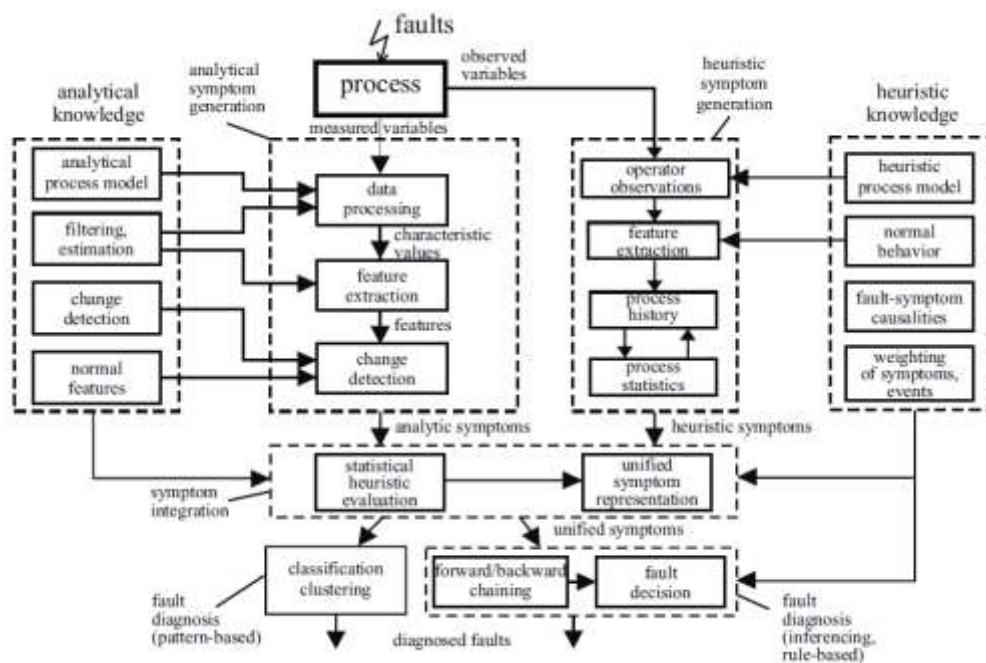
Figure 2.2. Layout of the knowledge-based FDD aproach [20]

In order to generate evaluable information, data processing besed on measured states/variables needs to be performed. Following approaches can be preferred for specific FDD applications.

- Limit value checking of directly measurable signals

- Signal analysis of measurable signals by the use of signal models like correlation functions, frequency spectra, autoregressive moving average (ARMA) or the characteristic values such as, variances, amplitudes and frequencies or parameters.
- Model-based mathematical process analysis using parameter/state estimation, parity equation and residual generation

Special information about the analytical sympthoms within the process can then be extracted by manipulating some characteristic values like physical system coefficients, filtered or transformed residuals. This information is then compared with the nominal values of the non-faulty process. Consequently, the resulting changes in the mentioned three methods can be identified as analytical symptoms. Alternatively, the symptom generation may also be achieved by heuristic methods through human obervation, inspection checks, etc.

After gathering information about the symtoms within the process, the diagnosis step comes where the type, size, magnitude and the location of the fault is determined. Time of detection is also one of the key point in fault diagnosis as it directly affects the overall results of the possible fault. Development of fault detection and diagnosis approaches can often be resulted with a fault tolerant control system design and a significant increase in the overall system robustness. Together with the processing data related with the symptoms in the system/process and the identification of this data for fault diagnosis, a complete FDD (fault detection and diagnosis) method is developed.

An FDD system design generally begins with the mathematical modelling of the process/system together with the signals to be focused. By doing so, faulty and non-faulty behaviours of the system can be simulated. Then it follows with the development of the FDD-method(s) with software-in-the-loop simulations. When the developed FDD system is ready and mature enough for the implementation of the final software, then the real system tests and tuning processes can be carried out

through hardware-in-the-loop simulations. Real time simulation of the process/system is achieved with an enhanced sensor-simulation interface.

2.3 Faults Detection and Diagnosis in Industrial and Flight Control Actuation Systems

Fault detection and diagnosis in hydraulic actuation system applications primarily refers to two distinct approaches, signal-based and model-based methods. In model-based approach, measured varibles or states in the system are analyzed in order to gather information on possible changes caused by faults. Analytical relations are used in form of process model equations which represent the relation between the reference input signal to be controlled and the measured output signals. Model-based fault detection methods then extracts certain information such as system parameters, state variables or residuals and comparing these information with their nominal values in order to make a decision about whether the change in the observed system features is categorized as faults or not. Wheres in signal-based detection methods, measured signals of processes in a system are used. If changes in the signals of concern are related to faults in the system, then the signal-based approaches migth be valid for FDD purposes. Especially, oscillations of harmonic or stochastic nature in a system or a machinery can be asssociated with system anomalies in signal-based fault detection methods [6].

Sepasi, M. utilized a novel model-based methodology for health-monitoring of a hydraulic actuation system [21]. Several different type of loads are studied like sudden loss of load, internal and external leakage of the actuator and dynamic friction due to the loading. An Unscented Kalman Filtering (UKF) algorithm is developed for system monitoring. Hydraulic system to be focused on is modelled in simulation environment. This model is also validated through a test rig. Leakage fault is realized

through a needle valve on the hydraulic test rig. FDD simulation results with UKF is then analysed for compatibility with the test results. By the help of antagonistic loading system including a pneumatic actuator, the author could also insert dynamic friction load failure to the system and compare the experimental results with the ones obtained through simulation.

Other than classical hydraulic servo actuators, similar approaches are also implemented and FDD is studied in Electro Hydrostatic Actuation (EHA) systems. Song, Y. used several filtering methods for an EHA test rig located at McMaster University. In the study, he used Extended Kalman Filter (EKF) and Smooth Variable Structure Filter (SVSF) methods together with Interacting Multiple Model (IMM) approach in order to develop the FDD algorithm for EHA prototype [22]. In the architecture of the real system, there is a throttling valve to simulate internal leakage in the cylinder and an auxiliary cylinder arrangement to replicate the friction fault without seal replacement. Without changing system parameters through adjustments in test rig, he inserted several fault cases and also simulated them through the FDD algorithms developed.

Chen, L. Focused on fault detection together with a fault tolerant control system design for a complete hydraulic actuation system (pump, control and check valves, reservoir, actuator, etc.) [23].In this study, leakage and pressure sensor faults are inserted to the modelled system and a fault detection observer is designed for FDD purposes. Estimated faults are compared with the system responses in simulation. After identifying the possible faults within the hydraulic system, the author also designed a fault tolerant control (FTC) system. Adaptive back stepping methodology, a recursive Lyapunov-based approach, is used for FTC purposes. The back stepping method is applied to the system which is subjected to varying load and the considered faults (leakage and pressure sensor). In the FTC algorithm, this method is employed to tolerate the uncertainties coming from possible changes in system parameters due to the fault cases. At the end, designed FTC algorithm is simulated for position and velocity tracking under several failures.

Early applications of FDD in flight control actuation systems were generally based on hydro mechanical fault detection circuits. Different logic structures are implemented into manifold of a control actuator for health monitoring purposes. Advances in electronics have increased level of confidence in both hardware and software used in aircraft equipment. The usage of integrated electronics for FDD applications in aviation have also significant advantages like weight saving, less number of mechanical components and higher reliability. [24]

Modern Fly-By-Wire aircraft flight control are getting more complicated with sophisticated actuators controlling different type of control surfaces. As one of the most important flight and safety critical system, the consequence of faults in in the flight control system hardware (flight control computer, actuators, sensors, etc.) and software may be extremely fatal for air vehicles. Due to such reasons, nearly all aircraft main contractor manufacturers try to be compliant with strict safety regulations of EASA (European Aviation and Safety Association), FAA (Federal Aviation Association) and other aviation authorities.

In some specific cases for aircraft systems, it may be assumed that the product will never fail during its operational life which is actually called safe-life. This concept can also be referred as resistance to failure and is essentially used for the design of several structural parts like landing gear. However, when loss of function is not tolerable, overall system performance should be insured either fully or in a degraded mode.

Current trend for safer flight control has been towards the health management, failure detection & diagnosis and prognostic air vehicle and/or flight control system design topics. Because of these safety issues, possible failures shall be predicted or may be identified way before the first flight of a new designed air platform from scratch, especially for flight and safety critical systems like flight controls, hydraulics, engine, etc. The traditional approach to fault diagnosis and fault tolerant system design relies on the hardware redundancy concepts which use multiple sensors, computers, electrical and hydraulic systems and dedicated software to

measure and control a predetermined variable and/or state. Despite the redundancy level, it might not still be possible to have a system design completely isolated from effects of failures. Furthermore, high redundancy concept could also increase weight, complexity, size and cost of the actuation system and after some point reliability of the overall system might not be enhanced significantly just by increasing number of power supplies or multiple input and output channels.

High number of study about failure detection & diagnosis (FDD) for flight control actuation systems are available in the literature. The paper written by Crepin P., Kress R. presents a model based method for fault detection of an aircraft actuator. Extended Kalman Filter (EKF) and parity space methods are applied for failure detection where EKF is used for the diagnosis of internal cylinder leakage and parity relations is used for the identification of direct drive valve (DDV) failures [25]. For this survey, three additive faults (coil voltage, coil current and valve position measurement faults) are simulated within the mathematical model of the DDV. EKF algorithms described here are also implemented on a DSP (digital signal processing) real-time platform and as an example, diagnosis graph of internal tandem cylinder leakage is given.

Some of the Airbus specialists have focused on FDD in their Electrical Flight Control System (EFCS) design stages. Goupil et al. 2015, investigates model-based detection of different control surface failures such as oscillatory failure case (OFC), jamming and runaway cases. In this study, they construct different techniques for both jamming and OFC fault cases [19]. Real-time estimations of the desired state (position of control surface or actuator rod) is accomplished by non-linear local filtering and non-linear observer methods for OFC. By comparing the estimated state with the real one, a residual is generated which is than evaluated considering prescribed threshold values. Another failure scenario studied in this paper is the jamming of actuation system. Dedicated Kalman Filtering is offered for monitoring of jamming and runaway situations. According to the author, the basic idea of using Kalman Filtering here is to early detect abrupt changes between two signal lanes that carry control surface (or actuator rod) position information. One of the proposed

model-based solutions in the study, has received certification on new generation Airbus A350 aircraft.

Another study about actuator lock-in-place failure are carried out again by Airbus specialists. Cieslak et al. 2014, develop a signal-based detection method for those kind of failures [18]. The strategy proposed in the paper is based on two successive steps. The first step comprises estimation of on-line derivatives of the pilot order inputs and also derivatives of control surface position. In the second step, for the diagnosis of jamming cases a dedicated decision making algorithm evaluates the signals generated from the first process. A second order discretized filter and a first order sliding mode differentiator (SMD) is used in order to estimate the derivatives of input signal. Once the derivatives mentioned are obtained, an evaluation rule, together with predefined threshold values, is applied for confirmation of the researched fault cases. The signal-based approach developed in the study is also tested and validated on an Airbus actuator test bench using recorded flight-test data from A380 elevator actuator.

A new method is proposed by Eykeren et al. [26] for the detection of solid, liquid jamming and surface disconnection cases in flight control actuators. The approach to detect those failures in the study is based on Aerodynamic Model Identification (AMI). Different type of faults are identified with their influence on the aerodynamic model of the aircraft and parameter changes in the aerodynamic under failures is compared with the initial or nominal values. Marton, L. and Ossmann, D. proposed a different approach for the surface disconnection type failures. Instead of comparing the changes in the aerodynamic model, they developed a model which compares the energy intake of the actuator and of the fault model [27]. With this way, the disconnection between the opposing load and the actuator is detected. They derive the energy balance of the acutator during faulty and fault-free cases where the input energy depends on the actuator's velocity and then obtain the residual signal to be explored. According to this method, the residual signal is constant during the disconnection and it varies in normal operation where the actuator is in motion.

Alternatively, model-based linear parameter varying (LPV) techniques are applied for fault detection purposes for flight control actuators. Ossmann, D. developed a methodology for the detection of jamming, OFC, and runaway type failure cases [28]. This study is based on a nonlinear first order actuator model derived before by Goupil [29]. The actuator model is actually quite dependent on the aerodynamic force acting on the control surface. Thus, a nonlinear gain is defined and it is scheduled with different aircraft parameters and flight conditions. According to different flight conditions, the model updates itself by changing its linear parameters. The residual signal for the fault detection is generated using this LPV actuator model and evaluated via a measurement method of the residual signal energy, so-called Narendra signal evaluation scheme [30]. After the evaluation process, fault decision is made based on a threshold based operation. It is quite important at this steep to define an appropriate threshold since it influences the overall performance of the FDD system. At the end, the validation of the FDD scheme developed in this study is performed on an AIRBUS actuator test bench for the monitoring of jamming at small actuator deflections under different manoeuvres and flight condition inputs given to the FDD system. The same model-based LPV technique is also used by Ossmann [10] for the detection of loss of efficiency type failures. The method is tested on different points in the flight envelope and it succesively detects stall loads observed in the real flight.

2.4 Model Based Fault Detection and Diagnosis Methods

Model-based fault detection and diagnosis (or often referred as identification) basically consists of two main steps residual generation and fault identification. There may also be several substeps such as residual evaluation where the norm of the residual signal is generated and decision making where the evaluated residual signal is used in a simple threshold based logic [31].

Faults in a system change the expected system dynamics and perhaps the nominal model parameters. High fidelity system models can be analyzed to predict discreapancies between estimations and measurements which in turn is used for fault detection purposes. Here, the residual generation is the critical point in the design of a FDD system. The residual signal is obtained based on the difference between the estimated and the measured system state, variable or parameter. Fault detection occurs if the generated residual signal exceeds a predefined threshold value. However, there are always some uncertanities within models and measurement noises in practical systems which can result in false alarms or keep faults to be undetected. This fact significantly degrades the fault detection performance. Therefore, specifying an optimum threshold may not be an easy task for most of the fault detection applications.

The residual signal should be very close to zero if no error exists in the system. However, this is not the case in reality as all engineering systems include unmodelled uncertanities and measurement noises. Residual signal should be picked according to the specific fault to be investigated. If the generation of residual signal does not contain information about the faulty state of the system or if it is not sensitive enoguh to the special fault, then the residual should be referred to other states or variables within the system. Moreover, generated residual signal should also be robust against modelling errors, disturbances and uncertainties. Generally, a trade-off between false alarm rate and fault detection sensitivity is to be made in order to achieve the 'optimum' fault detection results.

One of the most common method to generate a residual signal is to use an observer. David G. Luenberger introduced a widely used basic observer scheme to reorganize missing state variables for control purposes [32]. The Luenberger observer assumes a linear time invariant system described by the following equations:

$$\dot{x} = A_{sys}x + B_{sys}\, u_{in} \tag{2.1}$$

$$y = C_{sys}x \tag{2.2}$$

where x stands for the system states, u_{in} for the input(s) and y is the measurement. A_{sys}, B_{sys} and C_{sys} all are from the state space representation of the system. The Luenberger Observer is the constructed as:

$$\dot{\hat{x}} = A_{sys}\hat{x} + L_{obs}(y - \hat{y}) + B_{sys}u_{in} \tag{2.3}$$

$$\hat{y} = C_{sys}\hat{x} \tag{2.4}$$

Where the observer's estimation of the system states and the output are denoted by $\hat{x}$ & $\hat{y}$ and L is the gain matrix of the observer. Dynamic behaviour of the state estimation errors is determined by the eigenvalues of the $A_{sys} - L_{obs}C_{sys}$ matrix. Therefore, if matrix $A_{sys} - L_{obs}C_{sys}$ is stable, then the estimation errors will converge to zero for any initial error vector. Furthermore, if the eigenvalues of matrix $A_{sys} - L_{obs}C_{sys}$ are chosen in such a way that dynamic behavior of the state estimation error vector is asymptotically stable and adequately fast, then error vector will tend to zero with an adequate speed.

Based on this basic Luenberger Observer principle, various approaches have been developed to reconstruct the state vector of the system. Some of the examples are Internal Observers and Sliding Mode Observers. Robust residuals generation in FDD algorithms may also be achieved by using specific type of observers such as Unknown Input Observers (UIO) [33] and Sliding Mode Observers [34].

Another typical method used for residual generation is state and parameter estimation using special filters like Kalman and Smooth variable Structure filters

[35]. Rudolph Kalman first introduced his new approach to filtering and estimation problems in 1960 [36] and since then the Kalman Filter has been extensively used for many applications in industry. This filtering method is applicable for stochastic linear systems described by the following difference equation:

$$x_{k+1} = A_{sys} x_k + B_{sys} u_k + w_k \qquad (2.5)$$

and the measured output equation y_k is defined as

$$y_k = H x_k + v_k \qquad (2.6)$$

where A_{sys} is the state matrix, B_{sys} is the input matrix, H is the output matrix, x is the state vector, y is the system output, u is the input, w is the process noise and v is the measurement noise. Both process and measurement noises are assumed to have a zero-mean and to be Gaussian distribution with the following process noise Q, and measurement noise matrix R.

$$Q = E[w_k \quad w_k{}^T] \qquad (2.7)$$

$$R = E[v_k \quad v_k{}^T] \qquad (2.8)$$

The Kalman Filter performs the estimation in a predict and correct manner. Equations for prediction are responsible for the priori estimation of the state vector $\hat{x}_k^-$ at k$^{\text{th}}$ step. This so-called 'Time-update' equation uses *a priori* state estimate vector as follows.

$$\hat{x}_k^- = A_{sys} \hat{x}_{k-1} + B_{sys} u_k \qquad (2.9)$$

Here $\hat{x}_{k-1}$ is *a posteriori* (corrected) state estimate vector and u_k is the known input. By subtracting the measured and the estimated output, the residual is calculated as:

$$y_k - H\hat{x}_k^-$$ (2.10)

Measurement update or correction equation is then used together with *a posteriori* state estimation vector to obtain the *posteriori* estimates as follows.

$$\hat{x}_k = \hat{x}_k^- + K_k(y_k - H\hat{x}_k^-)$$ (2.11)

Here $\hat{x}_k$ is *a priori* (predicted) state estimate vector and K_k is the Kalman gain. The *priori* and *posteriori* estimate error covariances are described, respectively;

$$P_k^- = A_{sys}\, P_{k-1} A_{sys}{}^T + Q$$ (2.12)

$$P_k = (I - K_k H)P_k^-$$ (2.13)

Where Kalman Gain is obtained by the following equation as referred in [37].

$$K_k = P_k^- H^T (H P_k^- H^T + R)^{-1}$$ (2.14)

Kalman Filter is initialized with a *posterior* estimate $\hat{P}_{k-1}$ covariance and the state $\hat{x}_{k-1}$. Then, the defined predictor-corrector algorithm is recursively applied at each iteration k. The recursive relation of the Kalman filter is represented in Fig. 2.3.

$$\hat{x}_0 = E(x_0)$$
$$P_0 = E[(x_0 - \hat{x}_0)(x_0 - \hat{x}_0)^T]$$

Time Update

$$\hat{x}_k^- = A\hat{x}_{k-1} + Bu_k$$
$$P_k^- = AP_{k-1}A^T + Q$$

Measurement Update

$$K_k = P_k^- H^T (HP_k^- H^T + R)^{-1}$$
$$\hat{x}_k = \hat{x}_k^- + K_k(y_k - H\hat{x}_k^-)$$
$$P_k = (I - K_k H)P_k^-$$
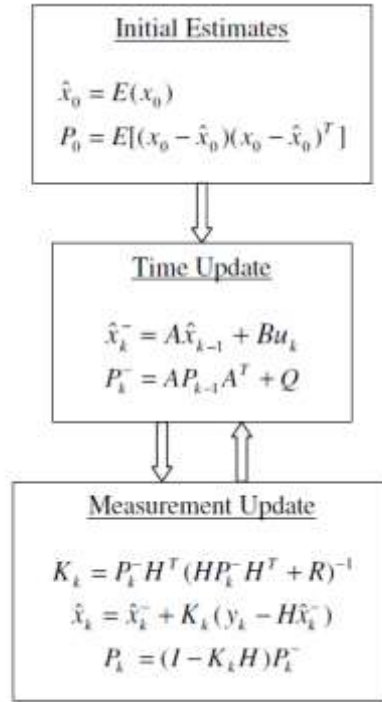
Figure 2.3. Kalman Filter Structure [21]

Besides its use in state estimation, Kalman filter has also been extensively used in fault detection and diagnosis applications. Goupil et al. [18] proposed a dedicated Kalman Filtering for monitoring of jamming and runaway situations. According to the author, the basic idea of using Kalman Filtering here is to early detect abrupt changes between two signal lanes that carry control surface (or actuator rod) position information. Proposed model-based solutions in the study, has received certification on new generation Airbus A350 aircraft. Okita et al. investigated foot slip detection with the Kalman Filter and the Unscented Kalman Filter (UKF) [38]. Sepasi also developed an Unscented Kalman Filter based methodology for the fault monitoring of an electro hydraulic actuation system [21]. He calculated the moving average of error (MAE) for the detection of various faults from external&internal leakages to sudden loss of load. Two different faults in EHA system are were diagnosed by Chinnah using Extended Kalman Filter method [39]. He followed a different approach than using Kalman Filter as a residual generator. Rather, changes in system parameters (bulk modulus and viscous friction coefficient) were

24

monitored. Entrapped air and the change in friction were successfully identified by tracking the change in those parameters.

Other model-based methods are also used for residual generation and fault detection purposes. Some examples are frequency domain approach by Frank and Ding [40], parity space approach by Willsky [41] and differential-geometric approach by Massoumnia [42].

2.5 Model-Based Linear Parameter Varying (LPV) Techniques for FDD

Since hydraulic actuation systems in aerospace applications exhibit a highly nonlinear and time varying behaviour, it is not easy to apply a linear mobel-based FDD scheme. One common approach is to linearize the mathematical model around given setpoints, then use gain scheduling method for control. This approach neglects the nonlinear nature of the missile model and the stability of the designed Fault Detection Filter (FDF) during the flight envelope lacks theoretical support.

The more efficient approach is based on Linear Parameter Varying (LPV) methodology. LPV methods can capture the nonlinearities within the system through state transformations to yield a quasi-LPV description and therefore allow some relatively mature linear-like control method to be applied. Based on that, many theoretical sound control system design methods are successfully applied to the missile LPV systems by Ganguli et al. [43] Yu et al. [44].

Among the existing FDI researches on LPV systems, Bokor and Balas [45] extends the fault detection filter for LTI system to a class of LPV systems using standard geometrical algorithms. Abadalla et al. [46] and Casavola et al. [47] proposed frequency domain based FDF design method for a class of polytopic LPV system using H∞/H- performance index. However, few literatures have applied these theoretical methods to aerospace applications. One of the first expamplew where the FDD problem for a missile in cruise phase is fully investigated, was accomplished by Yu, Cui, et al [48]. A fault detection system incorporating a LPV

fault detection filter bank was proposed in this study to detect and isolate the faults of tail actuator and pitch rate sensor. The LPV fault detection bank is designed based on the geometrical algorithms originally proposed by Bokor and Balas [45].

Ossmann and Varga [49] proposes a synthesis approach consisting of two steps of robust fault detection filters for model based diagnosis of sensor faults for a civil aircraft. As the first step, a linear parameter varying (LPV) fault detection filter is synthesized analytically using an extension of the nullspace based synthesis methods to LPV systems. In the second step, a multi-objective optimization problem is solved for the tuning of the LPV parameters in the filter to achieve a satisfactory fault detection performance. At the end of the study, proposed method is examined for the detection of failures in an angle-of-attack sensor.

Ossmann et al. [31] accomplished the verification and validation of a model based fault detection and diagnosis methodology for the detection and diagnosis of actuator jamming at small surface deflections. For the detection of jamming a discrete version of the LPV-model based fault detection approach of Varga et al. (2011) is proposed, extended with the fault identification functionality. The error residual $r(t)$ is generated based on the position output of this LPV based hydraulic actuator model and the position measurement by an LVDT. Then, the residual evaluation signal $\theta_r(t)$, representing an approximation of the norm of the residual signal, is obtained by using a Narendra type fault evaluator [30]. Overall method goes on with a threshold based decision making step and finally fault identification algorithm based on computing the variance of n many samples of measured actuator position signal after the jamming decision is made in the decision making process. The detection performances have been assessed by simulating the jamming failure scenario, during a classical ight and during special manoeuvres. The results have shown a high degree of robustness of the designed FDD system for the whole range of tests and a highly satisfactory detection performance.
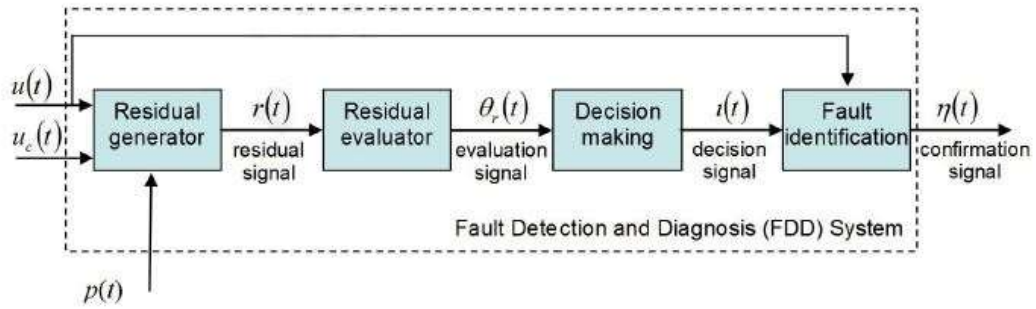
Figure 2.4. FDD System for monitoring of Jamming [31]

Details of the LPV-based FDD system for jamming detection is shown in Figure 5.2 above. The fault detection filter, here also called as Residual Generator, generates the residual signal using the actuator position measurmenet $u(t)$, actuator position command $u_c(t)$ and several aircraft states $p(t)$. Since the aerodynamic force, which may be considered as the disturbance on the actuator, has a great impact on the actuator dynamics, in the resarach this load is estimated and LPV actuator model is scheduled based on aerodynamic formulation together with the state of the aircraft such as calibrated air speed, center of gravity along x axis and the aircraft altitude.

Another study carried out by Ossmann [10], focused on the detection and identification of the stall load phenomenon which occurs when the sum of all opposing loads acting on the actuator exceeds the available hydraulic pressure times the piston area of the actuator. Main difference between the stall load case and the jamming is that the time of occurance of a stall load is limited whereas jamming is generally considered as a permanent system failure. A very similar LPV model-based FDD technique is also applied in this study except from the last fault identification step before applied by Varga et al. Therefore, a faster fault detection and identification is achieved without computing the variance of the measured position of some number of samples.

CHAPTER 3

METHEMATICAL MODELLING

In this chapter, mathematical modelling of both the EHA and the valve controlled system are performed for the development of the model-based FDD system. In section 3.1, mathematical equations are derived for the physical relations between the components within the load simulator and it follows with the modelling of the EHA system in section 3.2. Details of those EHA and load simulator models together with their design of control systems and the validation of the mathematical models are given in the Ph. D thesis study completed by Çalışkan [50] and the M.Sc. thesis study performed by Akova [51], respectively.

3.1 Mathematical Modelling of the Valve Controlled System

Physical relation between the servo proportional valve and the hydraulic actuator is illustrated in Figure 4-1 for modelling purposes. System dynamics of the load simulator can be basically modelled with a proportional control valve and a single piston actuator. Here, the signal u is the input from controller to the valve.
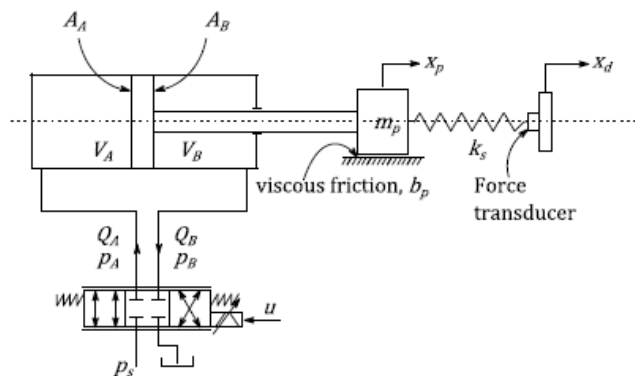
Figure 3.1. Components and their relations within the load simulator system [51]

In Figure 3.1, the position of the piston is denoted by x_p and the total mass of the piston and its attached parts is expressed by m_p. The spring mechanism between the piston of the load simulator and that of the EHA can also be seen in Figure 3.1 and the spring stiffness here is represented by k_s.

3.1.1   Proportional Control Valve Model

The control valve used in the load simulator is a four way, zero-lapped proportional control valve it is responsible for the drive of the control flow. Spool displacement x_v within the valve is proportional to the input voltage u to the valve. Since there is no force feedback spring like in classical two stage servo valves, a closed loop control strategy is needed. To that end an inner loop is utilized for the spool position control and related control electronics are onboard to the valve itself. An LVDT measures the position of the spool and this signal is fed back to the control electronics for the closed loop application.
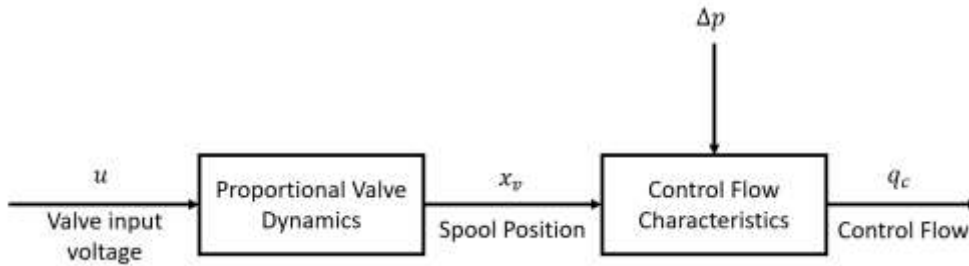
Figure 3.2. Schematic drawing of the load simulator system

The relation between the voltage command $U(s)$ and the valve spool position $X_v(s)$ can be considered as a following first order transfer function as the valve dynamics are much more rapid than dynamics of the piston. Here K_a is the steady state gain and the T_v is the time constant of the proportional valve.

$$G_V(s) = \frac{X_v(s)}{U(s)} = \frac{K_a}{T_v s + 1} \qquad (3.1)$$

The transfer function in the Eqn. 3.1 represents the motion of the spool with respect to the given valve input command. The next step is to generate the equations for the control flow with respect to the reulting spool opening. Depending on the extension ($x_v \geq 0$) and the retraction ($x_v < 0$) cases, control flow equations can be written as follows.

For extension, $x_v \geq 0$;
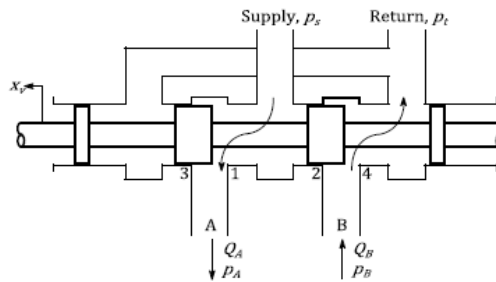
Figure 3.3. Schematic of the valve motion in the extension case

$$q_{cA} = C_d \omega x_v \sqrt{\frac{2}{\rho}(p_s - p_A)} \tag{3.2}$$

$$q_{cB} = C_d \omega x_v \sqrt{\frac{2}{\rho}(p_B - p_r)} \tag{3.3}$$

For retraction, $x_v < 0$
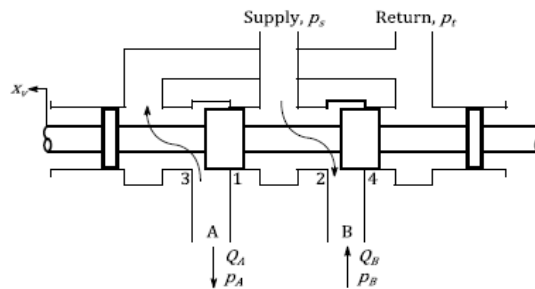
Figure 3.4. Schematic of the valve motion in the retraction case

31

$$q_{cA} = C_d \omega x_v \sqrt{\frac{2}{\rho}(p_A - p_r)} \tag{3.4}$$

$$q_{cB} = C_d \omega x_v \sqrt{\frac{2}{\rho}(p_s - p_B)} \tag{3.5}$$

In general, a combined flow gain can be defined as follows.

$$K_v = K_a C_d \omega \sqrt{\frac{2}{\rho}} \tag{3.6}$$

Inserting the above flow gain into Equations from (3.2) to (3.5), steady state flow equations are obtained as below.

For extension, $x_v \geq 0$;

$$q_{cA} = K_v x_v \sqrt{(p_s - p_A)} \tag{3.7}$$

$$q_{cB} = K_v x_v \sqrt{(p_B - p_r)} \tag{3.8}$$

For retraction, $x_v < 0$

$$q_{cA} = K_v x_v \sqrt{(p_A - p_r)} \tag{3.9}$$

$$q_{cB} = K_v x_v \sqrt{(p_s - p_B)} \tag{3.10}$$

3.1.2   Hydraulic Actuator Model

Once the flow equations are derived, then the mathematical modelling can go with the hydraulic actuator section. If it is assumed that the actuator piston and rod are rigid enough and the compressibility of the oil inside the actuator is not neglected, then the rate of change of volumes or the flow continuity equations can be expressed as follows.

$$q_{cA} = A_A \dot{x}_p + \frac{V_A}{\beta}\frac{dp_A}{dt} \tag{3.11}$$

$$q_{cB} = A_B \dot{x}_p - \frac{V_B}{\beta}\frac{dp_B}{dt} \tag{3.12}$$

Volumes of the actuator chambers according to the piston position can also be expressed as follows.

$$V_A = V_{A_0} + A_A x_p \tag{3.13}$$

$$V_B = V_{B_0} - A_B x_p \tag{3.14}$$

Where V_{A_0} and V_{B_0} are the chamber volumes at the mid stroke, i.e. $x_p = 0$. Since it is a single rod type actuator, load pressure is defined accordingly [52].

$$p_L = p_A - a p_B \tag{3.15}$$

Where a represents the areo ratio between the rod and the piston side. For simplification chamber areas may be expressed in terms of piston area and the area ratio only.

$$a = \frac{A_B}{A_A}, \quad A_p = A_A \tag{3.16}$$

For the steady state operation, compressibility terms in Eqn.s (3.11) and (3.12) vanish and this leads to;

$$q_{cA,ss} = A_P \dot{x}_{p0} \tag{3.17}$$

$$q_{cB,ss} = a A_P \dot{x}_{p0} \tag{3.18}$$

For the extension case where $x_v \geq 0$, combining the Equations (3.7), (3.8) with (3.17), (3.18) the control flow equations can be written as:

$$\frac{q_{cA,ss}}{q_{cB,ss}} = \frac{K_v x_v \sqrt{(p_s - p_{A0})}}{K_v x_v \sqrt{(p_{B0} - p_r)}} = \frac{A_P \dot{x}_{P0}}{a\, A_P \dot{x}_{P0}} \tag{3.19}$$

In order to represent a steady state relation between the chamber pressures, following expression can be derived using the above division. It correlate chamber pressures at the steady state case (3.19).

$$a^2 p_s = a^2 p_{A0} + p_{B0} \tag{3.20}$$

Inserting the load pressure definition will give the below steady state chamber pressures.

$$p_{A0} = \frac{1}{1 + a^3}(p_L + a^3 p_s) \tag{3.21}$$

$$p_{B0} = \frac{-a^2}{1 + a^3}(p_L - p_s) \tag{3.22}$$

Applying the same procedure for the negative valve opening where $x_v < 0$, will give:

$$p_{A0} = \frac{1}{1 + a^3}(p_L + a p_s) \tag{3.23}$$

$$p_{B0} = \frac{1}{1 + a^3}(p_s - a^2 p_L) \tag{3.24}$$

3.1.3 Linearization of the Control Flow Equations

Note that all the equations regarding control valve flow up to now is non-linear. In order to use the flow equation for control design and linear estimation purposes for FDD algorithms, these equations have to be linearized. By expressing it as a Taylor's series expansion about a particular operating point at a specific x_{v0} (valve spool position) and a specific p_o (operating pressure) values with eliminating the higher order terms will give the below relationships.

$$q = \frac{\partial q}{\partial x_v}\bigg|_{p_0,x_{v0}} x_v + \frac{\partial q}{\partial p}\bigg|_{p_0,x_{v0}} p \qquad (3.25)$$

And, the flow coefficients will be:

$$K_q = \frac{\partial q}{\partial x_v}\bigg|_{p_0,x_{v0}} \quad , \quad K_c = -\frac{\partial q}{\partial p}\bigg|_{p_0,x_{v0}} \qquad (3.26)$$

Simply, the flow equations for the control valve can be written as:

$$q_{cA} = K_{qA}\, x_v - K_{cA}\, p_A \qquad (3.27)$$

$$q_{cB} = K_{qB}\, x_v - K_{cB}\, p_B \qquad (3.28)$$

Where the flow gains are

$$K_{qA} = \frac{\partial q}{\partial x_v}\bigg|_{p_{A0},x_{v0}} = \begin{cases} K_v\sqrt{p_s - p_{A0}} & \text{for } x_v \geq 0 \\ K_v\sqrt{p_{A0}} & \text{for } x_v < 0 \end{cases} \qquad (3.29)$$

$$K_{qB} = \frac{\partial q}{\partial x_v}\bigg|_{p_{B0},x_{v0}} = \begin{cases} K_v\sqrt{p_{B0}} & \text{for } x_v \geq 0 \\ K_v\sqrt{p_s - p_{B0}} & \text{for } x_v < 0 \end{cases} \qquad (3.30)$$

And the flow-pressure coefficients are

$$
K_{cA} = \frac{\partial q}{\partial p_A}\bigg|_{p_{A0}, x_{v0}} =
\begin{cases}
\dfrac{K_v x_{v0}}{2\sqrt{p_s - p_{A0}}} & \text{for } x_v \geq 0 \\[4mm]
-\dfrac{K_v x_{v0}}{2\sqrt{p_{A0}}} & \text{for } x_v < 0
\end{cases}
\tag{3.31}
$$

$$
K_{cB} = \frac{\partial q}{\partial p_B}\bigg|_{p_{B0}, x_{v0}} =
\begin{cases}
-\dfrac{K_v x_{v0}}{2\sqrt{p_{B0}}} & \text{for } x_v \geq 0 \\[4mm]
\dfrac{K_v x_{v0}}{2\sqrt{p_s - p_{B0}}} & \text{for } x_v < 0
\end{cases}
\tag{3.32}
$$

In order to obtain the final equations in terms of load pressure, chamber pressure terms p_A & p_B in Eqn.s (3.28) and (3.29) must be eliminated. Using the derived Eqn.s (3.21) and (3.22), control flow equations in can be expressed as follows.

$$
q_{cA} = K_{qA}\, x_v - K_{cA} \frac{1}{1 + a^3} p_L
\tag{3.33}
$$

$$
q_{cB} = K_{qB}\, x_v + K_{cB}\, \frac{a^2}{1 + a^3} p_L
\tag{3.34}
$$

Time rate of change of the load pressure equation in (3.15) will result:

$$
\dot{p}_L = \dot{p}_A - a\dot{p}_B
\tag{3.35}
$$

Together with the above relation, the flow continuity Eqn.s in (3.11) & (3.12) and the control flow equations derived in (3.33) & (3.34), overall flow equations can be simplified further to a single load flow equation as follows.

$$
q_L = K_q x_v - K_c p_L = A\dot{x}_p + C\dot{p}_L
\tag{3.36}
$$

where

$$K_q = K_{qA} + a\frac{V_A}{V_A}K_{qB} \tag{3.37}$$

$$K_c = \frac{1}{1+a^3}K_{cA} - \frac{a^3}{1+a^3}\frac{V_A}{V_A}K_{cB} \tag{3.38}$$

$$C = \frac{V_A}{\beta} \tag{3.39}$$

$$A = \left(1 + a^2\frac{V_A}{V_B}\right)A_p \tag{3.40}$$

and Newton's second law of motion gives the force balance for the piston as:

$$F_L = A_A p_A - A_B p_B - F_f = m_P \ddot{x}_P \tag{3.41}$$

Where the friction force characteristics is simplified as having only a viscous force component.

$$F_f(\dot{x}_P) = b_P \dot{x}_P \tag{3.42}$$

After adding the effect of spring stiffness to the actuator force equation will come up to the following equation.

$$m_P \ddot{x}_P + b_P \dot{x}_P + F_d = A_p p_L \tag{3.43}$$

The ultimate control parameter for the electro-hydraulic load simulator is the force exerted to the elector hydrostatic actuator system F, is considered as the disturbance load acting on the actuator as follows. Since force control is not in the scope of this thesis and previously performed by Akova [51], the only concern here is the effect of disturbance on the system.

$$F = k_s(x_p - x_d) = F_d \tag{3.44}$$

Finally, the servo actuator dynamics between valve spool position command u and the actuator velocity $\dot{x}_p$ can be represented as in the below block diagram.
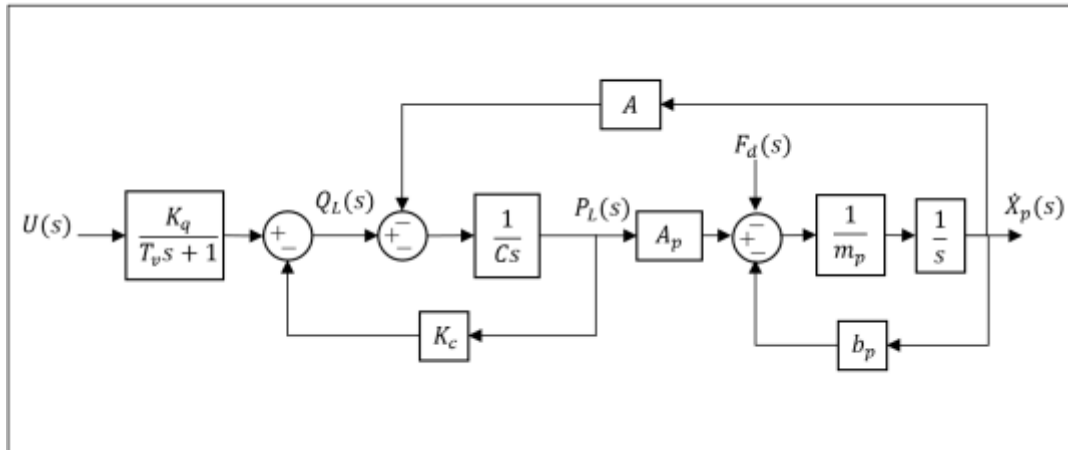
Figure 3.5. Block diagram representation of the open loop load simulator system

The parameters used for the mathematical modelling of the valve-controlled load simulator system are given in Table 3-1 below.

Table 3.1. Parameters of the Load Simulator system [51]

Parameter	Description	Value	Unit
A_A	piston side cross sectional area	2827.4	mm^2
A_B	rod side cross sectional area	2120.6	mm^2
m_p	mass of the piston	3	kg
K_v	flow gain of the proportional valve	22270	$\dfrac{mm^3}{sV\sqrt{MPa}}$
T_v	servo proportional valve time constant	0.002	s
V_{A_0}	initial volume of the piston side chamber	325200	mm^3
V_{B_0}	initial volume of the rod side chamber	243900	mm^3
b_p	viscous damping coefficient	6.5	$N \cdot s/mm$
p_s	supply pressure	12	MPa
β	bulk modulus of the hydraulic oil	1300	MPa

3.1.4   State Space Representation of the Open Loop System

Actuator system dynamics are described by the following three equation.

$$F_d + p_L A_p - b_p \dot{x}_p = m_p \ddot{x}_p \tag{3.45}$$

$$q_L = A\dot{x}_p + C\dot{p}_L = K_q x_v - K_c p_L \tag{3.46}$$

$$\dot{x}_v T_a + x_v = u \tag{3.47}$$

Selecting the state variables as below;

$$x_1 = x_p \; (piston\; position), x_2 = \dot{x}_p(piston\; velocity) \tag{3.48}$$
$$x_3 = p_L(Load\; Pressure), x_4 = x_v \; (Spool\; position) \tag{3.49}$$

Above differential equations can be re-written in state space form as follows;

$$\dot{x}_1 = x_2 \tag{3.50}$$

$$\dot{x}_2 = -\frac{b_p}{m_p}x_2 + \frac{A_p}{m_p}x_3 - \frac{1}{m_p}F_d \tag{3.51}$$

$$\dot{x}_3 = -\frac{K_c}{C}x_3 - \frac{A}{C}x_2 + \frac{K_q}{C}x_4 \tag{3.52}$$

$$\dot{x}_4 = -\frac{1}{T_a}x_4 + \frac{1}{T_a}u \tag{3.53}$$

In Matrix form, the equations become;

$$
\begin{bmatrix} \dot{x}_1 \\ \dot{x}_2 \\ \dot{x}_3 \\ \dot{x}_4 \end{bmatrix} = \begin{bmatrix} 0 & 1 & 0 & 0 \\ 0 & -\dfrac{b_p}{m_p} & \dfrac{A_p}{m_p} & 0 \\ 0 & -\dfrac{A}{C} & -\dfrac{K_c}{C} & \dfrac{K_q}{C} \\ 0 & 0 & 0 & -\dfrac{1}{T_a} \end{bmatrix} \begin{bmatrix} x_1 \\ x_2 \\ x_3 \\ x_4 \end{bmatrix} + \begin{bmatrix} 0 & 0 \\ \dfrac{1}{m_p} & 0 \\ 0 & 0 \\ 0 & \dfrac{1}{T_a} \end{bmatrix} \begin{bmatrix} F_d \\ u \end{bmatrix} \tag{3.54}
$$

$$
y = \begin{bmatrix} 1 & 0 & 0 & 0 \end{bmatrix} \begin{bmatrix} x_1 \\ x_2 \\ x_3 \\ x_4 \end{bmatrix} + \begin{bmatrix} 0 & 0 \end{bmatrix} \begin{bmatrix} F_d \\ u \end{bmatrix} \tag{3.55}
$$

3.2   Mathematical Modelling of the EHA System

The EHA system mainly consists of a hydraulic piston, a pump, an AC electric servo motor driving the pump, a shuttle valve and a hydraulic accumulator for differential flow compensation. Physical relations within the EHA system together with the variables used in modelling are illustrated in Figure 3-6 in order to get an insight to complex interactions between the system components. A basic schematic view is also supplied to simplify these relations in Figure 3-7.

In this section, a simplified linear model of the complete EHA system is performed together with the system dynamics regarding the components and the subsystems mentioned above. Besided, a state space representation of the whole system is also presented. A more detailed nonlinear modelling of the system with all the dynamics of its components and a sopishticated control system are successfully completed in the Ph. D. thesis of Çalışkan [53].

There are basically two working regions for the EHA. Depending on the load pressure value, the shuttle valve adjusts its opening and let the flow go into the accumulator and/or the actuator chambers. When the load pressure is low, about 7-8 bar, the shuttle valve is partially opened to either both chambers or only one of the chambers. The spool of the pilot-operated spool of the shuttle valve positions itself naturally. For the other case where the load pressure exceeds these 7-8 bar of differential pressure, then the shuttle valve becomes fully opened to either side. In this configuration, one of the two chambers is connected to the accumulator and thus the accumulator and the connected chamber can be assumed to have the same pressure. The direction of the load determines the opening side of the shuttle valve and which chamber is connected to the accumulator. Within the scope of this thesis study, the EHA is operated in the fully opened shuttle valve configuration. In the test scenario created for the detection of jamming and the validation of the designed observer models, the EHA is operated and the counter loading is adjusted so that the differential load pressure allows the shuttle valve to fully open.
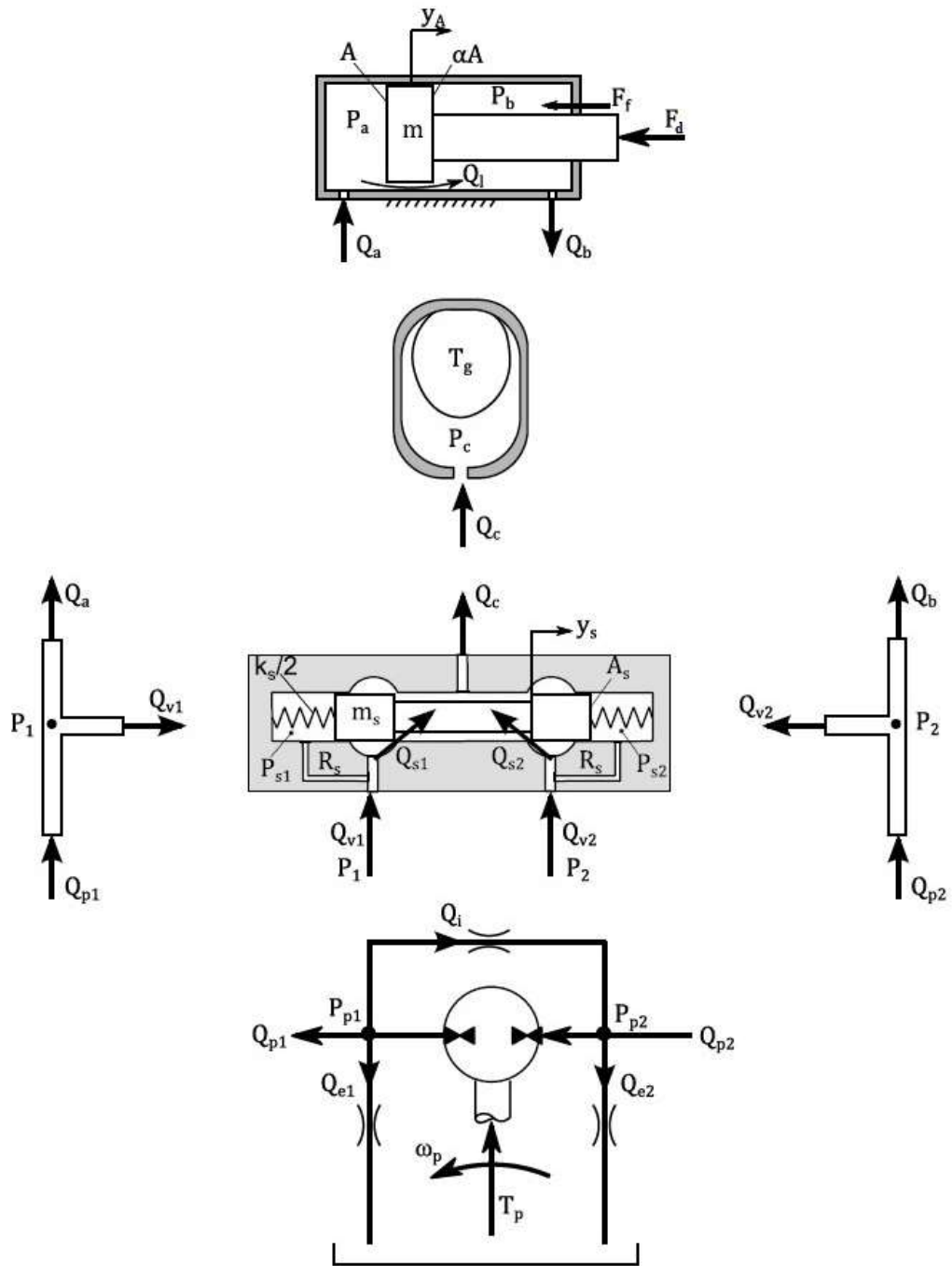
Figure 3.6. Components and their relations within the EHA system [50]
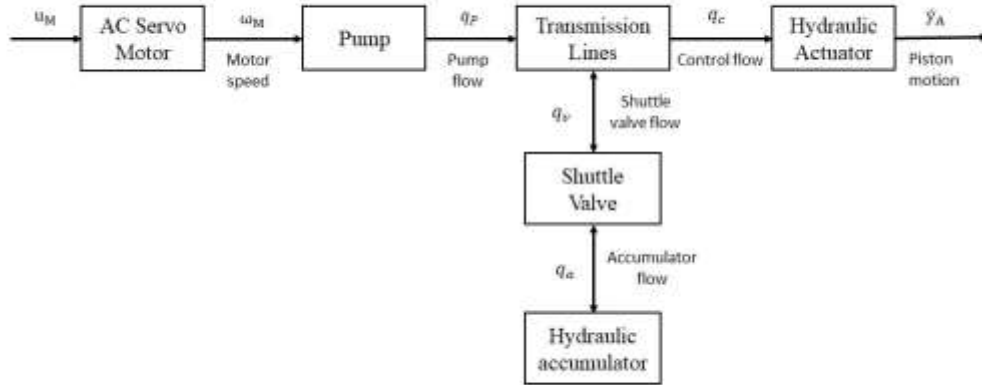
Figure 3.7. Simplified schematic drawing of the EHA system and its components [50]

In order to give an insight into the system dynamics, the electrical, rotational mechanical, hydraulic and the translational mechanical systems illustrated in Figure 3-7 are considered for the open loop plant model. A simplified linear version of the state space representation of the whole system is also derived at the end of this section. In order to develop a simplified mathematical model of complicated system dynamics of the EHA in figure 3.6, the following assumptions need to be referenced.

- The accumulator pressure and temperature responses are considerably slow, with respect to the other components so accumulator dynamics are neglected.

- The electric motor current dynamics very fast and they are neglected too.

- Shuttle valve is assumed to be fully opened for the test scenario described in section 5.2. Therefore, spool dynamics of the shuttle valve is not considered.

- In a fully opened shuttle valve condition, only one hydraulic chamber determines the pressure dynamics since the hydraulic accumulator capacitance together with the hydraulic conductance of the shuttle valve are considerably high. In other words, change in the load pressure will be equal to one of the chamber pressures as $\delta P_L = \delta P_a$ or $\delta P_L = \delta P_b$ depending on the open side of the shuttle valve. [50]
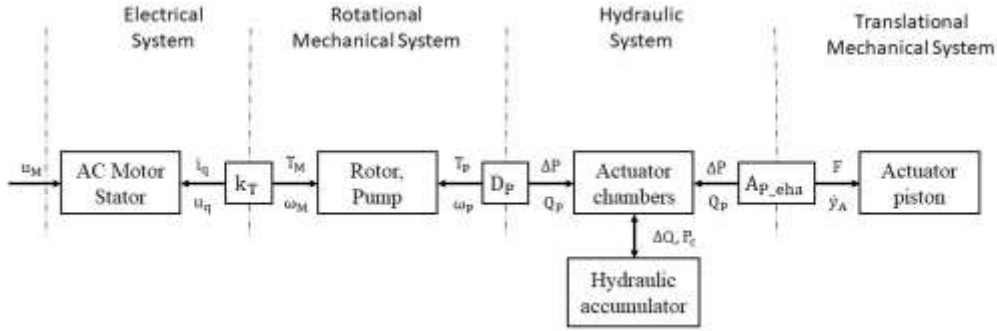
Figure 3.8. Physical subsystems and their relations included in the system dynamics of the EHA

3.2.1 Electrical and Rotational Mechanical System

The electric motor and the hydraulic pump are assumed to be coupled through a rigid coupling. Therefore, the pump inertia together with the frictional losses is lumped into electric motor dynamics. The resulting torque continuity equation on the motor shaft is written as follows

$$k_T i_q = (J'_M)\dot{\omega}_M + (b'_M)\omega_M + D_p(P_a - P_b) \cdot 10^{-3} \tag{3.56}$$

where, $J'_M = J_M + J_P$ and $b'_M = b_M + b_{p_{eha}}$ are the total effective inertia and friction coefficients, respectively. Note that for unit conversion, the last component in the above Equation 3.56, is multiplied by 10^{-3} as the $D_p \Delta P$ multiplication produces torque in Nmm where the unit for the pressures $(P_{a,b})$ is $MPa \; or \; simply \; N/mm^2$.

$k_T = $ electric motor torque constant in Nm/A

$\omega_M = $ angular speed of the electric motor and the pump in rad/s

$J_M = $ inertia of the rotor of the electric motor in $kg \cdot m^2$

$J_P = $ inertia of the hydraulic pump rotor in $kg \cdot m^2$

$D_p = $ pump displacement in mm^3/rad

$b_{p_{eha}} = $ viscous friction coefficient of the pump in Nms/rad

3.2.2 Hydraulic and Translational Mechanical System

Similar to the load simulator, the equation of motion for the actuator is written as follows.

$$A_{P_{eha}}(P_a - a_{eha}P_b) = m_{eha}\ddot{y}_A + F_D + F_{f_{eha}} \tag{3.57}$$

where,

$$y_A = \qquad \text{actuator piston position in } mm$$

$$P_a, P_b = \qquad \text{piston and ord side chamber pressures in } MPa$$

$$A_{P_{eha}} = \qquad \text{piston side cross sectional area in } mm^2$$

$$m_{eha} = \qquad \text{mass of the piston and rod of the actuator in } kg$$

$$a_{eha} = \qquad \text{pressure area ratio of the EHA hydraulic cylinder}$$

$$F_D = \qquad \text{disturbance force acting on the actuator in } N$$

$$H = \qquad \text{leakage flow coefficient of the pump } mm^3/s \cdot MPa$$

$$b_{eha} = \qquad \text{viscous friction coefficient of the actuator in } Ns/mm$$

The friction force here is modelled as having only the viscous friction compnent but a more detailed model such as the Stribeck model might also be preferred for high-fidelity simulation analysis.

$$F_{f_{eha}} = b_{eha}\dot{y}_A \tag{3.58}$$

The flow continuity equation for the piston and the rod side chambers can be written with considering the leakage flow proportional to the load pressure as follows.

$$C_a\dot{P}_L = D_p\omega_M - A\dot{y}_A - HP_L \tag{3.59}$$

$$C_b\dot{P}_L = -D_p\omega_M + a_{eha}A\dot{y}_A - HP_L \tag{3.60}$$

3.2.3 State Space Representation of the Pump Controlled Open Loop EHA System

Actuator system dynamics are described by the Equations presented from (3.56) to (3.60).

Selecting the state variables as below;

$$x_1 = y_A \; (piston \; position), \tag{3.61}$$

$$x_2 = \dot{y}_A (piston \; velocity), \tag{3.62}$$

$$x_3 = P_L = (P_a - a_{eha}P_b)(load \; pressure), \tag{3.63}$$

$$x_4 = \omega_M (electric \; motor \; speed) \tag{3.64}$$

In Matrix form, the open loop system becomes;

$$[\dot{x}] = [\mathbf{A_{eha}}] \, [x] + [\mathbf{B_{eha}}][u] \tag{3.65}$$

where, the system matrix $\mathbf{A_{eha}}$ and the input matrix $\mathbf{B_{eha}}$ and with u_M the motor torque & F_d disturbance load taken as input u as follows.

$$[u] = \begin{bmatrix} u_M \\ F_d \end{bmatrix} \tag{3.66}$$

$$\mathbf{A_{eha}} = \begin{bmatrix} 0 & 1 & 0 & 0 \\ 0 & -\dfrac{b_{p_{eha}}}{m_{eha}} & \dfrac{A_{P_{eha}}}{m_{eha}} & 0 \\ 0 & -\dfrac{A_{P_{eha}}}{C} & -\dfrac{H}{C} & \dfrac{D_p}{C} \\ 0 & 0 & -\dfrac{D_p}{J'_M} & -\dfrac{b'_M}{J'_M} \end{bmatrix} \tag{3.67}$$

$$\mathbf{B_{eha}} = \begin{bmatrix} 0 & -\dfrac{1}{m} & 0 & 0 \\ 0 & 0 & 0 & \dfrac{1}{J'_M} \end{bmatrix}^T \tag{3.68}$$

46

The parameters used for the mathematical modelling of the electrical and rotational mechanical subsystems are given in Table 3-2 below.

Table 3.2. Parameters of the electrical and rotational mechanical subsystems [50]

Parameter	Description	Value	Unit
k_T	torque constant	1.52	Nm/A
J_M	rotor inertia of the electric motor	$27.3 \cdot 10^{-4}$	$kg \cdot m^2$
J_P	hydraulic pump rotor inertia	$1.93 \cdot 10^{-4}$	$kg \cdot m^2$
D_p	pump displacement	8	cm^3/rad
b_M	motor viscous friction coefficient	$7 \cdot 10^{-3}$	Nms/rad
$b_{p_{eha}}$	pump viscous friction coefficient	0.035	Nms/rad

The parameters used for the mathematical modelling of the hydraulic and translational mechanical subsystems are given in Table 3-3 below.

Table 3.3. Parameters of the hydraulic and translational mechanical subsystems [50]

Parameter	Description	Value	Unit
A_{p_eha}	piston side cross sectional area	2827.4	mm^2
a_{eha}	area ratio	0.75	–
m_{eha}	mass of the piston and the rod	9.6	kg
b_{eha}	viscous friction coefficient of the actuator	6.3	Ns/mm
C_a	piston side hydraulic chamber capacitance	302.5	$mm^3/s \cdot MPa$
C_b	rod side hydraulic chamber capacitance	302.5	$mm^3/s \cdot MPa$

Capacitance values of C_a and C_b are assumed to be constant to a value of C that is calculated at a stroke where the two chamber volumes are equal.

CHAPTER 4

EXPERIMENTAL TEST SETUP

4.1   Overview of the Hydraulic Test Setup

A schematic drawing of the hydraulic test bench which is designed and constructed by Çalışkan [50] and Akova [51] is shown in Figure 4-1. It consists of two distinct electro hydraulic actuation systems. The one on the left is an electro hydrostatic actuation system controlled by a hydraulic pump whereas the one on the right is a conventional hydraulic actuated load simulator system controlled by a servo proportional valve. Two system are connected to each other via a spring mechanism and a force sensor. Closed loop force control of the load simulator is accomplished using the output of this sensor. Besides the force transducer between the two actuator, there are four more sensors in the load simulator. Two position transducers provide the measurement of the piston position which is used in a disturbance feedforward controller.

EHA is a closed loop position controlled system where the position tracking is achieved through a closed loop feedback and feedforward control. An AC servo motor is placed to drive the hydraulic pump in the system. One of the most significant novelty in the system is that unequal flowrates for the retraction and extension sides are compansated using a hydraulic accumulator and a 3-position 3-way shuttle valve. Together with the position of the piston of the EHA, speed of the motor is controlled in closed loop manner. Speed and torque of the servo motor, pressures in the two piston chambers and in the accumulator is measured simultenously together with the actuator position.
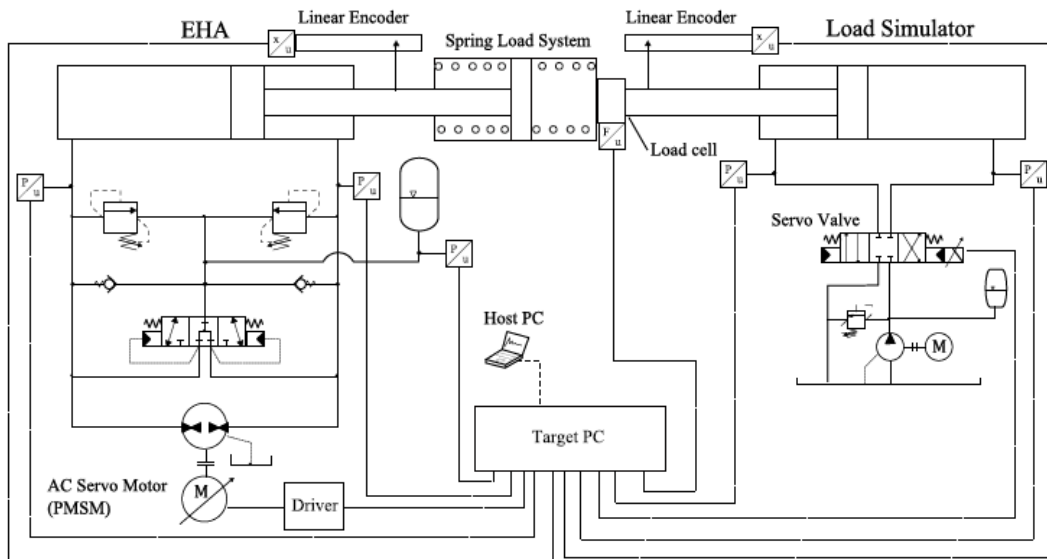
Figure 4.1. *Schematic drawing of the hydraulic test bench [50]*

4.2   Components of the EHA System

Electro hydraulic actuation (EHA) system includes the following components;

- A Siemens 1FK7083 series 3-phase permanent magnet AC synchronous motor,
- A Bucher Hydraulics QXM22 series constant displacement pump (with a displacement of 8 cm^3/rev),
- A Hanchen single rod actuator with a 200 mm total stroke, 60/30 mm of piston and rod diameters, respectively,
- A 5 l accumulator with a 25 bar gas charge pressure. At the beginning of each test, the hydraulic accumulator is charged up to a desired pressure level.

50

- A hydraulic monifold circuit including a shuttle valve, two pressure relief valves, and two check valves. All of the valves are of cartridge type.

- Three TRAFAG 8472 pressure transducers with a rated pressure of 250 bar and 0-10 V of analog output signal,

- A Novotechnik position sensor inside the EHA with an analog output signal of 0-10 V,

- An ATEK linear encoder with a grid spacing of 20 μm and a resolution of 5 μm at 4X decoding.

The hydraulic ports of the single rod actuator and those of pump are connected together with the accumulator and return tank lines as shown in the below figure 4-2.
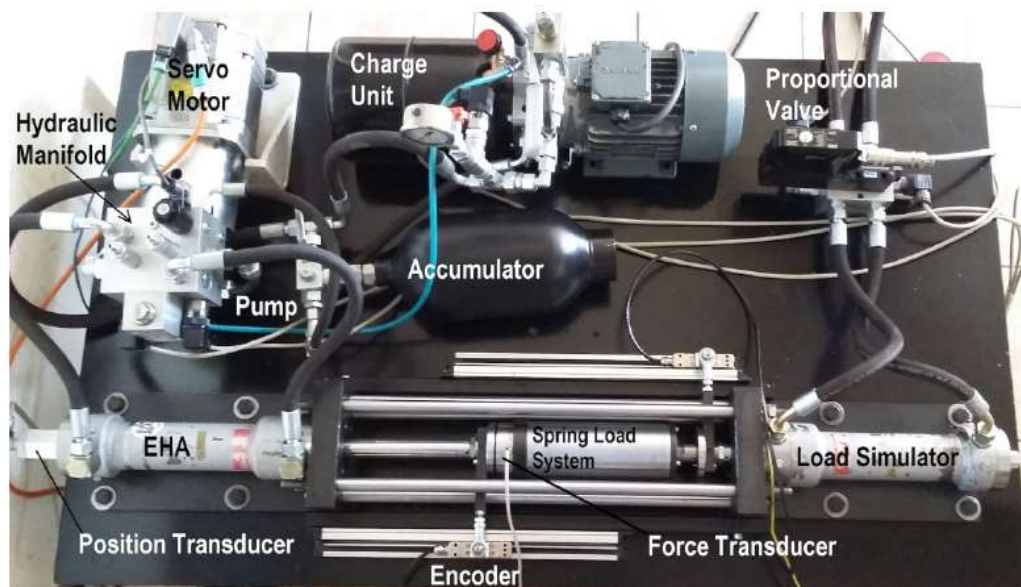
Figure 4.2. *A photo showing the experimental test rig [50]*

4.3   Components of the Load Simulator

Load simulator system consists of the following components;

- A Parker Hannifin DFplus Servo proportional control valve,
- A Hydraulic Power Pack including;
  - A Gamak cage 3-phase induction motor with a power rating of 11 kW,
  - A Bucher Hydraulics QXM31-032 series constant displacement pump (with a displacement of 31.2 cm^3/rev,
  - A Bucher hydraulics DVPA-1-10-SM pressure relief valve
  - A 1.5 l SAIP bladder type hydraulic accumulator with a maximum operating pressure of 350 bar
  - FIREFLEX DIN EN 853 SAE1000R2 AT 1/2″ hydraulic hoses as transmission line elements
  - PO Hydro Oil HD 46 Series hydraulic oil with a cleanliness level of NAS 7 (according to NAS 1638)
  - Hydraulic Reservoir of 120 $liters$
  - An EATON HP 61 10VG series pressure line, stainless steel wire mesh filter

- A Burster Model 8524 tension and compression force transducer with a maximum measurable load of 20kN and a natural frequency of 4 kHz [54]. Output signal of the transducer, which is in the range of 7.5 mV, is amplified with an amplifier having a bandwidth of 1 kHz.
- Two TRAFAG 8472 pressure transducers with a rated pressure of 250 bar and 0-10 V of analog output signal. Chamber pressures are measured using these sensors.
- A Novotechnik position sensor with an analog output signal of 0-10 V,
- An ATEK linear encoder with a grid spacing of 20 μm and a resolution of 5 μm at 4X decoding.
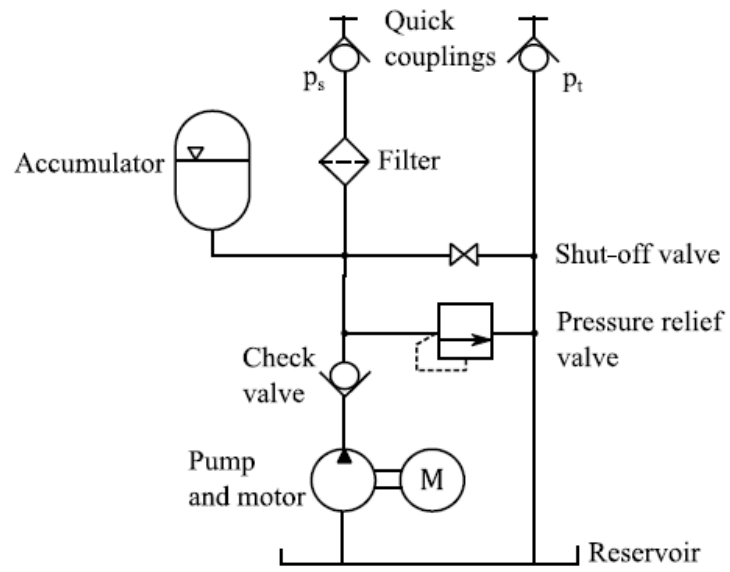
Figure 4.3. *Hydraulic Power Unit of the Load Simulator [51]*

4.4   Control System Hardware Components

Both the EHA and the load simulator system is controlled and monitored using a Speedgoat modular real-time target machine with a variety of analog and digital IO (Input-Output) modules. The target machine is utilized as the DAQ (data acquisition) and system and the control computer. This system is called as 'target PC' in figure 4-1. MathWorks® xPC Target™ real time kernel is running on the target PC, and it accomplishes the real time control of the two actuation system. The target PC has an Intel Core 2 Duo 2.26 GHz processor and a memory of 2048 MB DDR3 RAM.

Control and FDD algorithms are designed and developed in a personel computer, which is called as 'host PC' in figure 4-1. The MATLAB® R2011a software, together with Simulink®, Real-Time Workshop®, xPC Target™ and necessary SpeedGoat IO drives are installed on the host PC. The designed controller and FDD algorithms in MATLAB®/Simulink® environment is compiled by a VisualC compiler in the host PC and downloaded to the real-time target machine via an Ethernet communication. The solver of the control algorithm is selected as 4th order Runge-Kutta (ode4) with 1 ms fixed step.

Additionally, the SpeedGoat target machine is equipped with IO105 analog input, IO111 analog output, IO401 TTL/SSI encoder and IO203 digital input/output modules. The IO105 module comprises 32 differential analog input channels of 16-bit resolution. This module acquires the voltage outputs of the pressure, position and force transducers. The IO111 module comprises 16 analog output channels and drives the servo proportional valve of the load simulator. The IO401 module acquires the output of the encoders.

Servo motor speed and torque, pressures of the two chambers and the accumulator are measured for EHA together with the actuator position with a 1 kHz sampling frequency. The pressure transducers are installed on the hydraulic manifold in the EHA system. Speed and torque control of the servo motor is

performed via a Siemens CU320 control unit. An analog communication interface is established between the real time Target Pc and CU320 control unit using Siemens TM31 terminal module. There is also a CAN-bus communication between the CU320 and the target PC. A supervisory controller manages this interface.

Figure 4.4. *Speedgoat Real Time Target Machine [51]*

CHAPTER 5

IMPLEMENTATION OF THE MODEL BASED FDD TECHNIQUE

In this chapter, a structure for the detection and diagnosis of the faults is developed. In section 5.1, a disturbance observer based FDD method is proposed for the detection and identification of different jamming cases. Then, a fault identification step is introduced where the diagnosis of jamming condition is achieved. At the end of the chapter, experimental data acquired using the proposed FDD method is given.

5.1   Proposed Method

In this section, an observer based method is proposed for the detection of jamming cases in the electro hydraulic actuation system. As the residual generation method, observer design is commonly used for FDD purposes. Opposing load on an actuator could be considered as the main source of that actuator's being unable to generate further control movement permanently or temporarily. Therefore, it is vital to observe the disturbance load which the control actuator is exposed in order to detect jamming conditions. By doing so, a state observer is first designed then its output is connected to a disturbance observer which gives the desired load estimation.

At this point, estimated disturbance is used to extract information about the fault. For the case where jamming occurs at small actuator inputs, changes in the load is analyzed. In order to distinguish whether the actuator is jammed, observed force is used. If the time rate of the disturbance force exceeds a predefined threshold, then the fault detection process is triggered for this kind of failure case. Diagnosis of the fault is ensured by checking one more indicator by analyzing the tracking error between the reference and the measured position of the actuator. Basically, moving

average of the position feedback is calculated and compared with a defined threshold value in the fault identification.

5.1.1   State Observer Design for the Load Simulator System

A Luenberger observer is to be designed initially for the valve controlled load simulator system assuming it as a linear time invariant system described by the state space equations derived in section 3.1.4. Using state space form in (3.56) and (3.57) together with the system parameters given in section 3.1.3, following matrix equations can be obtained.

$$[\dot{x}] = \begin{bmatrix} 0 & 1 & 0 & 0 \\ 0 & -2.168 & 942.47 & 0 \\ 0 & -19.78 & 0 & 452.66 \\ 0 & 0 & 0 & -500 \end{bmatrix} [x]$$
$$+ \begin{bmatrix} 0 & 0 \\ -0.333 & 0 \\ 0 & 0 \\ 0 & 500 \end{bmatrix} [F_d \ u]$$

$$(5.15)$$

$$y = \begin{bmatrix} 1 & 0 & 0 & 0 \end{bmatrix} [x] + \begin{bmatrix} 0 & 0 \end{bmatrix} \begin{bmatrix} F_d \\ u \end{bmatrix} \qquad (5.2)$$

where x stands for the system states, u for the input(s) and y is the measurement and system matrices $\mathbf{A_{lsin}}$ and $\mathbf{B_{lsim}}$ are defined for the load simulator system as below.

$$\mathbf{A_{lsim}} = \begin{bmatrix} 0 & 1 & 0 & 0 \\ 0 & -2.168 & 942.47 & 0 \\ 0 & -19.78 & 0 & 452.66 \\ 0 & 0 & 0 & -500 \end{bmatrix} \qquad (5.3)$$

$$B_{lsim} = \begin{bmatrix} 0 & 0 \\ -0.333 & 0 \\ 0 & 0 \\ 0 & 500 \end{bmatrix} \qquad (5.4)$$

Open loop poles of the valve controlled system is calculated as:

$$p_{o\_lsim} = \begin{matrix} 0 + 0i \\ -1.08 + 136.54i \\ -1.08 - 136.54i \\ -500 + 0i \end{matrix} \qquad (5.5)$$

Fourth pole of the open loop system corresponds to the dynamics of the servo proportional valve and a build-in control electronics is installed within the valve manifold. Thus, a closed loop control already exists for the valve dynamics and its root can be assumed as stable. The first pole comes from the position response of the actuator and in the observer structure the position feedback is used and it helps the observer to estimate the position response. Therefore, these two poles may not need to be placed much further to the negative real side. Whereas there isn't any available feedbacks for the velocity (second pole) and the load pressure (third pole) dynamics and their real parts are too close to the origin. Therefore, real parts of the second and the third observer poles should be placed to further left. Accordingly, the desired poles for the Observer is chosen as:

$$p_{c\_lsim} = \begin{matrix} -5 + 0i \\ -30 + 140i \\ -30 - 140i \\ -500 + 0i \end{matrix} \qquad (5.6)$$

Finally, the gain matrix of the Observer can be found using 'place' command in Matlab as below:

$$L_{lsim} = \begin{bmatrix} -0.0179 & 1.4720 \cdot 10^{-5} \\ -0.0034 & 2.5707 \cdot 10^{-6} \\ -0.0244 & 5.9680 \cdot 10^{-7} \\ -0.0035 & -1.0014 \cdot 10^{-6} \end{bmatrix} \qquad (5.7)$$

The MATLAB®/Simulink® model of the designed Luenberger Observer, implementing Eq.s from (5.3) to (5.4), is given in Figure 5.1. The model accepts the

proportional valve input command u, measured position signal y and the estimated disturbance from the disturbance observer designed in section 5.1.3. As mentioned before, state and disturbance observers works simultenously. The desired output of the state observer is the piston velocity $\dot{x}_p$ and using this signal, disturbance observer estimates the load acting on the piston. This estimated disturbance signal is simultenously used in the state observer.
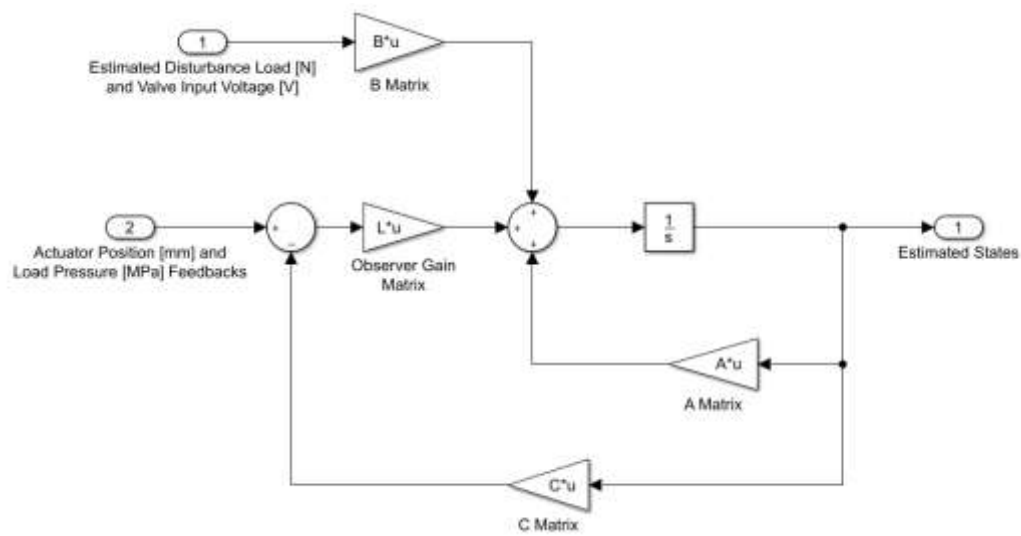
Figure 5.1. State observer model for velocity estimation

5.1.2 State Observer Design for the EHA System

Another Luenberger observer is to be designed for the pump controlled system assuming it as a linear time invariant system described by the state space equations derived in section 3.2.3. Using state space form in (3.72) and (3.73) together with the system parameters given in section 3.2.3, following matrix equations can be obtained.

$$
[\dot{X}] = \begin{bmatrix} 0 & 1 & 0 & 0 \\ 0 & -673.07 & 302072.645 & 0 \\ 0 & -9.35 & 0 & 0.4408 \\ 0 & 0 & -5369.86 & -2.39 \end{bmatrix} [X]
$$
$$
+ \begin{bmatrix} 0 & 0 \\ -0.107 & 0 \\ 0 & 0 \\ 0 & 342.465 \end{bmatrix} [F_d \ u]
$$
(5.8)

$$
y = \begin{bmatrix} 1 & 0 & 0 & 0 \\ 0 & 0 & 0 & 1 \end{bmatrix} [X] + \begin{bmatrix} 0 & 0 \end{bmatrix} \begin{bmatrix} F_d \\ u \end{bmatrix}
$$
(5.9)

where x stands for the system states, u for the input(s) and y is the measurement and system matrices A and B are defined for the EHA system as below.

$$
A_{EHA} = \begin{bmatrix} 0 & 1 & 0 & 0 \\ 0 & -673.07 & 302072.645 & 0 \\ 0 & -9.35 & 0 & 0.4408 \\ 0 & 0 & -5369.86 & -2.39 \end{bmatrix}
$$
(5.10)

$$
B_{EHA} = \begin{bmatrix} 0 & 0 \\ -0.107 & 0 \\ 0 & 0 \\ 0 & 342.465 \end{bmatrix}
$$
(5.11)

Open loop poles of the EHA system is calculated as:

$$
p_{o\_EHA} = \begin{matrix} 0 + 0i \\ -336.26 + 1646.9i \\ -336.26 - 1646.9i \\ -2.9594 \end{matrix}
$$
(5.12)

Fourth pole of the open loop system corresponds to the servo motor speed dynamics. Servo motor dynamics are already controlled with a PI controller and in the Observer motor speed feedback is used as well. The first pole comes from the position response of the actuator and in the observer structure the position feedback is used and it helps the observer to estimate the position response like in the load simulator. Therefore, these two poles may not need to be placed much further to the negative real side. Whereas there isn't any available feedbacks for the velocity (second pole) and the load pressure (third pole) dynamics and fast estimation response is required for this states as they are used in the disturbance observer. Therefore, real parts of the second and the third observer poles should be placed to further left. Accordingly, the desired poles for the Observer is chosen as:

$$p_{c\_EHA} = \begin{matrix} -0.1 + 0i \\ -400 + 1646.9i \\ -400 - 1646.9i \\ -3.0 + 0i \end{matrix} \qquad (5.13)$$

Finally, the gain matrix of the Observer can be found using 'place' command in Matlab as below:

$$L_{EHA} = \begin{bmatrix} 30 & 0.5 \\ 2.25e + 05 & 125 \\ 1.2e + 03 & 0.1 \\ 3.2e + 02 & 20 \end{bmatrix} \qquad (5.14)$$

The MATLAB®/Simulink® model of the designed Luenberger Observer, implementing Equations from (5.10) to (5.11), is given in Figure 5.3. The model accepts the servo motor torque command u_M, measured position signal y_A and the estimated disturbance from the disturbance observer designed in the next section 5.1.3. At the end, state and disturbance observers works simultenously for the EHA. The desired output of the state observer is the piston velocity $\dot{y}_p$, the load pressure P_L and using these signals, disturbance observer estimates the load acting on the piston. This estimated disturbance signal is simultenously used in the state observer.
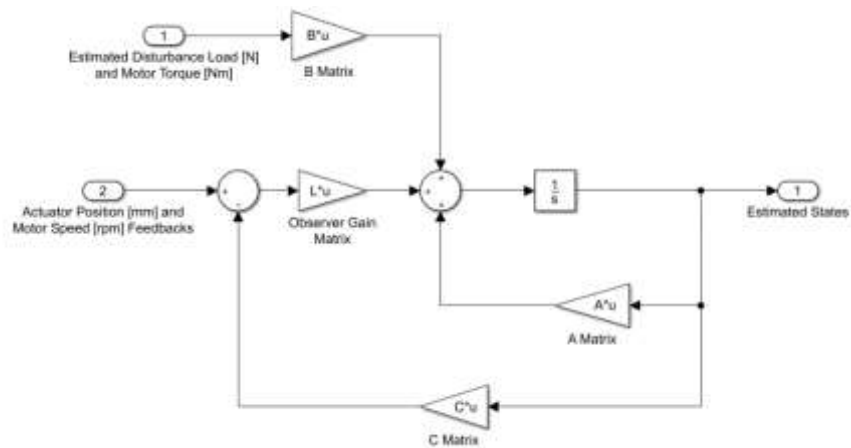
Figure 5.2. State observer model for velocity and pressure estimation

Eventual aim of the designed state observer is to supply unknown state information to a disturbance observer. However, the disturbance load acting on the actuator (load simulator or EHA) is an unknown too. Therefore, a structure including two observers working simultanously is developed for both state and disturbance estimations. Two observer work together with one estimating the state variables while the other estimating the disturbance. Designed observer structure for the EHA system is shown in the following Fig. 5.3. The only difference for the Observer structure of the load simulator is that load pressure is not estimated in its state observer, rather the available pressure feedbacks are used. The state observer in the following structure (Fig. 5.3) uses the equations derived in Section 3.2 before while the equations for the disturbance observer is to be defined later in the following Section 5.1.3.
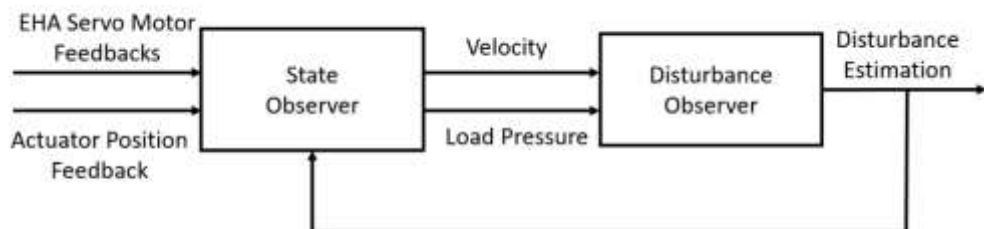
Figure 5.3. Observer Structure of State and Disturbance Estimations for the EHA

5.1.3   Disturbance Observer Design

Since the dynamics are the same for both piston (EHA and load simulator), the force equilibrium on the either can be re-written as below.

$$F_d = -m_p\ddot{x}_p + p_L A_p - b_p \dot{x}_p \qquad (5.15)$$

Which may also be expressed in terms of state variables as;

$$F_d = -m_p \dot{x}_2 + A_p x_3 - b_p x_2 \qquad (5.16)$$

Estimation of the disturbance load is defined as $\hat{d}$ and the dynamics of this estimation with an observer gain L_0 can be designed as follows. [55]

$$\dot{\hat{d}} = -L_1(m_p \dot{x}_2 - A_p x_3 + b_p x_2 + \hat{d}) \qquad (5.17)$$

In the above equation, derivative of the disturbance uses the derivative of the state x_2 which will probably cause a noise amplification by the high observer gain L_1. Thus, it might not be practical to go on with the implementation of this method. In order to avoid this problem, an auxiliary variable ζ can be preferred, as represented by [56].

$$\zeta = -\hat{d} - L_1 m_p x_2 \qquad (5.1816)$$

and the dynamics of this variable is

$$\dot{\zeta} = -L_1(\zeta + L_1 m_p x_2) + L_1(b_p x_2 - A_p x_3) \qquad (5.19)$$

By using load pressure and piston position information and the velocity estimation, is accepted in the disturbance observer model. Therefore, having the load pressure and the velocity state information, the observer can be examined. The MATLAB®/Simulink® models of the designed disturbance observers for

the load simulator and the EHA systems, implementing Equations (5.18) and (5.19), is given in Figures 5.4 and 5.5.
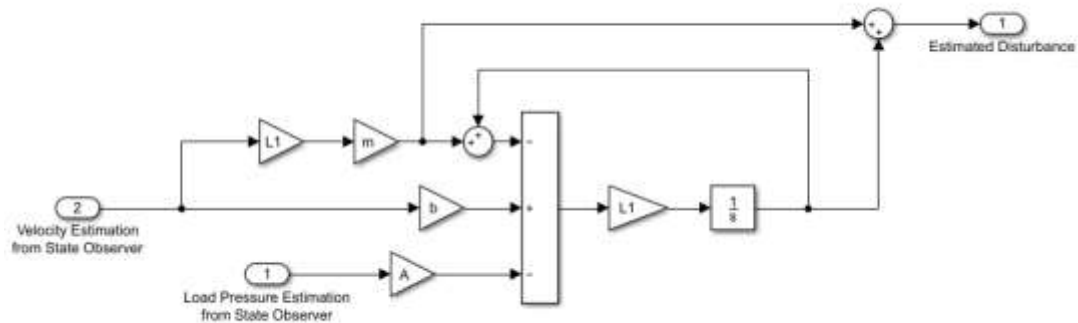
Figure 5.4. Disturbance Observer model for the Load Simulator
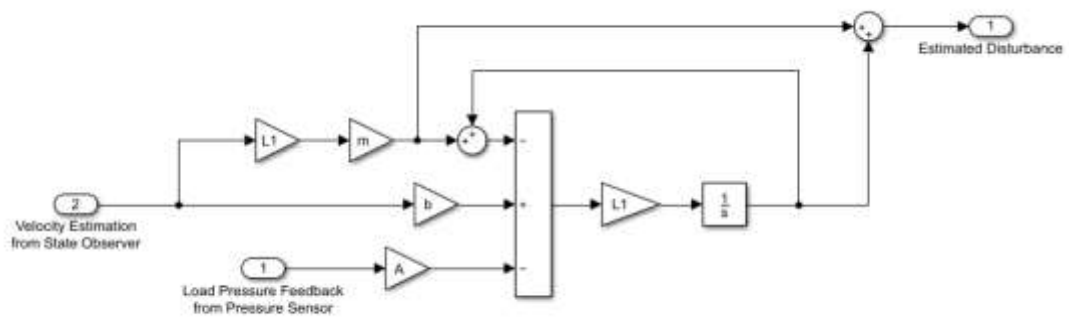
Figure 5.5. Disturbance Observer model for the EHA

At this point, its worth noting that the direct usage of the chamber pressure information significantly increases the fidelity of the disturbance observer model. Yet, pressure feedback might not always be available for an aircraft fly-by-wire actuator [5]. Even if a pressure sensor is implemented to an actuator, it might be trivial to estimate the disturbance load using this pressure information. Rather, it would be more logical to directly use this pressure information if it is available. Considering the case for this thesis study with the absence of the pressure information, the state estimation described in section 5.1.2 could still be decent for disturbance estimation for an electro-hydrostatic type actuator.

65

State and disturbance estimations of the observer models are verified by using the experimental test results and the measurements of the force transducer as this sensor is directly related with the disturbance load acting on the piston. Note that a comparison is made for the disturbance estimations with and without using pressure information. The same disturbance observer model is valid for both actuators in the test setup and the pressure information in any actuator's chambers could be preferred. The pressure estimation is performed through the state observer detailed in section 5.1.2 for the EHA and thus this estimation is used in the disturbance observer for this actuator. For comparison, pressure feedbacks from the chambers of the load simulator is used for another estimation and state estimation for the load simulator is used together with this pressure feedback for this system in the designed disturbance observer.

A set of test data is used where the reference position of the EHA and the force of the load simulator is controlled as shown in the following Figures 5.6 and 5.7.
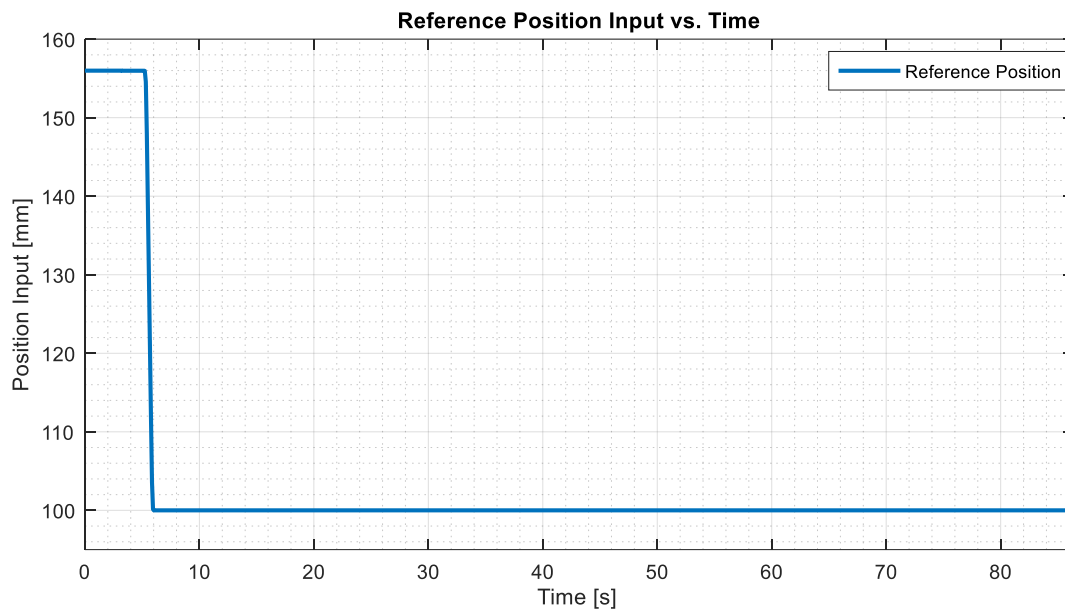
Figure 5.6. Reference Position Input to the EHA

66
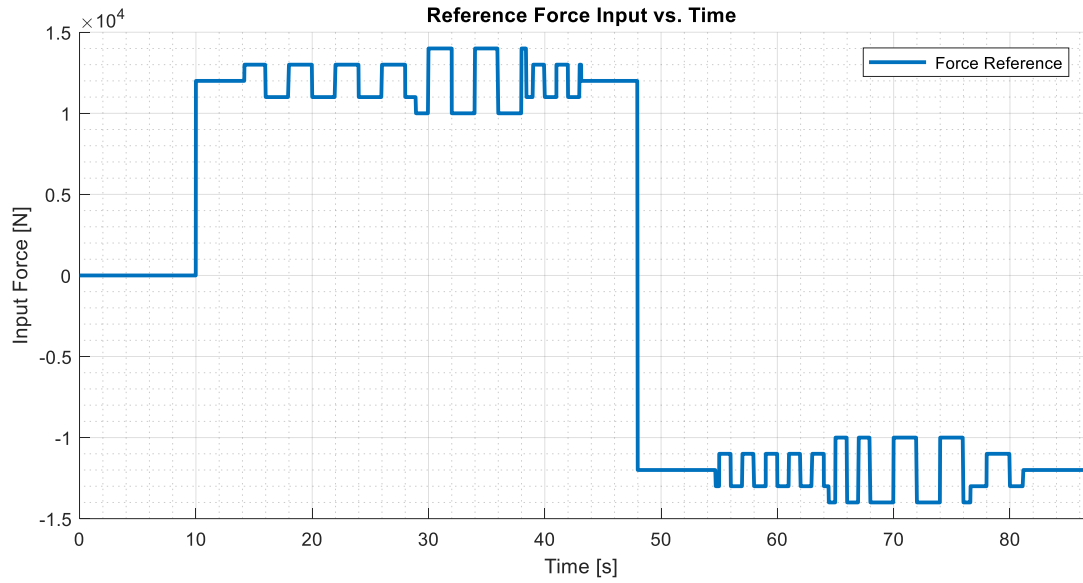
Figure 5.7. Reference Force Input to the Load Simulator

In the closed loop tests, position of the EHA is kept constant at 100mm after t =6seconds. (see Fig. 5.6). Force signal with varying its amplitude and frequency values is generated as the reference input for the the load simulator in order to evaluate the estimation performance of the disturbance and the state observers better. Both positive and negative disturbance loads of 14kN are applied and its amplitude its changed between 1-2 kN interval while the frequency values are adjusted between 0.5-2 Hz (see Fig. 5.7).   Data acquisition is achieved with two system operating simultaneously. Velocity estimation via a dedicated Kalman Filter performed by Çalışkan [50] is also given together with the velocity estimation output of the state observer designed in section 5.1.2. Some operating regions in the following test results are zoomed in to show the estimation performance of the observers. Especially, the region where the disturbance load is varied is tried to be focused on. Comparison of the estimated states and disturbances with measured feedbacks, via the transducers in the setup, is given in the following figures.

67
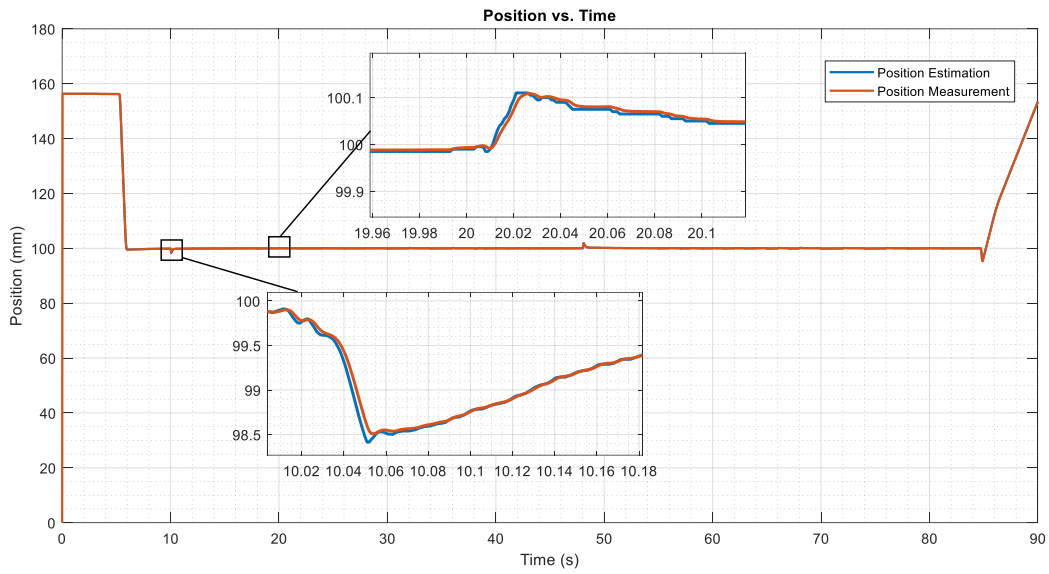
Figure 5.8. Measured Position Response and the Position Estimation of the EHA
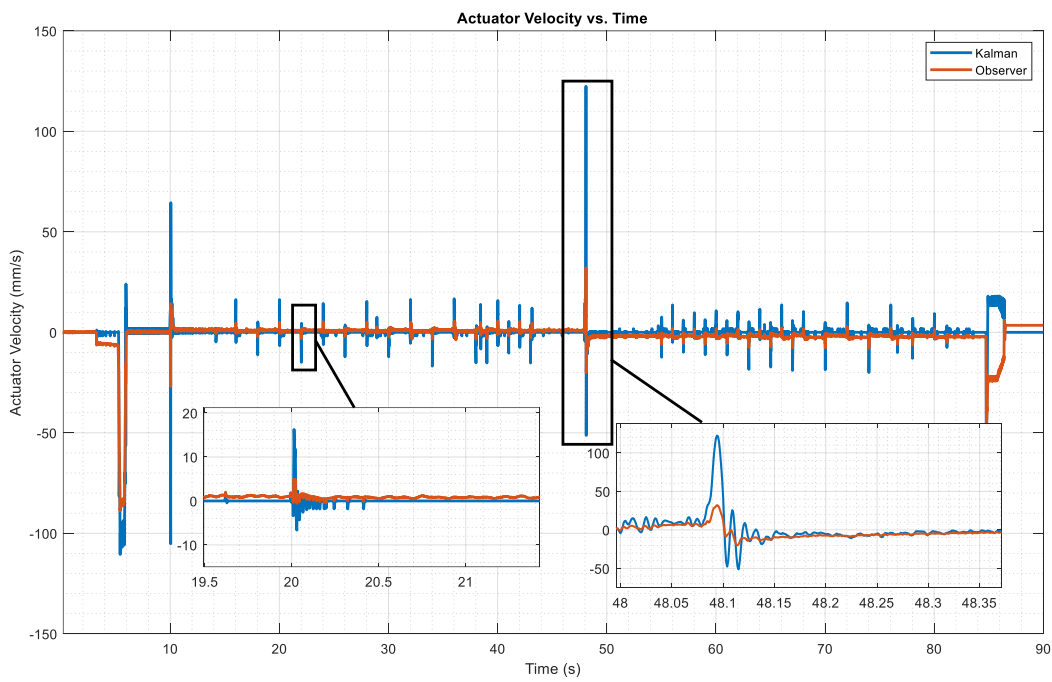
Figure 5.9. Kalman Filtered Velocity Estimation vs. Observer based Velocity Estimation of the EHA

68

The state observer gives accurate results, with less than 0.1 % of error, for the estimation of position (see Fig. 5.8). This is in fact an expected situation since feedback is available for this state variable.

Velocity estimation plot (see Fig. 5.9) shows some differences between the estimation by state observer and the estimation by a Kalman Filter [50]. This can be explained by the fact that the estimation, performed by Çalışkan, uses a Kinematic Kalman filtering method whereas in the velocity estimation using by the state observer in this study relies more on the system dynamics and the state equations. There is also very small error in the estimation of Observer for the zero velocity region which might be overcomed by increasing the related gain term in the Observer gain matrix.
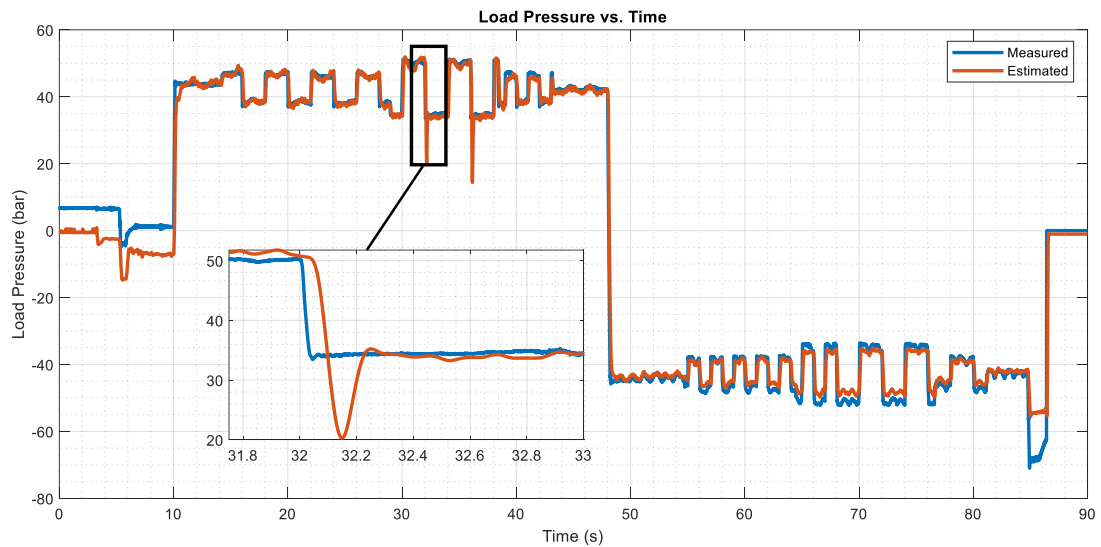
Figure 5.10. Measured Load Pressure and the Load Pressure Estimation of the EHA

For the estimation of the load pressure, some undesirable peak points are observed like the ones in 32th and 34th seconds of the simulation as in the Figure 5.10. Apart from those points, load pressure estimation includes slight deviations in the transient regions and gives better results for the steady state regions.
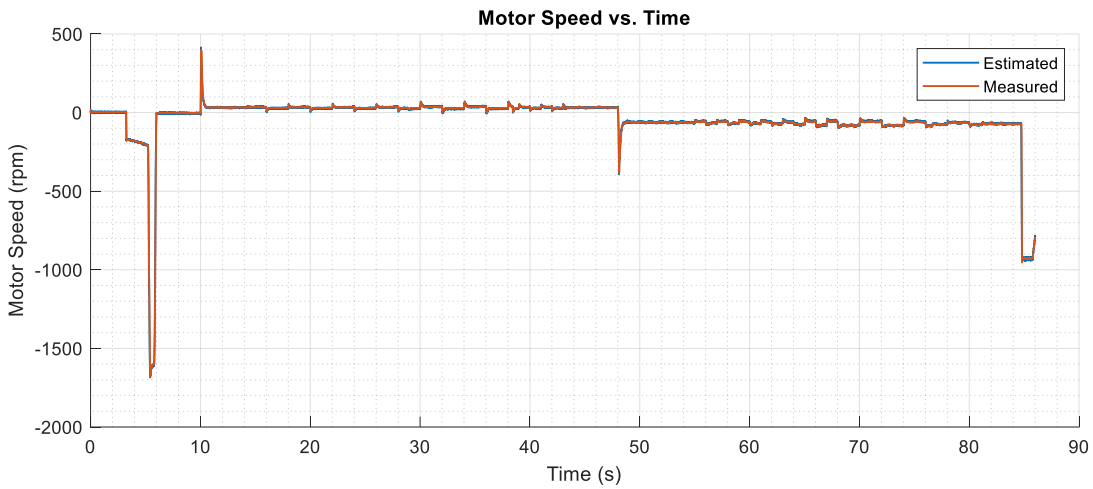
Figure 5.11. Measured Motor Speed and the Motor Speed Estimation for the EHA

The state observer gives accurate results for the estimation of the servo motor speed as can be seen in Fig. 5.11. This is also an expected situation since feedback ist available for this state variable. In addition to the state estimations, the comparison for the disturbance force estimation is also given with the following figures.
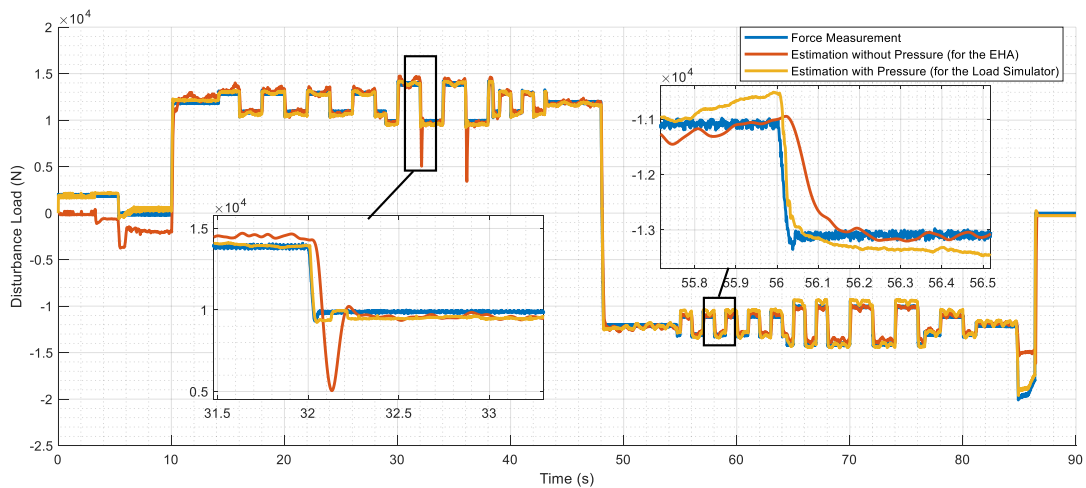
Figure 5.12. Disturbance Force Estimation (with & without Pressure Feedback) and the Measured Disturbance
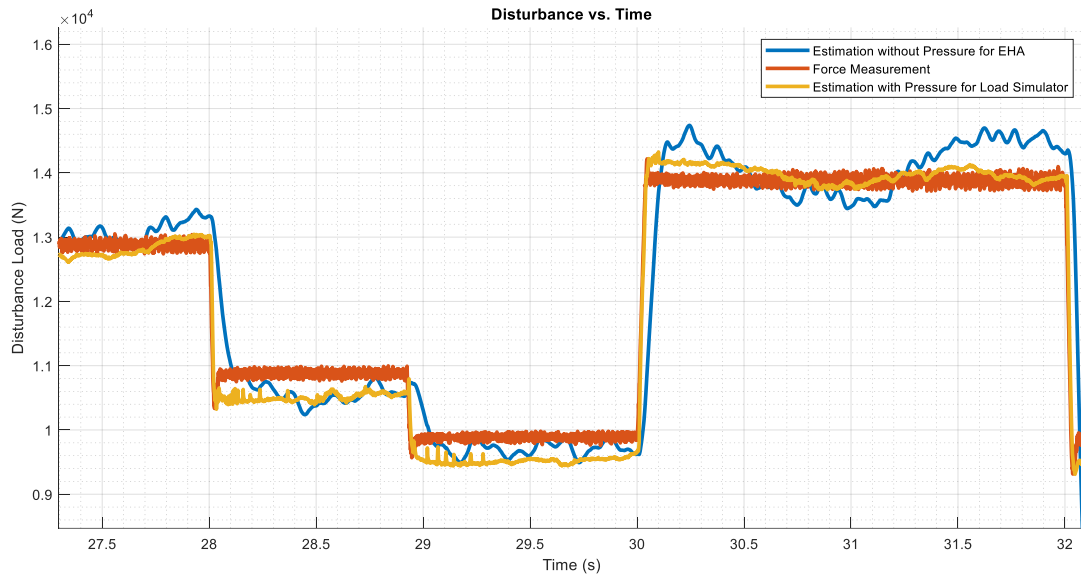
Figure 5.13. Disturbance Estimation (Zoomed)

Considering the results for the disturbance estimation, it could be concluded that the designed disturbance observer gives good estimation results for the steady state cases as can be seen in Figures 5.12 and 5.13. Though, there is some deviations from the measured force between the disturbance estimation without using pressure feedback especially in transient regions (for example around a 0.2-0.3 second difference in rise time), the estimation still reflects the disturbance dynamics with an adequate level of reliability. The usage of pressure feedback might cause the difference between the estimation dynamics of the two methods (with and without pressure feedback).

After about 7-8 bar differential of the load pressure, the disturbance and the state observer starts to give much better results with much little errors. This is an expected situation since the shuttle valve inside the EHA system becomes fully opened after about 7-8 bar differential pressure and in the observer dynamics the shuttle valve is assumed to be fully opened to one side.

71

5.1.4   Fault Identification

In the first step of the fault identification process, rate of the output of the disturbance observer, i.e. time rate of change of the disturbance load, is analyzed as the residual signal and using simple threshold based logic, fault detection can be initiated. A detection signal $i(t)$ is generated which triggers the fault identification process if the variance σ of the disturbance rate $\left|\dot{F}_{d\_obs}\right|$ exceeds a predefined threshold. The threshold value τ for jamming cases is chosen according to results with unjammed test cases. It is obvious that the jamming would result in a considerable amount of increase in the time rate of change of the disturbance load and thus it affects the variance of this rate data. Using that fact, an initial fault information could be extracted from output test data.

$$i(t) = \begin{cases} 1 & \text{if } \sigma\left|\dot{F}_{d\_obs}\right| \geq \tau \\ 0 & \text{if } \sigma\left|\dot{F}_{d\_obs}\right| < \tau \end{cases} \tag{5.20}$$

Where calculation for the variance of the rate of the estimated disturbance can be summerized with following steps.

1. Collection of n samples of the estimated disturbance rate $\dot{F}_{d\_obs}(t)$: such that

$$\dot{F}_{d\_obs_1} = \dot{F}_{d\_obs}(t_i + t'), \dots, \dot{F}_{d\_obs_n} = u(t_i + nt') \tag{5.21}$$

where t' is the sampling time and the t_i is the initial time

2. Computation of $\dot{F}_{d_{obs},jam}$ as the mean of n samples:

$$\dot{F}_{d_{obs},jam} = \frac{1}{n}\sum_{i=1}^{n} \dot{F}_{d\_obs_i} \tag{5.22}$$

72

3. Computation of the variance of n samples:

$$\sigma = \frac{1}{n-1} \sum_{i=1}^{n} \left(\dot{F}_{d\_obs_i} - \dot{F}_{d\_obs_{jam}} \right)^2 \qquad (5.23)$$

Another parameter is needed to enhance the reliability of the designed FDD methodology. Since the actuator rod stays approximately constant at the jammed position, moving average $\bar{x}$ of the position tracking error may be analyzed to create a jamming signal. Where the tracking error is defined as follows.

$$e = y_{reference} - y_{measured} \qquad (5.24)$$

A fault confirmation signal $\mu(t)$ is generated which decides the presence or absence of a fault if the moving average $\bar{x}$ of the position tracking error $|e|$ exceeds a predefined threshold. The threshold value τ_j for jamming cases is chosen according to results with unjammed test cases. It is obvious that the jamming would result in a considerable amount of tracking error thus it affects the moving average of the position measurement. Using that fact, an additional fault information could be extracted from output test data. Two threshold based steps consolidate the fault detection function and increase the reliability of the developed FDD system.

$$\mu(t) = \begin{cases} 1 & \text{if } \bar{x}|e| \geq \tau_j \\ 0 & \text{if } \bar{x}|e| < \tau_j \end{cases} \qquad (5.25)$$

One possible drawback of this computation approach is that it requires the storage of n many samples, which may not be desirable for real time applications. One alternative way is to use recursive computational formulas for the mean and the variance based on a numerically stable computational method [57]. To avoid additional storage needs the following method is implemented with setting $m_1 = u_1$ and $s_1 = 0$.

$$m_k = m_{k-1} + (u_k - m_{k-1})/k \qquad (5.26)$$

$$s_k = s_{k-1} + (u_k - m_{k-1})/(u_k - m_k) \qquad (5.27)$$

for $k = 2, .., n$. Therefore,

$$u_{jam} = m_n \text{ and } \sigma = s_n/(n-1) \qquad (5.28)$$

A varying counter loading is applied to the system in order to compare the rate of the disturbance estimation with the rate of the measured disturbance load. The results is given in the following figures.
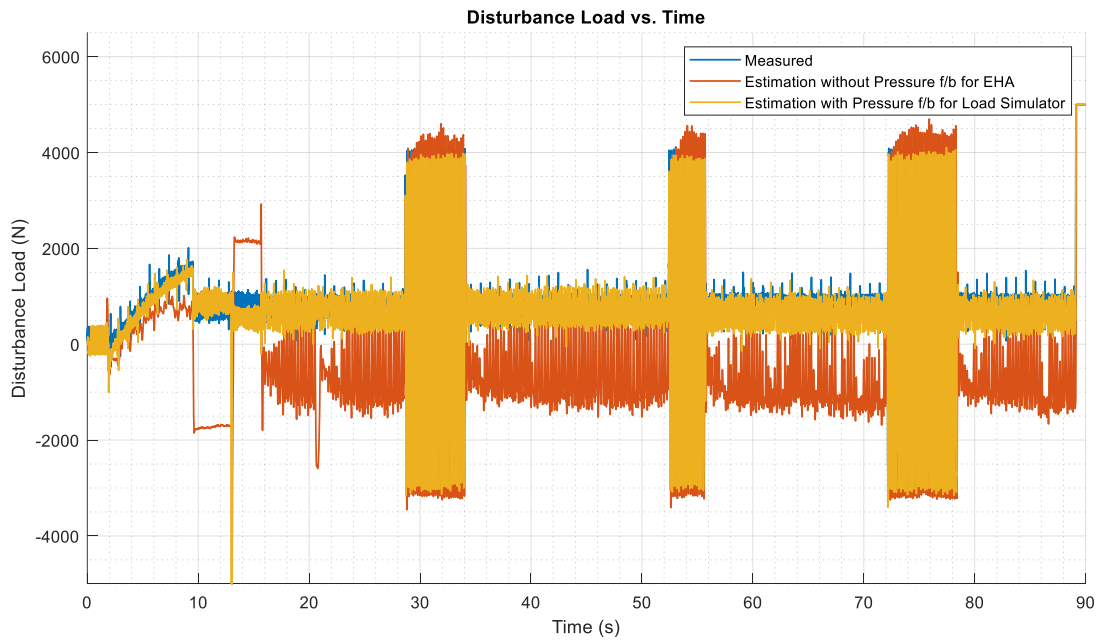
Figure 5.14. Disturbance Estimation under Varying Counter Loading

74
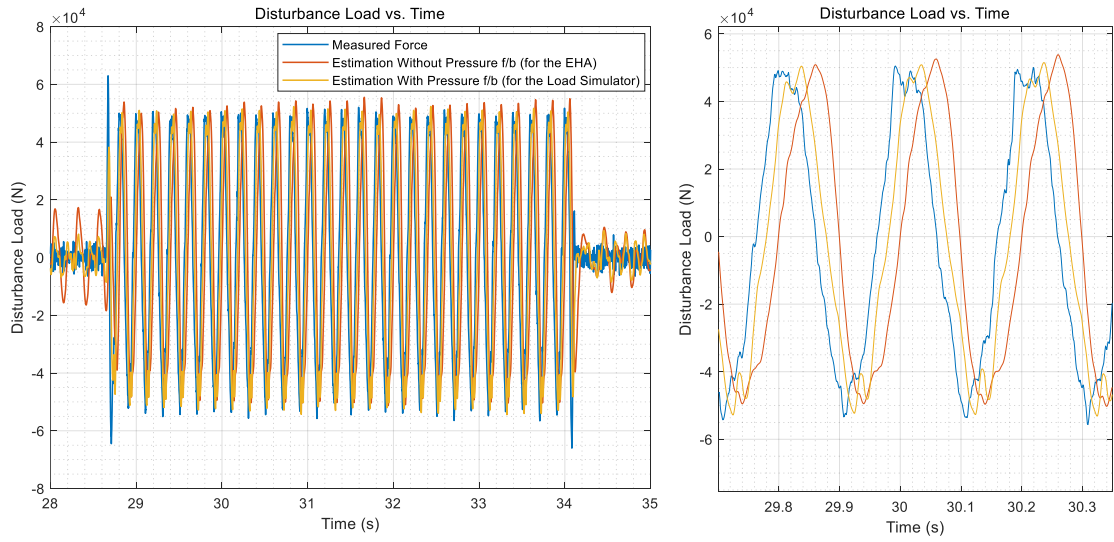
Figure 5.15. Disturbance Estimation under Varying Counter Loading (Zoomed)
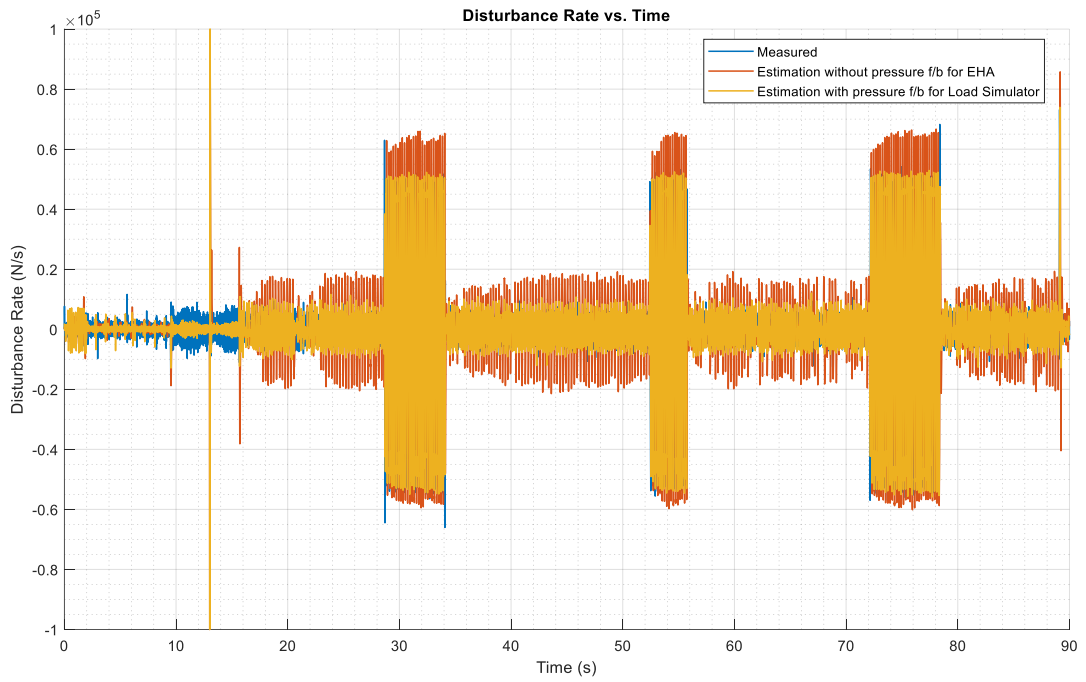
Figure 5.16. Disturbance Rate under Varying Counter Loading
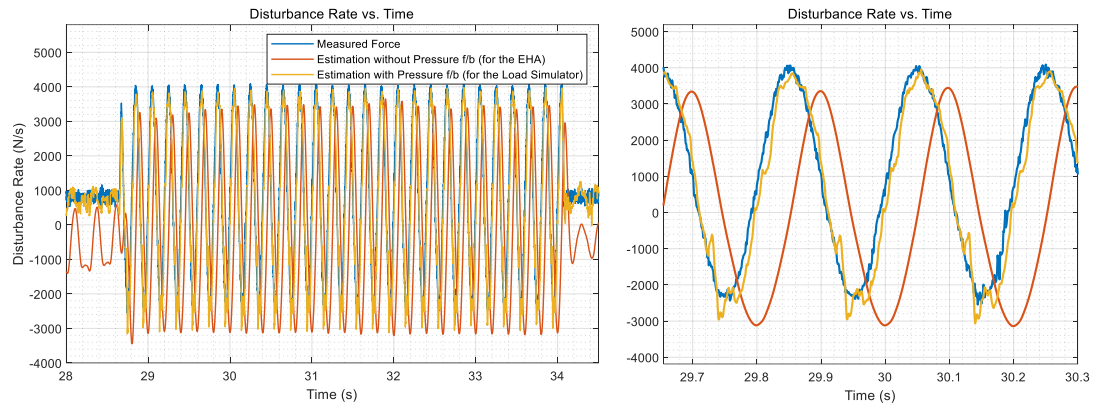
Figure 5.17. Disturbance Rate under Varying Counter Loading (Zoomed)

Considering the test results given for the counter load varied as a sinusoidal wave, the region where the disturbance estimation without the chamber pressure feedback is valid can be seen more clearly. In Figures 5.10 and 5.11 around 1000 N of load, the disturbance estimation without pressure feedback fails because of the neglected changes in the system dynamics due to the partially opening configuration of the shuttle valve. Yet, in the dynamic loading cases above 2-3 kN the estimation could give accurate results as the shuttle valves becomes fully opened to one side of its operation in this regions. A very similar situation is observed for the derivative of the disturbance loads as in Figures 5.12 and 5.13. Where the disturbance estimation without pressure feedback becomes valid, its rate could be used too.

5.2   Test Scenario

In accordance with the critical considerations (jamming or stuck at neutral position) discussed in the motivation and the objection of the thesis parts, several faulty cases are simulated in the real time environment and the detection performance of the proposed method is analyzed in this subsection.

In order to simulate the jamming phenomena, the load simulator is used to hold the EHA piston at a desired position. As explained in Chapter 4, two actuator rods are connected to each other via a spring attachment. The electrohydrostatic actuator (EHA) is a closed loop position control system and the load simulator is a force control system. Therefore, any position input (within the position limits) can be simulated with any counter loads (wtihin the supply pressure limit) acting on the actuator to be controlled. By adjusting the counter load provided by the load simulator and by locking the piston rod physically, see Section 5.3., required friction force for jamming action is created. After holding the actuator in a prescribed position with the help of the closed loop control, its rod is stopped by phsically locking it and then the real time hardware in the loop tests are carried out to simulate the jamming failure.

As mentioned, the most critical and difficult cases in terms of detection and identification of jamming are at low deflection signals where the reference position input to the actuator is quite low especially in cruise (steady state flight) cases. Therefore, low amplitude input signals around the jammed position are inserted to the control system. To simulate several different cases, both sinusoidal and sawtooth signals are used in jamming conditions. In order not to result in an excessive sudden increase in the load and not to damage the overall structure in the setup, step signals are not preferred for jamming simulations. The test scenario is applied under both jammed and non-jammed situations to compare the performance of the developed FDD system under faulty and non-faulty cases. The test cases investigated are listed in table 5.1. Amplitude and frequency values of the selected reference position signals are presented in the fifth column of the table. Since the actuator input demand

77

is relatively low in cruise condition with the control surface being quite close to its neutral position, amplitudes of 0.25 mm, 0.5 mm and 1 mm are chosen. To reflect different demand behaviors of actuator position sinusoidal and sawtooth signals with two different frequency values are taken. All of the faulty jamming conditions are also simulated for the non-jammed nominal case. It should be noted that jammed position are taken as 50mm. Yet, it does not have any effect on performance of the proposed FDD method and does not change the overall philosophy followed in this study for jamming detection. Developed method here could also be applicable for the detection of jamming at other low control surface deflections or actuator strokes as well. For all of the jamming conditions in the following table, a disturbance load of 14000N is applied as this value is very close to the maximum force that can be measured by the load cell in the test setup. Unjammed cases are simulated under a load of 4000N.

Table 5.1. Test Cases for Jamming

Test Case	Condition	Initial Condition	Input Signal	Signal Amplitude and Frequency	Disturbance Load
1	Jammed	50 mm	Sine Wave	0.25 mm, 2 Hz	14000 N
2	Non-Jammed	50 mm	Sine Wave	0.25 mm, 2 Hz	4000 N
3	Jammed	50 mm	Sine Wave	0.5 mm, 1 Hz	14000 N
4	Non-Jammed	50 mm	Sine Wave	0.5 mm, 1 Hz	4000 N
5	Jammed	50 mm	Sine Wave	1 mm, 0.5 Hz	14000 N
6	Non-Jammed	50 mm	Sine Wave	1 mm, 0.5 Hz	4000 N
7	Jammed	50 mm	Sawtooth	0.25 mm, 2 Hz	14000 N
8	Non-Jammed	50 mm	Sawtooth	0.25 mm, 2 Hz	4000 N
9	Jammed	50 mm	Sawtooth	0.5 mm, 0.5 Hz	14000 N
10	Non-Jammed	50 mm	Sawtooth	0.5 mm, 0.5 Hz	4000 N
11	Jammed	50 mm	Sawtooth	1 mm, 0.5 Hz	14000 N
12	Non-Jammed	50 mm	Sawtooth	1 mm, 0.5 Hz	4000 N

Before giving results of real time simulation cases, main assumptions of the test scenario should be noted here as follows.

- First assumption for this type of fault is the fact that low control surface deflections (actuator movements) around the point to be interested, i.e. the null position of the surface, would not result large variations in the aerodynamic forces acting on the actuator. It is fairly a reasonable assumption as aircraft meneuvers are relatively smooth in cruise phase, which corresponsd to a considerably large proportion of a whole flight envelope and not come up with sharp increases in control surface loads [58].

- The counter loading load simutor system is used within the measurement ranges of the load cell in the test bench and the disturbance rejection characteristics of the EHA is reduced by cancelling its integral gain. The jamming conditions are simulated under a proportional control.

- Actuator position input for maneuvers requiring lower demands would not be more than a couple of mm of stroke length. It is sensible to assume an actuator demand around 1mm for control surface deflections around a couple degrees. As actuator lever, which converts linear motion of the actuator into rotary motion of control surface, has a length of around 100mm depending on installation requirements for the control surface. For example, the lever length of the horizontal tail of F-16 is about 150mm [59] which would result in an actuator demand about 2mm for 1degree of surface deflection at the neutral (zero) position of the surface, which is the investigated point for the jamming case.

- Control surface demand would be in the order of 1 degree (about 1-2 mm actuator stroke) for the cases that requires low demand such as cruise level flight. Though the control surface demand depends on different parameters like flight condition, control surface kinematics, aircaft type, aircraft aerodynamics, so and so forth, it is reasonable to assume the control surface demand anywhere between 0-1 degrees for low demanded cruise conditions [60].

- Resolution of the control surface movement is assumed as about 0.1 degree which corresponds to a stroke around 0.24mm for a control surface having a very typical lever length of 150mm. The more the lever length value the higher stroke corresponding to the resolution of the control surface. At this point, such an assumption is to be made whether the developed FDD system is capable of detecting jamming failures even for the smallest deflection of a typical control surface movement. This resolution assumption might even be constrained below 0.1 degree depending on specifications of a control surface.

5.3   Experimental Results

Real time simulations are performed according to the test scenario stated in Table 5.1. As explained before, jamming cases are tried to be simulated under the counter load by the load simulator and with using a mechanical locking assembly. By this way, EHA piston is kept being stuck at the desired position.

Before conducting tests for the jamming cases defined in Table 5.1, a comparison is made between the two possible jamming conditions; with the counter loading by the load simulator and with the mechanical locking assembly. A quick installed mechanical system is designed for this purpose. It includes an upper and a lower steel body. Inside these two parts, two bronze bushings are installed to create the necessary friction power for jamming. Overall locking assembly is given in Figure 5.18.
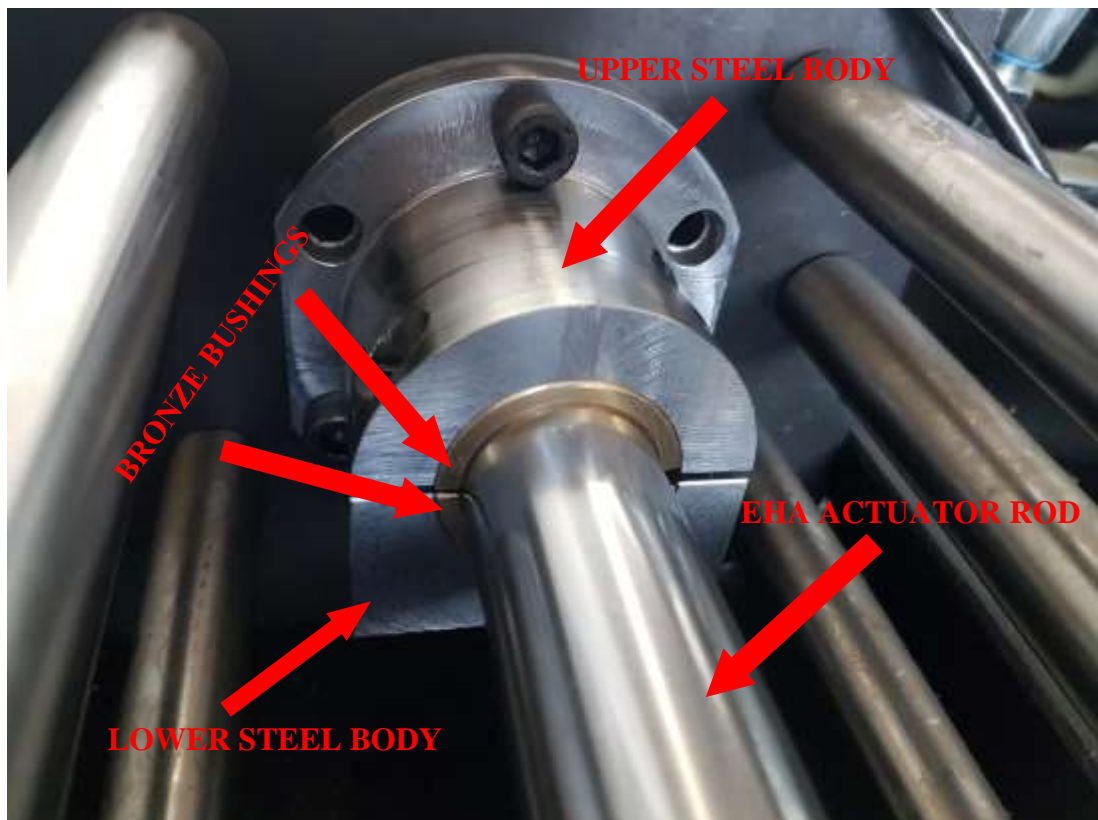
Figure 5.18. Mechanical locking assembly used for jamming

A sawtooth signal wave having 0.25 mm of amplitude and 2 Hz frequency is given as the reference position for both counter loaded and mechanical jammed conditions. Position responses and the reference position, load pressure variations and the responses (torque and speed) of the servo motor of the EHA are plotted in the following figures. Note that the actuator is not loaded for the unjamming case, the same amount of load is applied for both jannimg cases, and only the proportional control is active for all cases.
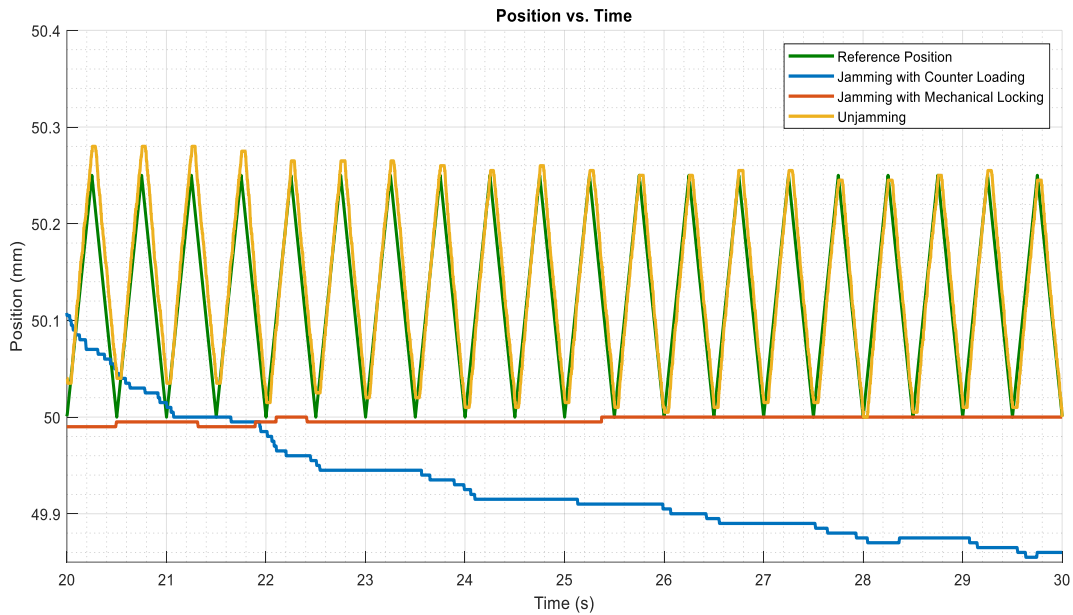
Figure 5.19. EHA position response under different conditions
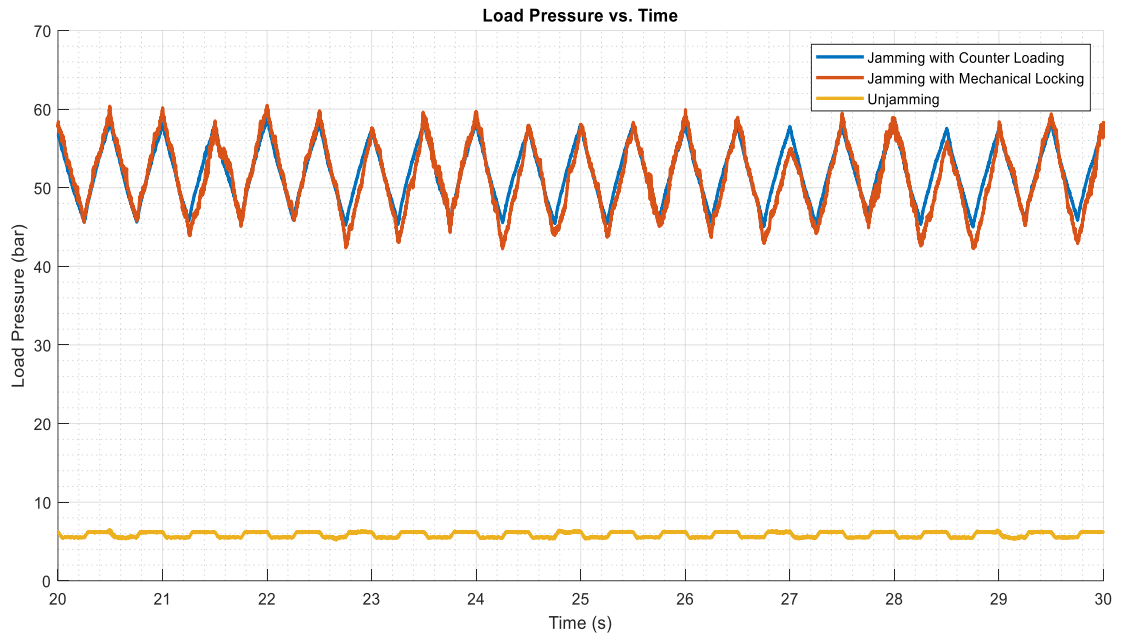
Figure 5.20. EHA load pressure under different test conditions
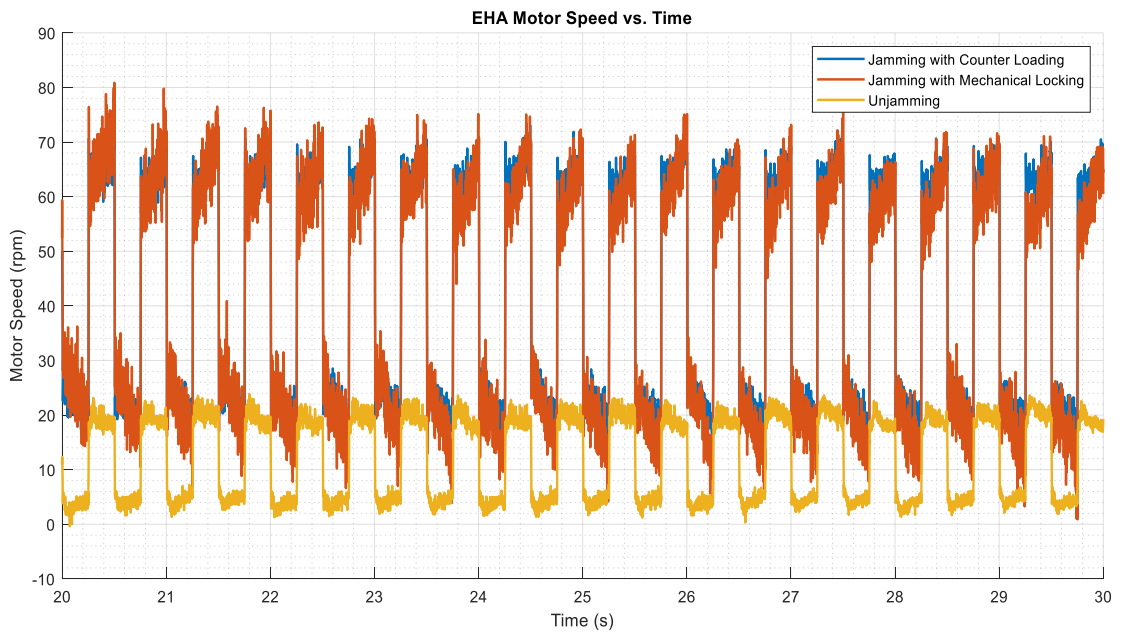
Figure 5.21. EHA motor speed under different conditions
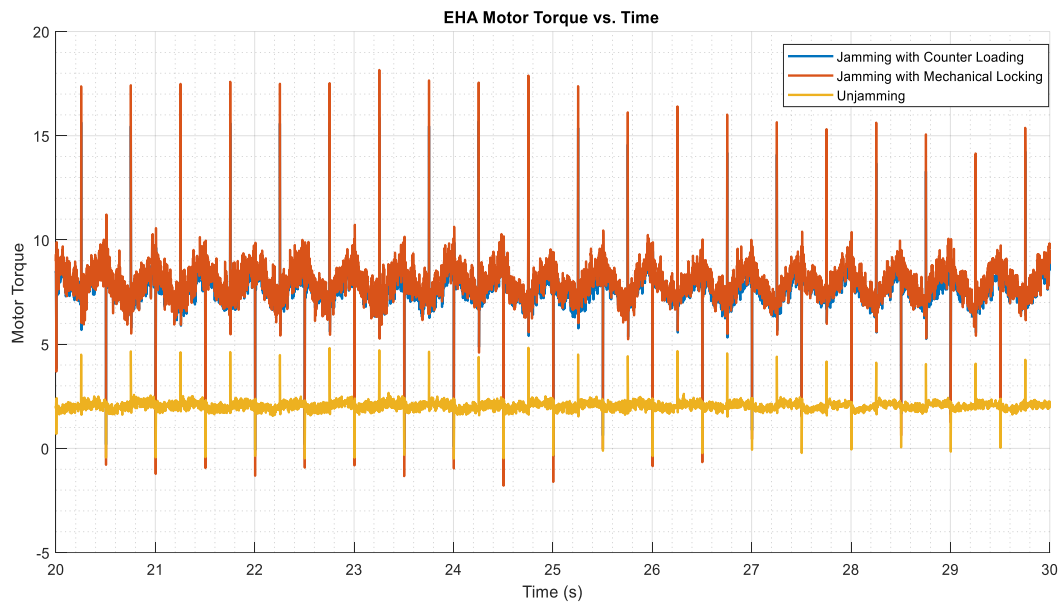
Figure 5.22. EHA motor torque under different conditions

All in all, the EHA piston is tried to be stuck at a certain position by using two alternative methods. In the first one, the counter loading actuator (the load simulator) is used to simulate the disturbance load due to the jamming whereas in the second condition a locking assembly is used after the same load is applied to the EHA as for the first condition. At the end, both technqiues give considerably similar results in terms of EHA servo motor responses (see Figures 5.21 and 5.22) and the chamber pressure dynamics. One of the main difference is that under the counter loading EHA piston cannot stay steady at the desired jamming position because it exceeds the disturbance rejection of the EHA at that specific condition. Unlike, the mechanical jamming condition well reflects the expected jamming situation since the EHA piston cannot move as seen in in Figure 5.19 even if the chamber pressures change as in Figure 5.20. After this validation step, all of the test scenario is to be examined with the faulty condition where jamming is simulated through the mechanical locking.

84

Reference and measured position, rate of the estimated disturbance, recursive variance calculation of disturbance rate, moving average of the tracking error and the eventual output of the developed FDD system, which is the fault signal, are plotted in the results of the test cases. Moving average of the position tracking error, disturbance rate and its variance are given including both jammed and unjammed cases in the same figures. Note that both jamming and unjamming conditions are simulated by cancelling integral gain of the controller. Therefore, developed FDD system are analyzed under proportional controller for all jamming and unjamming conditions. Disturbance loads of 14kN and 4kN are applied (at t=19s) for jamming and unjamming cases, respectively. After the counter load (disturbance), the reference position is inserted to the EHA at t=20s. Results are given for just one set of test case (Test Cases 9&10) in the following figures while the remaining test results are included in the Appendix part.

Test cases 9 and 10:
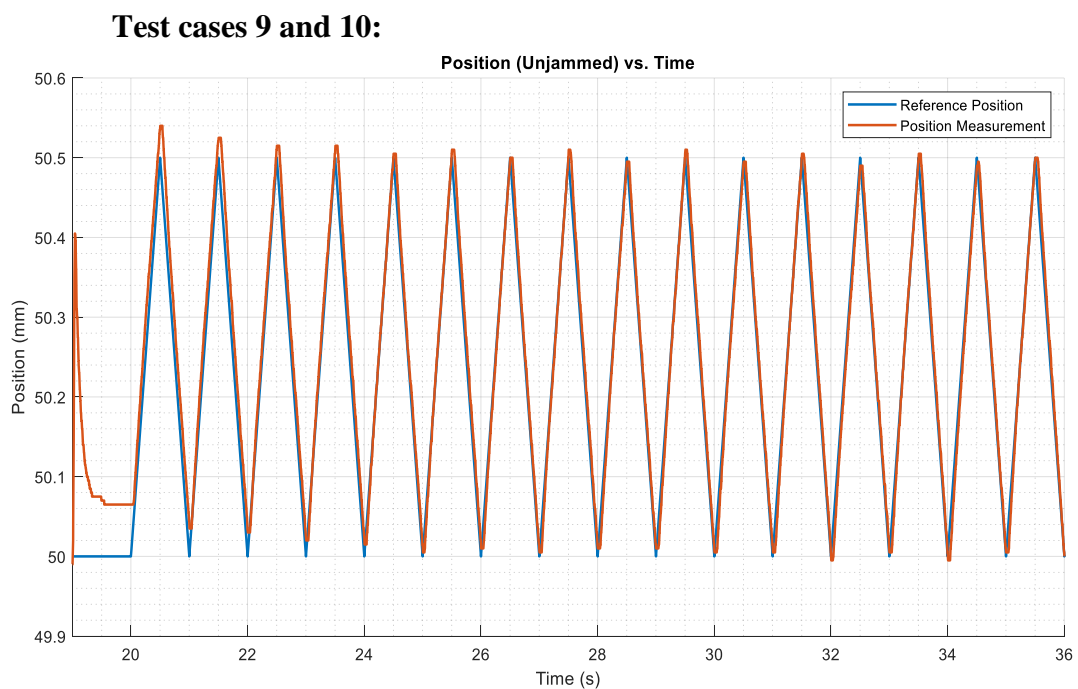
Figure 5.23. EHA Position Response under the Unjammed Case

85
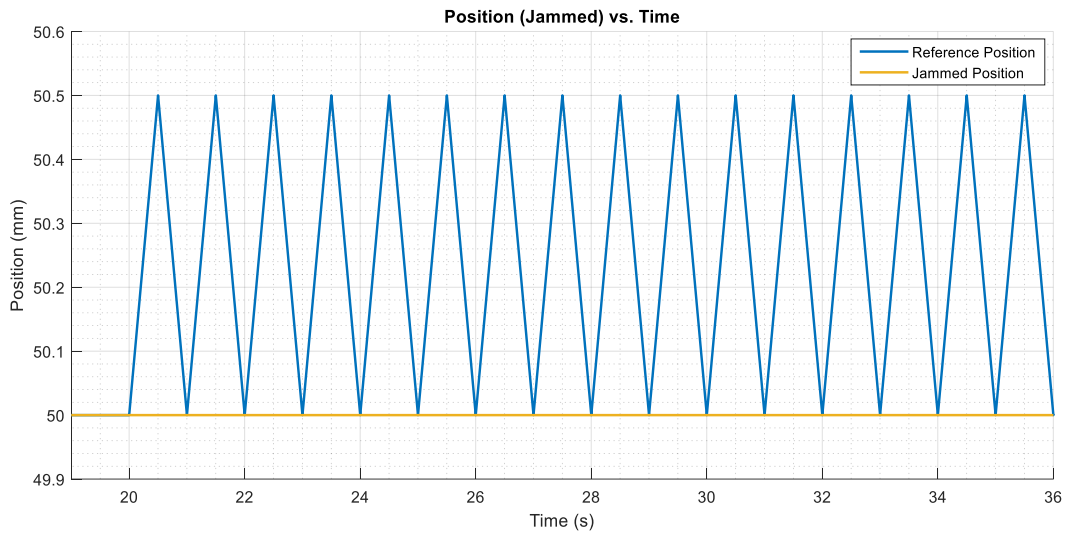
Figure 5.24. EHA Position Response under the Jammed Cases
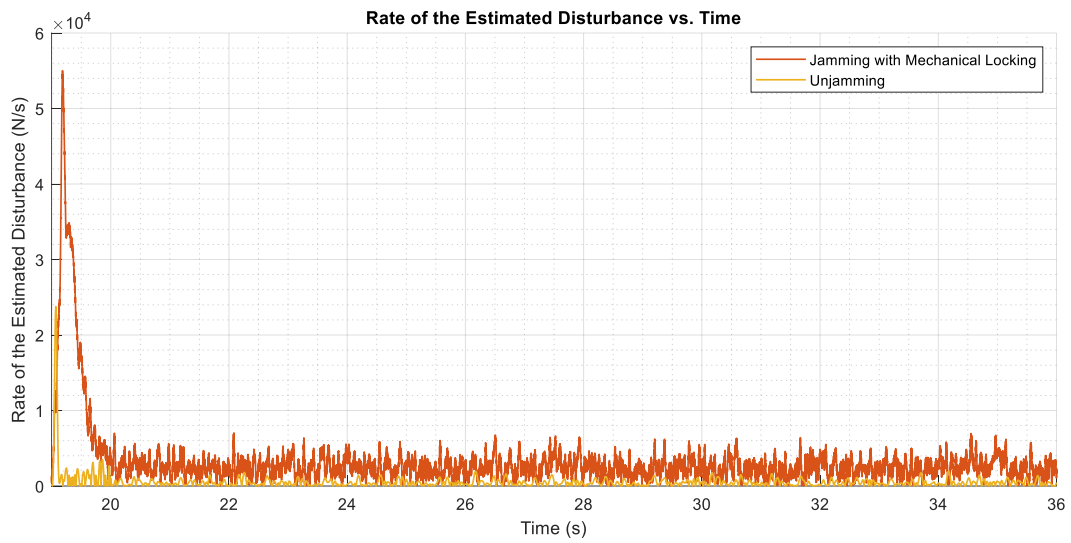
Figure 5.25. Rate of the Estimated Disturbance
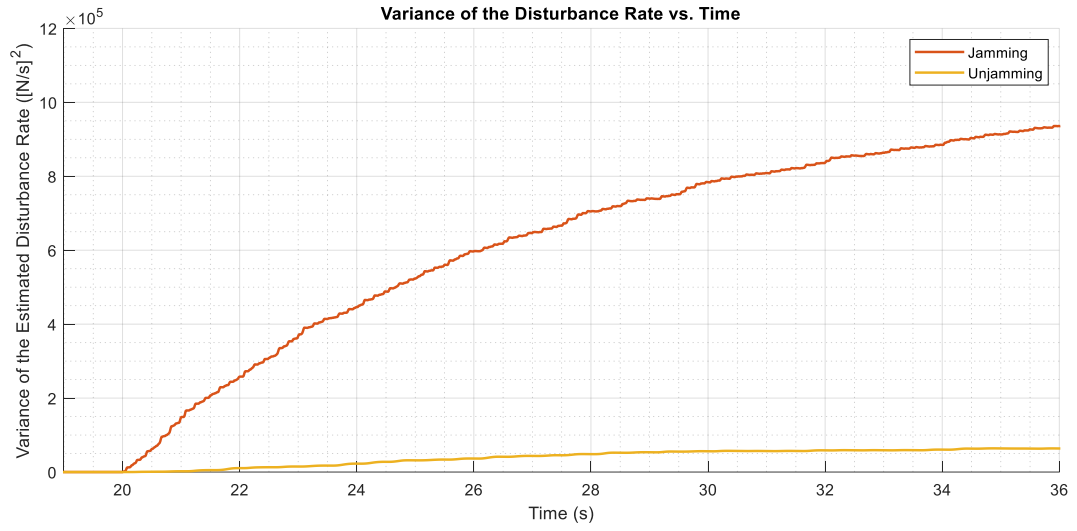
Figure 5.26. Variance of the Estimated Disturbance Rate
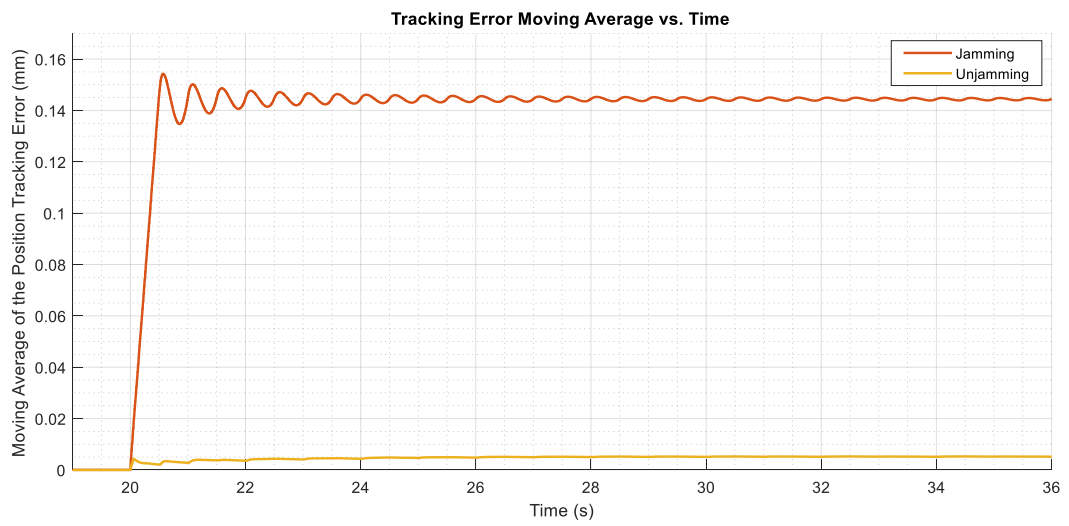
Figure 5.27. Moving Average of the Position Tracking Error
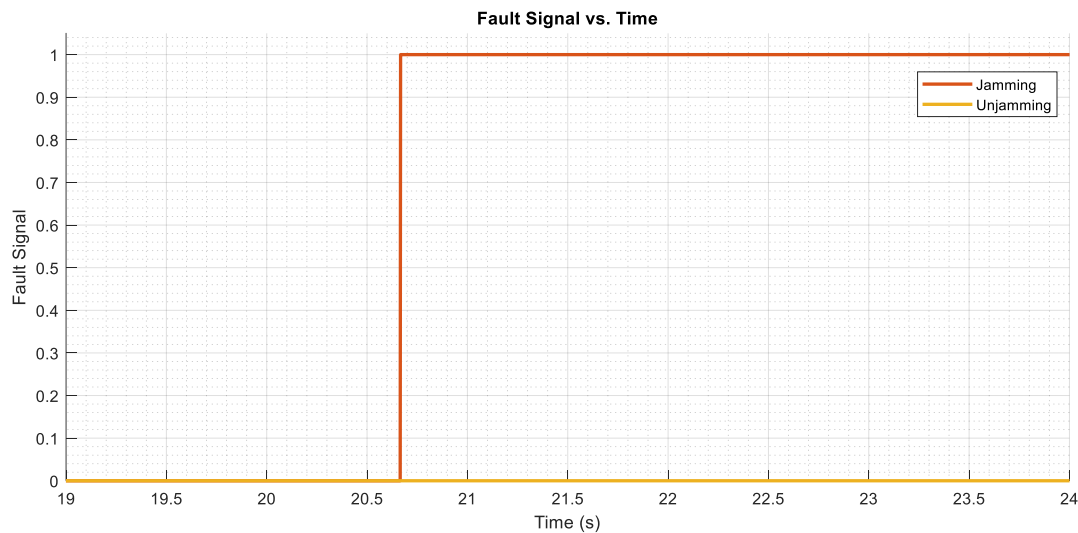
Figure 5.28. Generated Fault Signal

Several remark regarding the given plots for the fault detection and diagnosis of jamming failures are highlighted as follows;

- Position responses of the EHA under jamming and unjamming cases are actually expected. Because of the high disturbance load (14kN) the actuator cannot track the given position input as can be clearly seen in Figure 5.24. Whereas little tracking error occurs (see Figure 5.23) for the unjamming case due to the considerably lower disturbance load (4kN). Note that control system is the same for all jamming and unjamming cases so the only difference is created by changing the external disturbance load by means of counter loading and the mechanical locking which have been discussed before.

- Rate of the estimated disturbance load seems quite noisy and it is difficult to extract valuable information about the faults from Figure 5.25. Therefore, the variance of this disturbance rate is calculated in Figure 5.26. It is obvious that there is a quite bit of difference between the jamming cases and the unjamming. It might also be expected to see some disparity between two faulty cases (mechanical locking and counter locking) as the EHA motor responses and the chamber pressure dynamics vary slightly for these two cases (see Figures 5.20-21-22).

88

- High position tracking errors are inevitable for jamming cases because of the low disturbance rejection characteristics under mechanical locking or counter loading as can bee seen in Figure 5.27. Though, there is little difference between two jamming methods in the tracking error. Yet, the deviation between the tracking error for the unjamming case and these two jamming cases are quite large as might be expected.

- At the end, the fault is identified (see Fig. 5.28) in a considerably small time interval for this test case because of the high deviations in the indicators (disturbance rate and the tracking error) between jamming and unjamming conditions.

For all of the simulated test cases, developed FDD system gives very similar results for the fault indicators, detection time and deviations between jamming and unjamming conditions (see Appendix part). The responses of the system under two faulty cases, i.e. mechanical locking and the counter loading, are quite similar to ones given for the test cases 9-10 before. Using the developed FDD methodology all of the failure cases could be identified under a 1 seconds of time interval. It should be noted that detection time of the faults strictly depends on the chosen threshold values in the fault identification step. The higher threshold value chosen, the later the system identifies the jamming cases. In order to be more robust and reliable against false alarms, higher threshold might be chosen but this would considerably increase the lag between the occurrence of the error and the detection time. Overall results are summerized in the following table.

Table 5.2. Summary of the Results for the Sine Wave Inputs

Test Case	Input Signal	Variance of the Estimated Disturbance ($[N/s]^2$)	Moving Average of the Tracking Error (mm)	Detection Time (s)
1 – 2	0.25mm Sine	$7.2x10^5$ – Jammed $6x10^4$ – UnJammed	0.09 – Jammed 0.025 – UnJammed	0.62
3 – 4	0.50mm Sine	$9.1x10^5$ – Jammed $5x10^4$ – UnJammed	0.17 – Jammed 0.022 – UnJammed	0.51
5 – 6	1.00mm Sine	$10x10^5$ – Jammed $5x10^4$ – UnJammed	0.28 – Jammed 0.02 – UnJammed	0.47

Table 5.3. Summary of the Results for the Sawtooth Wave Inputs

Test Case	Input Signal	Variance of the Estimated Disturbance ($[N/s]^2$)	Moving Average of the Tracking Error (mm)	Detection Time (s)
7 – 8	0.25mm Sawtooth	$6.6x10^5$ – Jammed $6.5x10^4$ – UnJammed	0.06 – Jammed 0.023 – UnJammed	0.68
9 – 10	0.50mm Sawtooth	$9x10^5$ – Jammed $6x10^4$ – UnJammed	0.14 – Jammed 0.02 – UnJammed	0.66
11 – 12	1.00mm Sawtooth	$9.6x10^5$ – Jammed $6x10^4$ – UnJammed	0.23 – Jammed 0.025 – UnJammed	0.62

Considering the results provided in Table 5.2 & Table 5.3, a number of comment can be made regarding failure dynamics, fault detection performance and the overall effectiveness of the developed methodology;

- Fault detection time starts to decrease as the amplitude of the reference position signal rises. This is an expected result since the tracking error increases for higher strokes and the control system of the EHA tries to compensate this error harder. Eventually, the oscillations in the chamber pressures rise and that makes the variance of the disturbance rate to exceed the selected threshold much quickly. Not only the disturbance rate, but also the moving average of the tracking error becomes diverging further from the unjammed case.

- A single threshold value is selected in the developed FDD algorithm for both the moving average of the tracking error and the variance of the estimated disturbance rate. Yet, a single threshold set could give comparibly good detection times.

- There is a considerable amount of gap between the variance values for jammed and unjammed conditions as there is a huge difference, 10kN, between the counter loads applied for the two cases.

- In the real-time simulations, the EHA could not be completely jammed because of the disturbance rejection characteristics of the control system even though its integral gain is diminished for both jammed and unjammed cases. It affected the moving average of the tracking errors. If the EHA motion was fully stopped, then both fault indicators could exceed the thresholds even much faster.

Maximum fault detection time, 0.68s, occurs at the amplitude of 0.25mm. In the assumption part it was assumed that an actuator stroke of 0.25mm nearly corresponded to a minimum surface deflection of a typical flight control surface. Since the detection time would decrease as the given input is increased at the time of jamming, this 1.26s of detection time might be considered as the maximum detection time for a jamming failure of a flight control surface. This maximum detection time is actually lower thant the minimum detection time of 3seconds, achieved in the study performed by Ossmann et al. [31]

CHAPTER 6

CONCLUSION

6.1 Summary

The aim of this research was to develop a fault detection and diagnosis (FDD) methodology for the specific fault called ''jamming'' that might be encountered in a flight control actuation system. An Observer based detection methodology was modelled in Matlab/Simulink environment. This scheme was embedded into a real-time simulation model of a hydraulic test rig to diagnose the emulated faults. The hydraulic test setup included two distinct actuation system connected to each other via a spring attachment.

In order to estimate the state variables correctly, first system dynamics of two actuators, a pump-controlled electrohydrostatic actuator (EHA) and a valve-controlled actuator, were investigated and modelled with proper justifications. Then, linear time-invariant state space representations of both actuators were developed. According to the state space models, state and disturbance observers were designed to estimate both unknown system states and the disturbance load acting on the actuators. Both EHA and the load simulator systems were modelled with four system states. Available pressure feedbacks were used in the disturbance observer for the load simulator whereas in the EHA disturbance observer, pressure information was provided by the estimation of the state observer.

Outputs of the designed state and disturbance observers were compared for the validation of the observer models. Comparisons of the state variables were only performed for the EHA actuator since this actuator was then analyzed for the detection of jamming. In the validation of the disturbance observer, the EHA disturbance estimation without the pressure feedback and the load simulator disturbance estimation with the pressure feedback were both used just for the

comparison. In the fault detection processes of this study, the EHA disturbance estimation was used without any pressure measurement. Because the shuttle valve dynamics were neglected and it was assumed as in a fully opened configuration in the observer designs for the EHA, the state and disturbance estimations deviated quite a lot from the real values coming from the available sensors in the test setup. However, this fact did not affect the validity of the proposed detection method for jamming since the EHA system was tested in an operating region where the shuttle valve is fully opened and hence the state and the disturbance estimations of the observers were valid.

A Fault Detection and Diagnosis scheme was then developed based on the output of the designed disturbance observer. The whole FDD methodology was based on checking of two distinct indicators about the jamming. One parameter used in the fault detection was selected as the change in the disturbance rate as the disturbance load does not vary too much around a neutral (or null) point of a flight control actuator. Variance of the rate of the observed disturbance was computed through a recursive calculation method. When this variance exceeded a predefined threshold value then a second indicator regarding the fault would also be checked. This parameter was the moving average of the tracking error since it considerably diverged from an unjammed case in a jamming case. Two threshold based steps were then combined with an and gate to confirm jamming and to improve the reliability of the developed FDD procedure.

In order to test the performance of the proposed methodology, a fault scenario was created based on some estimations about the operating conditions defined in the scenario. Low amplitude sine and sawtooth waves with different frequency values around a specific actuator position (50mm) were taken as the reference inputs. The actuator was first forced to be stuck at that specific position by physically tightening its rod via a quick locking mechanism. Then, the reference inputs were inserted to the EHA actuator. By this way, the jamming failure was tried to be emulated. In order to compare whether different possible methods could resemble the jamming dynamics, a locking mechanism was designed and the jamming was tested with that

mechanical locking assembly. Results with both the mechanical locking and the locking with the counter loading were given. Considering the results, it might be stated that both technique gave very similar system responses except with small deviations. One significant drawback of counter loading method is that it could not stop the EHA piston completely for any reference position input even if the motion of the actuator might seem to be negligable. Therefore, in order to reflect the failure dynamics better the jamming was simulated with the mechanical locking option. After giving a high counter loading the EHA was tightened via the mechanical locking assembly and the position command was given.

It should be noted that a 'pure' jamming failure could not be emulated through the counter loads in the test setup. The EHA could not be completely jammed for the inputs with highest amplitudes (1mm) given to the system even though the counter loading system was forced to the maximum load that the load cell in the setup could measure. Therefore, in order not to cause any catastrophic damage to the test bench, the counter load was increased no further. In order to jam the actuator and decrease its disturbance rejection, its integral gain was degraded for both jammed and unjammed test cases. Although the integral controller gain was reduced, the EHA were still be able to track the given position signal in the unjammed test cases with still a considerable amount of counter load.

If it was possible to have and use a much more capable locking mechanism as in [61], then the designed FDD algorithm could have been examined for fault conditions closer to a realistic jamming case. After considering the results, it was realized that the disturbance rejection characteristics of the actuator had a great influence on the fault detection performance of the designed algorithm. Depending on the disturbance rejection of an actuator, its estimated disturbance rate under the jamming case could diverge rapidly from the unjammed nominal condition. Therefore, a more powerful locking mechanism with a highly robust controlled actuator against disturbances might be really exciting to be investigated for the detection of jamming.

At the end of the thesis, results were given for each test case with jamming inserted and not inserted to the EHA. Faults was successfully detected for all of the jammed cases and no false fault signal was observed for non-jamming cases. Detection times were observed to be quite low, less then one second for each case since for the jammed conditions the disturbance observer rate and the position tracking error deviates rapidly from the unjammed test cases.

6.2   Contributions

This thesis consists of several contributions to the literature, which have been made to both fields of hydraulic control and fault diagnosis. The major contributions are outlined as below;

- A state and a disturbance observer were designed for a pump speed controlled EHA type system. Using these observers unknown states which are the actuator velocity and the load pressure as well as the disturbance load acting on the actuator were estimated with an uccaptable level.
- Jamming failure was correlated with the disturbance load acting on a hydraulic actuator both in theory and in practice.
- An Observer-based fault detection and diagnosis methodology was developed for online monitoring of an electro hydraulic actuation system and the related algorithms were embedded into a real-time simulation system.
- A challenging fault case (jamming), which might be observed in an electro hydraulic flight control actuator, was investigated.

6.3   Suggestions for Future Work

In this thesis study, shuttle valve dynamics is completely neglected for pressure and disturbance estimations for the electro hydrostatic actuator. This assumption however brought a challenge during the tests. The actuator needed to be tested for the operating conditions where the shuttle valve is fully opened. For lower disturbance forces, the actuator chamber pressures become quite lower and this would result in partially opening of the shuttle valve. Therefore, the designed state and disturbance observer cannot be valid for lower counter loads. In the tests, higher forces are required for the observers to be properly used in the fault detection and diagnosis steps. In addition, pressure estimation fails for the valve-controlled load simulator without using the available pressure feedback. Disturbance estimation for the load simulator is performed with taking the pressure measurement and it is used just for the comparison of the estimation without pressure feedback. Thus, a more comprehensive and detailed estimation method might be developed for state and disturbance estimations for all working regimes of both valve and pump controlled actuation systems.

The developed method is validated for lower actuator demands with small amplitudes and it is validated accordingly due to the limitations in the test setup. Even thoguh this might be the case for flight control actuators during cruise maneuvers, it does not reflect all of the working envelope of a flight control actuator. Nevertheless, the developed method, with little modifications, could be easily applied for different maneuver cases requiring more actuator demands with higher aerodynamic loads.

Different failure conditions such as leakage, excessive friction, supply pressure loss, etc. which might occur in an electro hydraulic actuation system can also be investigated. The FDD methodology can be extended to cover those failures and a more comprehensive methodology could be obtained with minor modifications and additions.

REFERENCES

[1] R. Isermann and R. Balle. *Trends in the application of model-based fault detection and diagnosis of technical processes*. Control Engineering Practice,5:709–719, 1997.

[2] Findeisen, Dietmar. *Ölhydraulik: Handbuch für Die Hydrostatische Leistungsübertragung in Der Fluidtechnik*. Springer, 2006.

[3] Maré Jean-Charles. *Aerospace Actuators 2 Signal-by-Wire and Power-by-Wire*. John Wiley & Sons, 2017.

[4] Watton, J. *Fundamentals of Fluid Power Control*. Cambridge University Press, 2014.

[5] Maré Jean-Charles. *Aerospace Actuators 1 Needs, Reliability and Hydraulic Power Solutions*. UK, 2016.

[6] Isermann, R. (2011). *Fault-diagnosis systems: An introduction from fault detection to fault tolerance*. pp. 24. Berlin: Springer.

[7] Vanek, B., Szabó, Z., Edelmayer, A., & Bokor, J. (2012). Fault detection of electrical flight control system actuators using parameter dependent estimation*. *IFAC Proceedings Volumes,45*(20), 1358-1363. doi:10.3182/20120829-3-mx-2028.00218

[8] Samadani, M., Kwuimy, C., & Nataraj, C. (2014). Fault Detection and Severity Analysis of Servo Valves Using Recurrence Quantification Analysis. *ANNUAL CONFERENCE OF THE PROGNOSTICS AND HEALTH MANAGEMENT SOCIETY 2014*.4

[9]   Jayakumar, M., & Das, B. (2006). Diagnosis of Incipient Sensor Faults in a Flight Control Actuation System. *2006 SICE-ICASE International Joint Conference*. doi:10.1109/sice.2006.315126

[10] Ossmann, D., & Varga, A. (2013). Detection and identification of loss of efficiency faults of flight actuators. *2013 Conference on Control and Fault-Tolerant Systems (SysTol)*. doi:10.1109/systol.2013.6693841

[11] Model-Based Approaches for Fast and Robust Fault Detection in an Aircraft Control Surface Servo Loop: From Theory to Flight Tests [Applications of Control]. (2013). *IEEE Control Systems,33*(3), 20-84. doi:10.1109/mcs.2013.224941

[12] Zavarehi, M. K., Lawrence, P. D., and Sassani, F., 1999, "*Nonlinear Modeling and Validation of Solenoid-Controlled Pilot-Operated Servovalves,*" IEEE/ASME Transactions on mechatronics, 4(3), pp. 324-334.

[13] Niksefat, N., and Sepehri, N., 2002, "*A QFT Fault-Tolerant Control for Electrohydraulic Positioning Systems,*" IEEE Transactions on Control Systems Technology, 10(4), pp. 626-632.

[14] Crowther, W. J., Edge, K. A., Burrows, C. R., 1998, "*Fault Diagnosis of a Hydraulic Actuator Circuit using Neural Networks—An Output Vector Space Classification Approach,*" Proceedings of the Institution of Mechanical Engineers,Part I: Journal of Systems and Control Engineering, 212(1), pp. 57-68.

[15] Varga, A., & Ossmann, D. (2014). LPV model-based robust diagnosis of flight actuator faults. *Control Engineering Practice*, 31, 135-147. doi: 10.1016/j.conengprac.2013.11.004

[16] Boskovic, J., Bergstrom, S., & Mehra, R. (n.d.). Adaptive accommodation of failures in second-order flight control actuators with measurable rates. *Proceedings of the 2005, American Control Conference, 2005*. doi: 10.1109/acc.2005.1470096

[17] Boskovic, J. D., Mehra, R. K. (2010.). A Decentralized Fault-Tolerant Control System for Accommodation of Failures in Higher-Order Flight Control Actuators. *IEEE Transactions on Control System Technology, 18(5), 1103-1115*.
doi: 10.1109/tcst.2009.2033805

[18] Cieslak, J., Efimov, D., Zolghadri, A., Gheorghe, A., Goupil, P., & Dayre, R. (2014). A Method for Actuator Lock-in-place Failure Detection in Aircraft Control Surface Servo-loops. IFAC Proceedings Volumes, 47(3), 10549-10554. doi:10.3182/20140824-6-za-1003.02158

[19] Zolghadri, A., Cieslak, J., Efimov, D., Henry, D., Goupil, P., Dayre, R., Leberre, H. (2015). Signal and model-based fault detection for aircraft systems. IFAC-PapersOnLine, 48(21), 1096-1101. doi: 10.1016/j.ifacol.2015.09.673

[20] Isermann, R. (2011). *Fault-diagnosis systems: An introduction from fault detection to fault tolerance*. pp. 25-113. Berlin: Springer.

[21] Sepasi, M. (2007). Fault monitoring in hydraulic systems using unscented Kalman filter (Master's thesis).

[22] Song, Y. (n.d.). Electro-hydrostatic Actuator Fault Detection and Diagnosis (Master's thesis). McMaster University.

[23] Chen, L. (n.d.). Model-based fault diagnosis and fault-tolerant control for a nonlinear electro-hydraulic system (Master's thesis). Kaiserslautern, Techn. Univ., Diss.

[24] *Actuation System Failure Detection Methods*, SAE (Society of Automotive Engineers). 5273, Aerospace Information Report.

[25] Crepin, P., & Kress, R. (2000). *MODEL BASED FAULT DETECTION FOR AN AIRCRAFT ACTUATOR*. 1-8.

[26] Eykeren, L. V., Chu, Q., & Mulder, J. (2012). Actuator Fault Detection by Aerodynamic Model Identification*. IFAC Proceedings Volumes,45(20), 1353-1357. doi:10.3182/20120829-3-mx-2028.00193

[27] Márton, L., & Ossmann, D. (2012). Energetic Approach for Control Surface Disconnection Fault Detection in Hydraulic Aircraft Actuators. IFAC Proceedings Volumes,45(20), 1149-1154. doi:10.3182/20120829-3-mx-2028.00040

[28] Varga, A., & Ossmann, D. (2014). LPV model-based robust diagnosis of flight actuator faults. *Control Engineering Practice,31*, 135-147. doi: 10.1016/j.conengprac.2013.11.004

[29] Goupil, P., 2010. Oscillatory failure case detection in the A380 electrical flight control system by analytical redundancy. Control Engineering Practice 18, 1110–1119.

[30] Narendra, K., Balakrishnan, J., 1997. Adaptive control using multiple models. IEEE Trans. Automat. Control 42, 171–187.

[31] Varga, A., Ossmann, D., Goupil, P., & Sabot, G. (2013). Verification and validation of a FDD system for identification of aircraft control surface jamming*. *IFAC Proceedings Volumes*, *46*(19), 84–89. doi: 10.3182/20130902-5-de-2040.00007

[32] David G. Luenberger, "Observing the state of a linear system," Military Electronics, IEEE transactions, vol. 8, no. 2, pp. 74-80, April 1964.

[33] Chen, J., Patton, R. J., & Zhang, H.-Y. (1996). Design of unknown input observers and robust fault detection filters. *International Journal of Control*, *63*(1), 85–105. doi: 10.1080/00207179608921833

[34] Li, S., Wang, H., Aitouche, A., & Christov, N. (2018). Sliding mode observer design for fault and disturbance estimation using Takagi–Sugeno model. *European Journal of Control*, *44*, 114–122. doi: 10.1016/j.ejcon.2018.09.006

[35] Venkat Venkatasubramanian, Raghunathan Rengaswamy, Kewen Yin, and Surya N. Kavuri, "A review of process fault detecion and diagnosis Prat1: Quantitative model-based methods," Computers and Chemical Engineering, vol. 27, pp. 293-311, 2003.

[36] R.E.Kalman, "A New Approach to Linear Filtering and Prediction Problems," Journal of Basic Engineering, Transactions of ASME, vol. 82, pp. 34-45, 1960.

[37] Zarchan, P., and Musoff, H., 2005, "Fundamentals of Kalman Filtering: A Practical Approach," Aiaa.

[38] Nori Okita and H.J. Sommer III, "A Novel Foot Slip Detection Algorithm Using Unscented Kalman Filter Innovation," in 2012 American Control

[39] Y. A. Chinniah, "Fault Detection in the Electrohydraulic Actuator Using the Extended Kalman Filter," Department of Mechanical Engineering, University of Saskatchewan, Saskatoon, Saskatchewan, Ph.D. Thesis 2004.

[40] Frank, P. M., and Ding, X., 1994, "Frequency Domain Approach to Optimally Robust Residual Generation and Evaluation for Model-Based Fault Diagnosis," Automatica, 30(5), pp. 789-804.

[41] Willsky, A. S., 1976, "A Survey of Design Methods for Failure Detection in Dynamic Systems," Automatica, 12(6), pp. 601-611.

[42] M. A. Massoumnia. A geometric approach to the synthesis of failure detection filters. IEEE Transactions on Automatic Control, 31:839–846, 1986.

[43] Ganguli, S., A. Marcos and G. Balas, 2002. Reconfigurable LPV controller design for boeing 747-100/200 longitudinal axis. Proc. Am. Control Conf., 5: 3612-3617.

[44] Yu, J.Q., L. Liu and H.X. Zhao, 2006. Robust gain-scheduled controller design for air defense missile. Proceedings of the Chinese Control Conference, August 7-11, 2006, Harbin, pp: 713-718.

[45] Bokor, J. and G. Balas, 2004. Detection filter design for LPV systems-a geometric approach. Automatica, 40: 511-518.

[46] Abadalla, M.O., E.G. Nobrega and K.M. Grigoriadis, 2001. Fault detection and isolation filter design for linear parameter varying systems. Proc. Am. Control Conf., 5: 3890-3895.

[47] Casavola, A. Famularo and D. Franze, 2008. A fault-detection, filter-design method for linear parameter-varying systems. Proceedings of the 16th Mediterranean Conference on Control and Automation, June 25-27, 2008, Ajaccio, pp: 1681-1686.

[48] Yu, Cui, et al. "Missile Fault Detection Based on Linear Parameter Varying Fault Detection Filter." Information Technology Journal, vol. 8, no. 3, 2009, pp. 340–346., doi:10.3923/itj.2009.340.346.

[49] Ossmann, D., and A. Varga. "Optimization-Based Tuning of LPV Fault Detection Filters for Civil Transport Aircraft." Progress in Flight Dynamics, Guidance, Navigation, Control, Fault Detection, and Avionics, 2013. doi:10.1051/eucass/201306263.

[50] H. Çalışkan, "Development and Control of a Single Rod Electro Hydrostatic Actuator" Ph.D. Thesis, Middle East Technical University, Mechanical Engineering Department, 2015.

[51] H. U. Akova, "Design, Contruction and Control of an Electro-Hydraulic Load Simulator for Testing Hydraulic Drives," M.Sc. Thesis, Middle East Technical University, Mechanical Engineering Department, 2014.

[52] Jelali, M., Kroll, A., Hydraulic Servo-systems: Modelling, Identification and Control, Springer, 2003.

[53] Çalışkan, H., Balkan, T., and Platin, B. E. "A Complete Analysis and a Novel Solution for Instability in Pump Controlled Asymmetric Actuators." ASME. J. Dyn. Sys., Meas., Control. September 2015; 137(9): 091008. https://doi.org/10.1115/1.

[54] Burster Tension and Compression Load Cell Model 8524, Burster, retrieved from http://www.burster.com/fileadmin/Documents/Products/Data_Sheets/Section_8/8524_EN.pdf, last viewed on 10.06.2019.

[55] Won, D., & Kim, W. (2015). Disturbance Observer based backstepping for position control of electro-hydraulic systems. International Journal of Control, Automation and Systems, 13(2), 488-493. Doi:10.1007/s12555-013-0396-y

[56] W. Chen, D. Balance, P. Gawthrop, and J.O'Reilly (2000). ''A nonlinear disturbance observer for robotic manipulators,'' IEEE Trans. Ind. Electron., vol. 47, no. 4, pp. 932-938.

[57] Welford, B.P. (1962). Note on a method for calculating corrected sums of squares and products. Technometrics, 4, 419-420.

[58] Cooper, M. A., "Simulating actuator energy demands of an aircraft in flight", Ph.D. Thesis, Cranfield University, Department of Aerospace Engineering, 2014.

[59] Description of Actuation Systems for Aircraft with Fly-by-Wire Flight Control Systems, SAE (Society of Automotive Engineers). 4253, Rev B, Aerospace Information Report.

[60] Kienitz, K. H., Kaden, A., & Luckner, R. (2013). Modeling and Design Considerations for Robust Control of Aircraft in Tight Cruise Formation. AIAA Guidance, Navigation, and Control (GNC) Conference. doi: 10.2514/6.2013-4858

[61] HH Series with Hydraulic Rod Lock, Air Inc., retrieved from https://airinc.net/wp-content/uploads/2019/06/BimbaTRD_HYD-0514_HH_ROD_LOCK.pdf, last viewed on 16.11.2019.

APPENDICES

Appendix A. Test Results

Test Cases 1 and 2:
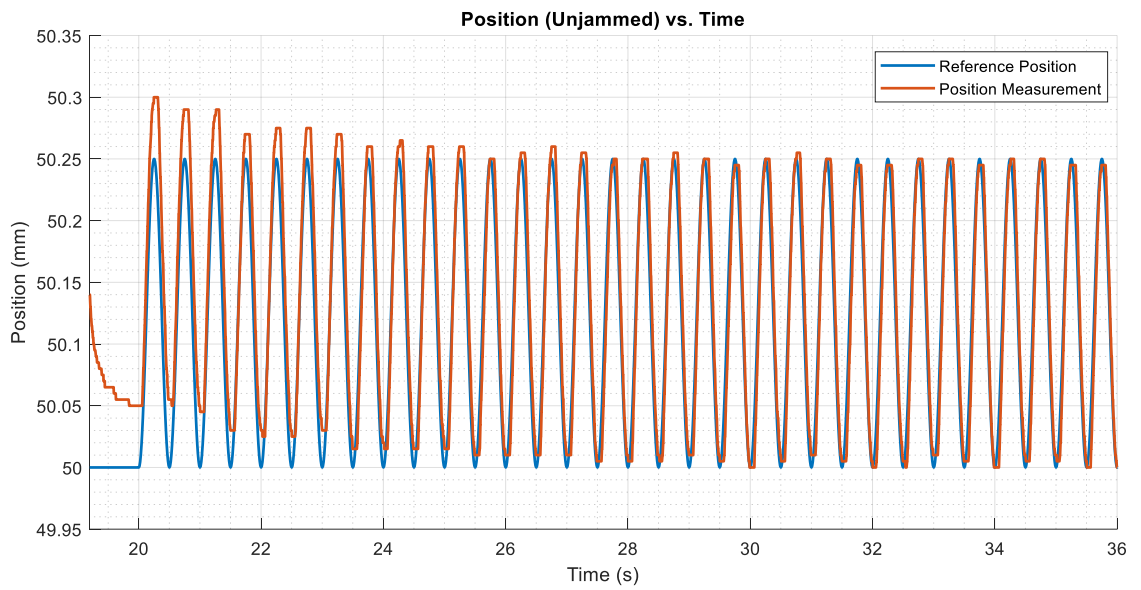
Figure A.1. EHA Position Response under the Unjammed Case
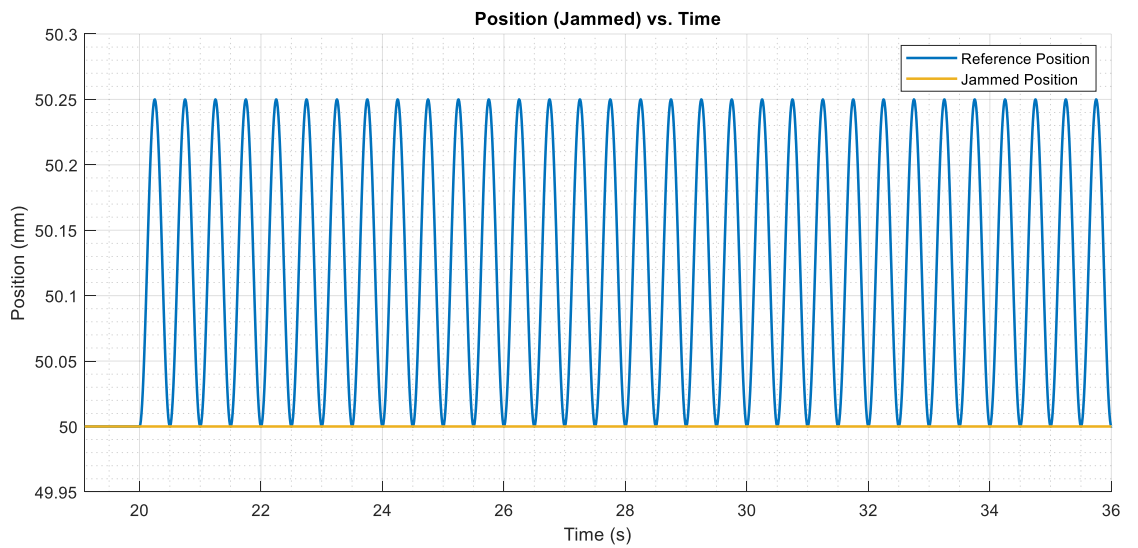
Figure A.2. EHA Position Response under the Jammed Case
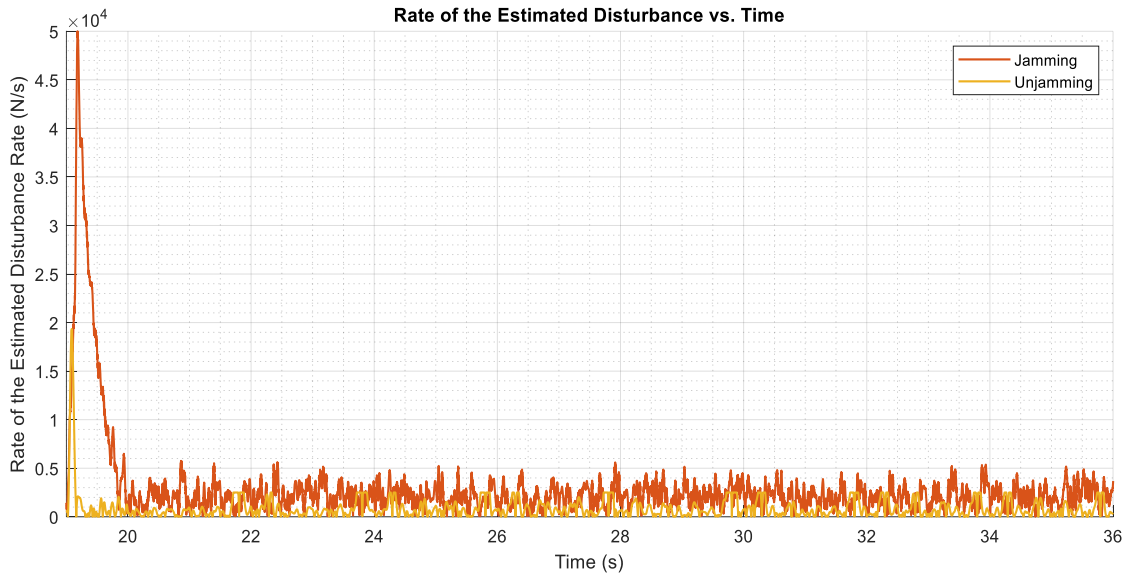
Figure A.3. Rate of the Estimated Disturbance
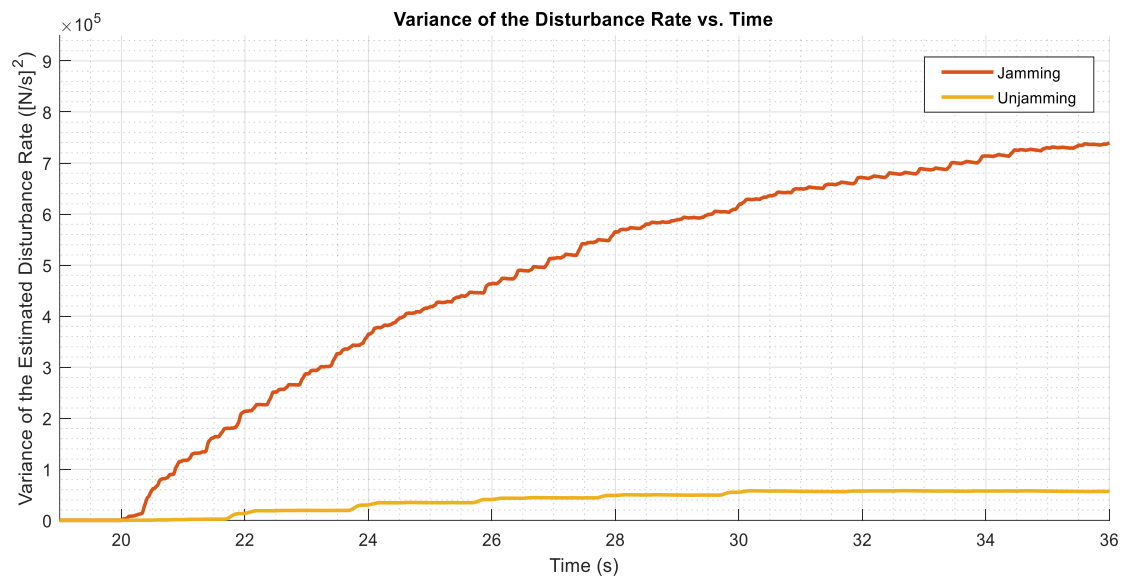
Figure A.4. Variance of the Disturbance Rate
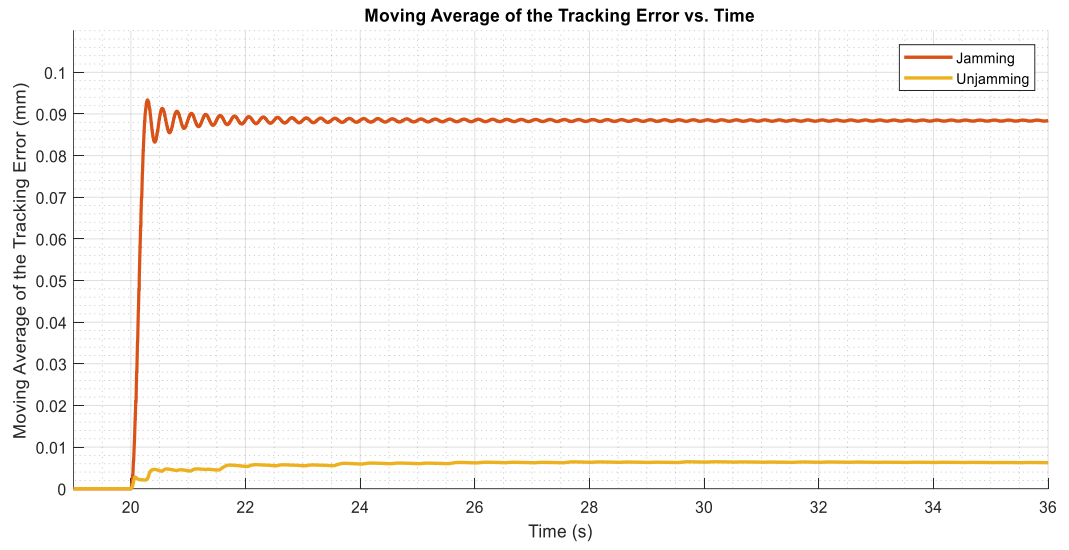
Figure A.5. Moving Average of the Tracking Error
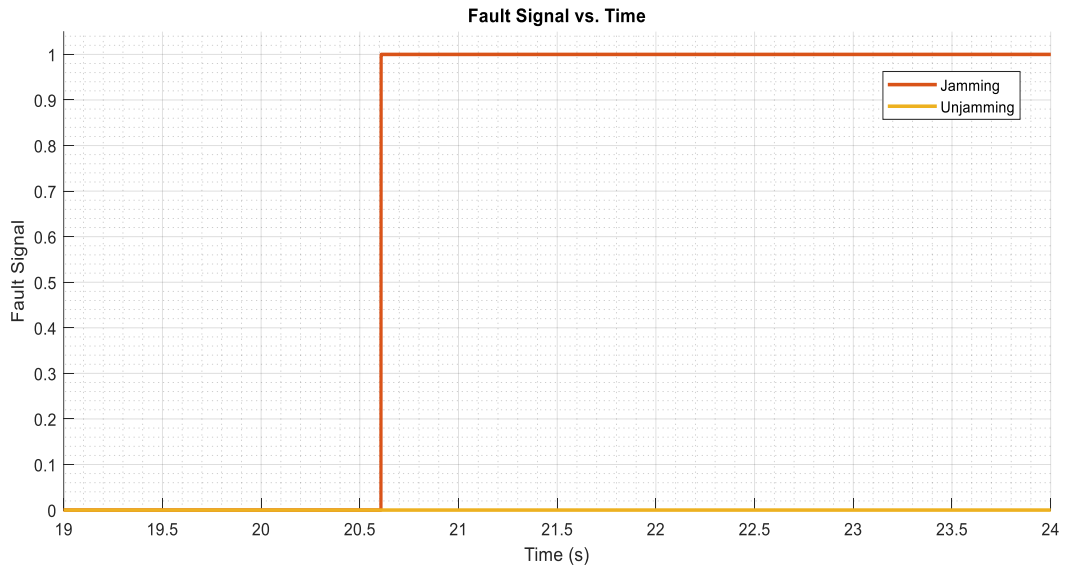
Figure A.6. Generated Fault Signal

Test Cases 3 and 4:
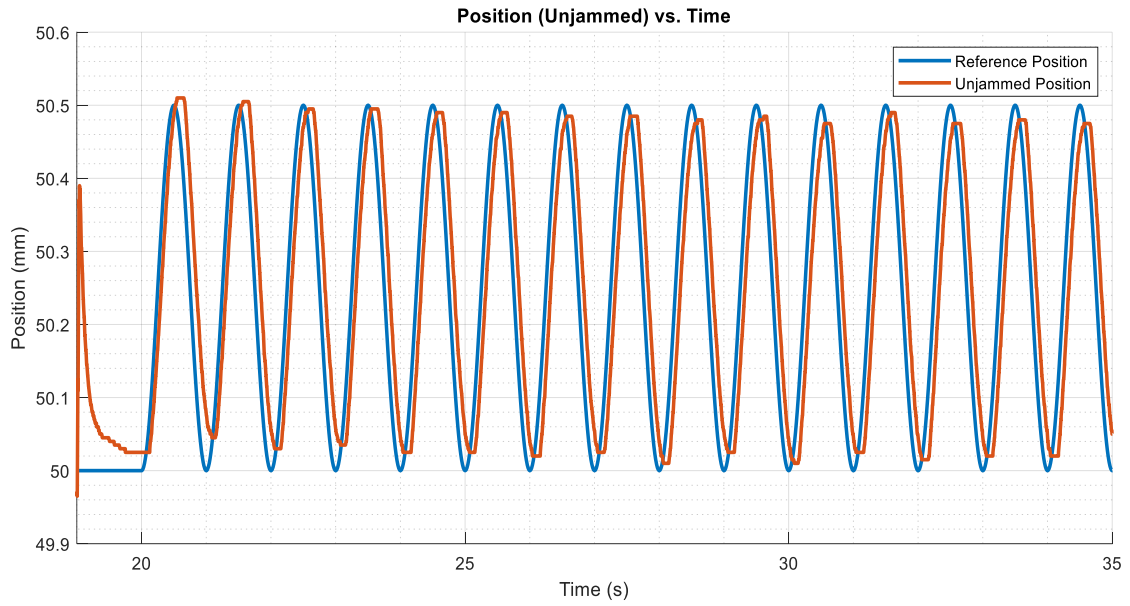
Figure A.7. EHA Position Response under the Unjammed Case
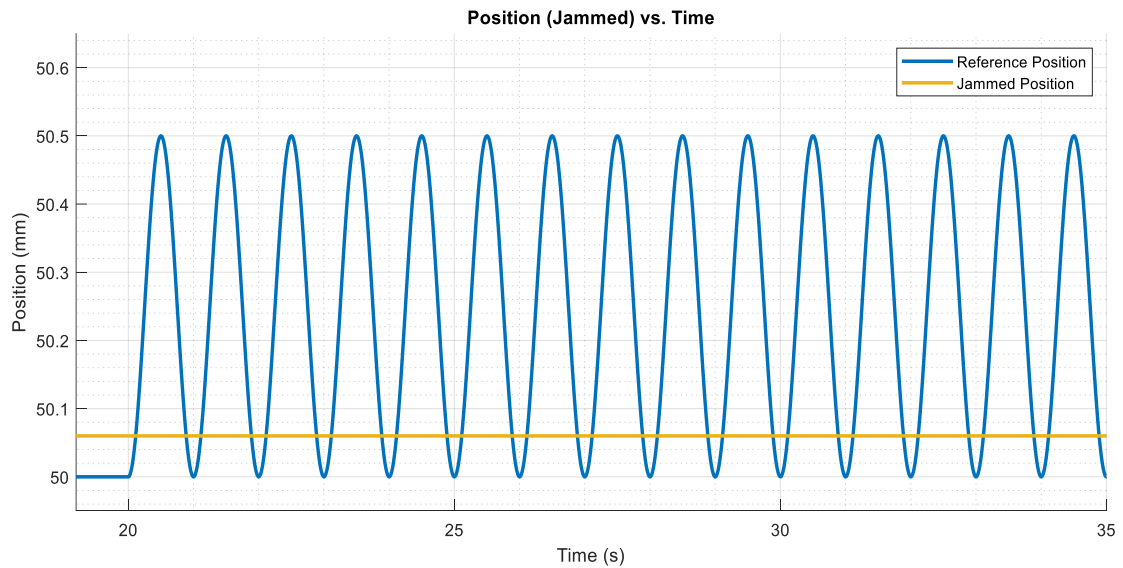
Figure A.8. EHA Position Response under the Jammed Case
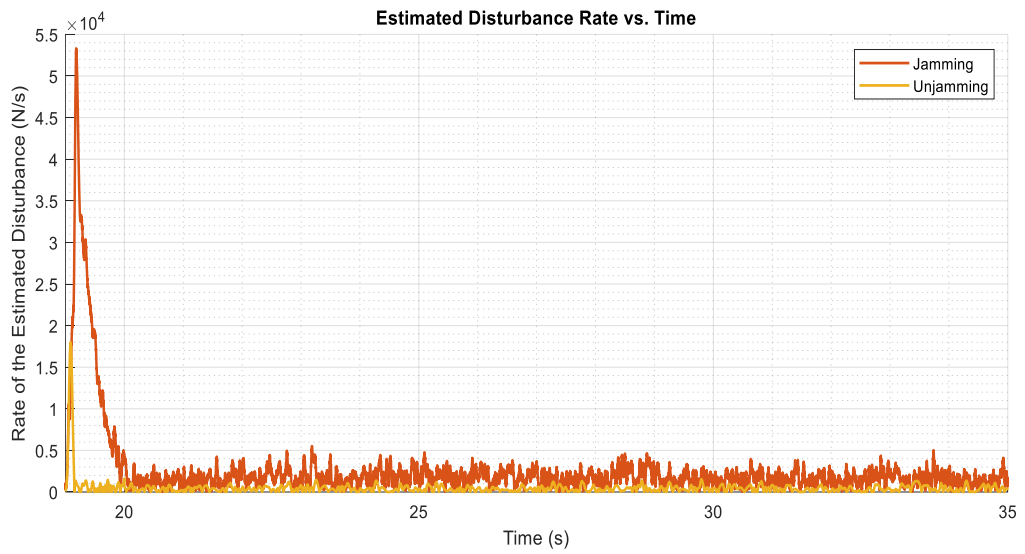
Figure A.9. Rate of the Estimated Disturbance
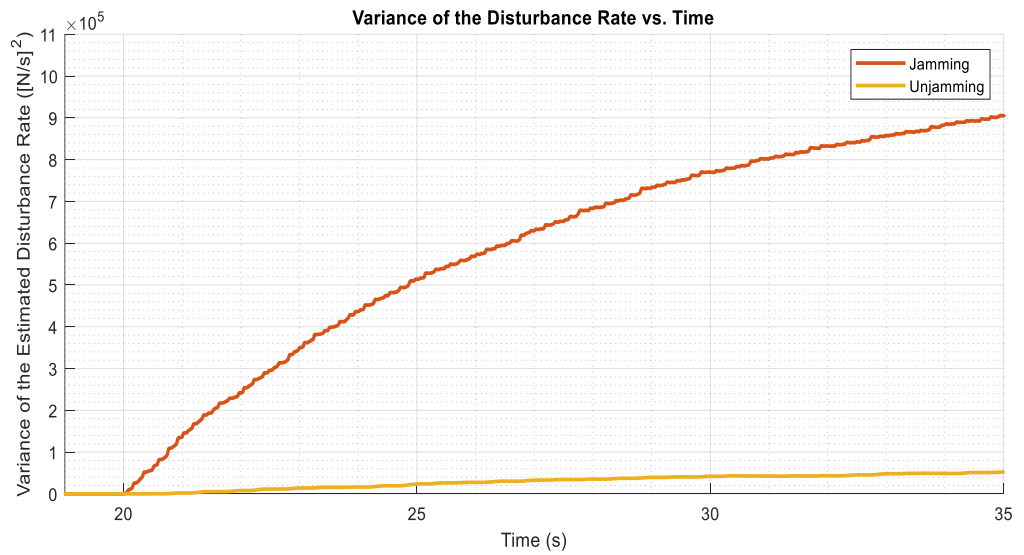
Figure A.10. Variance of the Estimated Disturbance Rate

113
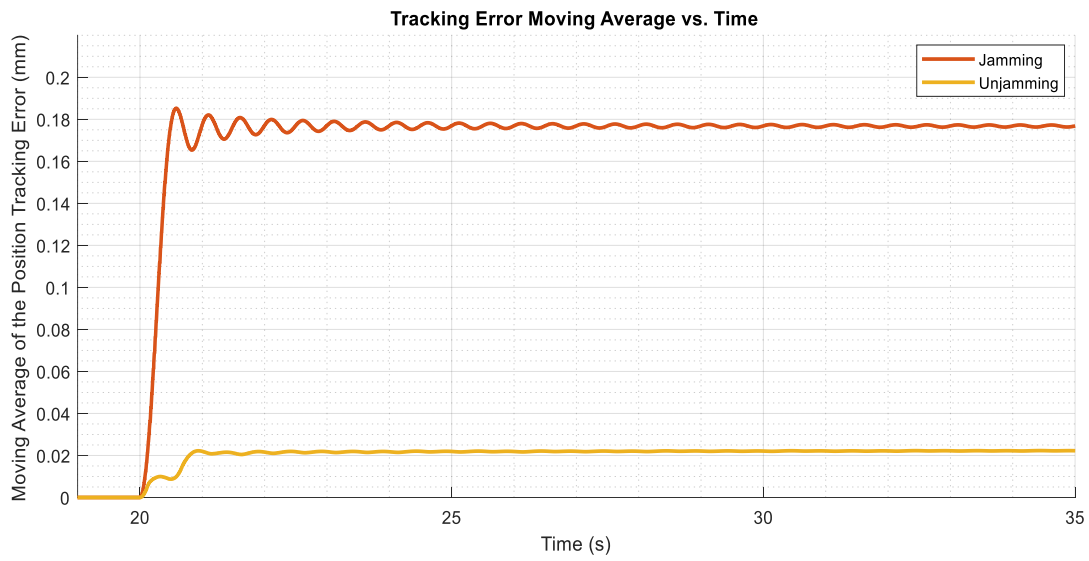
Figure A.11. Moving Average of the Tracking Error
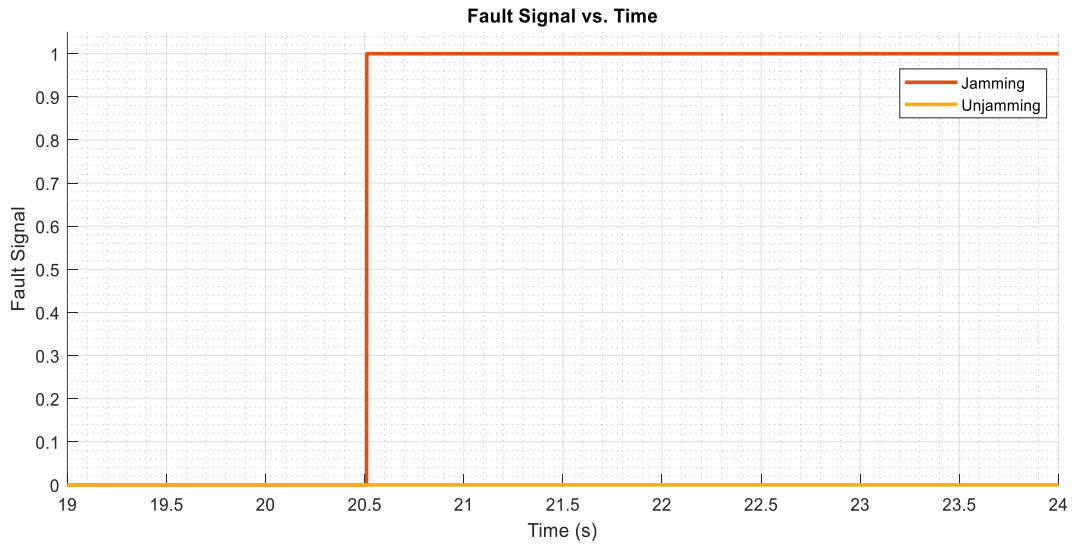
Figure A.12. Generated Fault Signal

114

Test Cases 5 and 6:
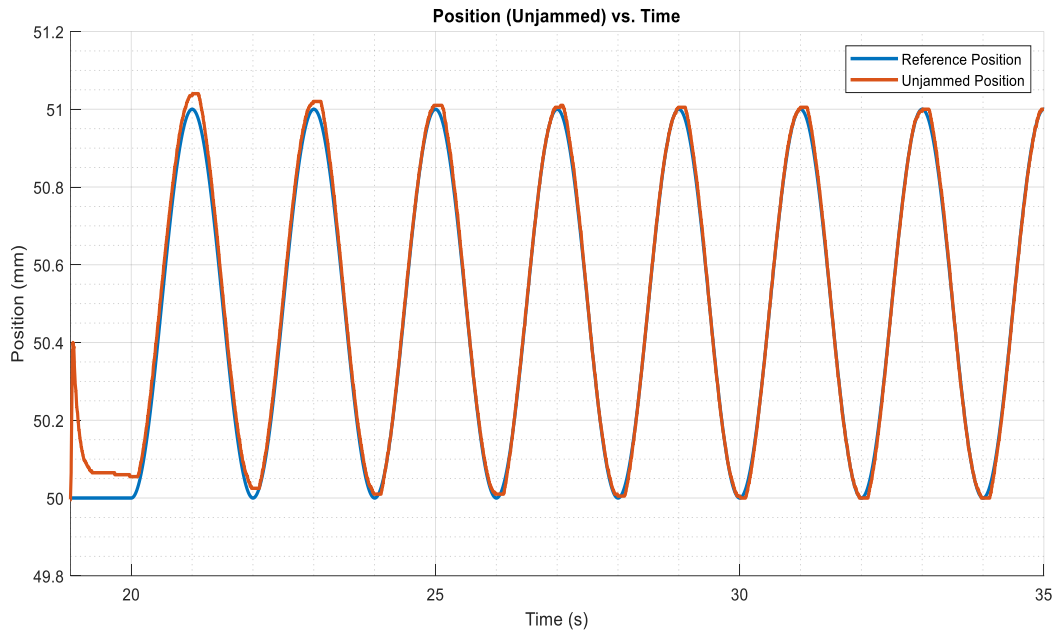
Figure A.13. EHA Position Response under the Unjammed Case
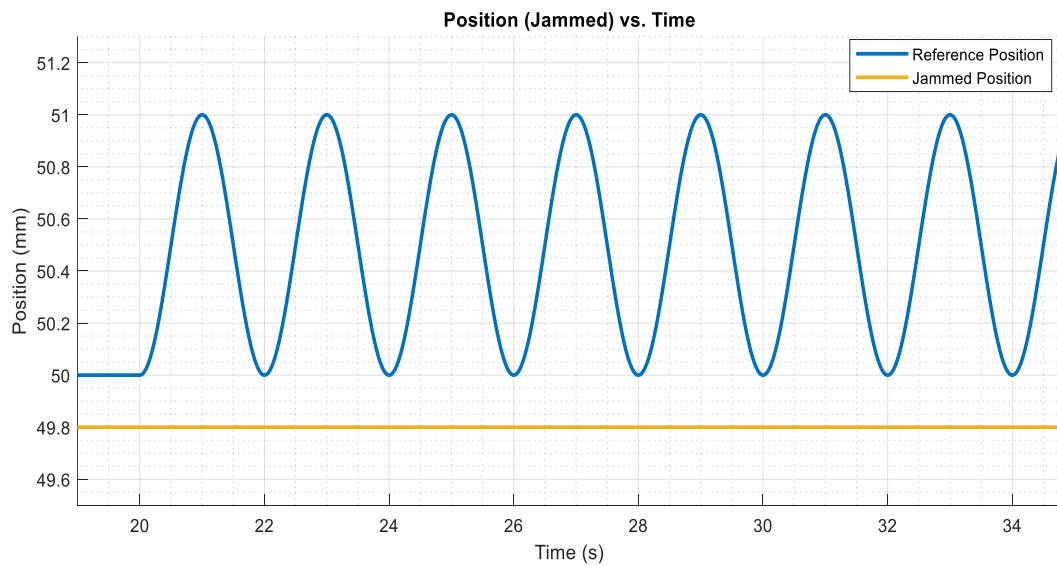
Figure A.14. EHA Position Response under the Jammed Case

115
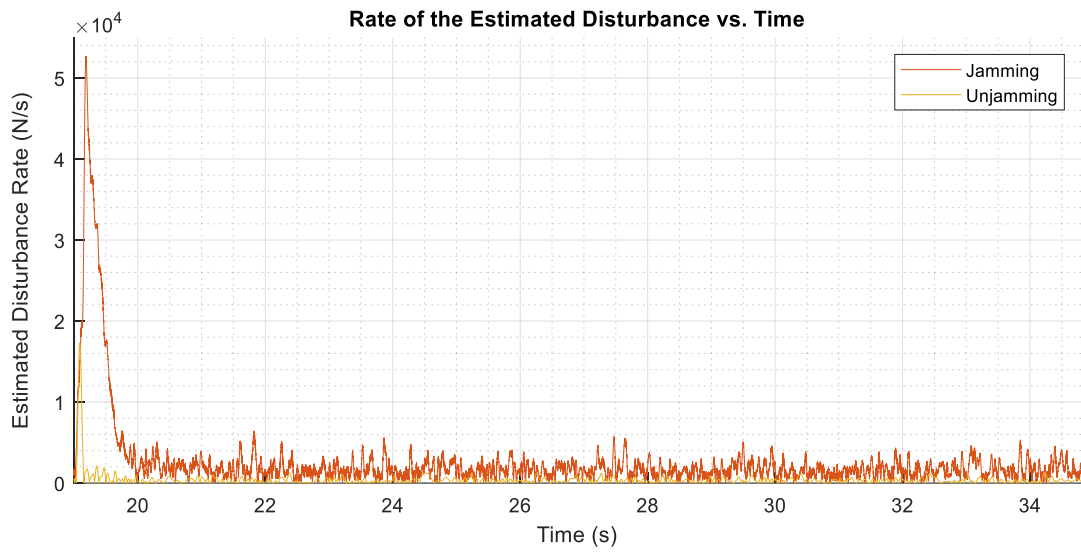
Figure A.15. Rate of the Estimated Disturbance
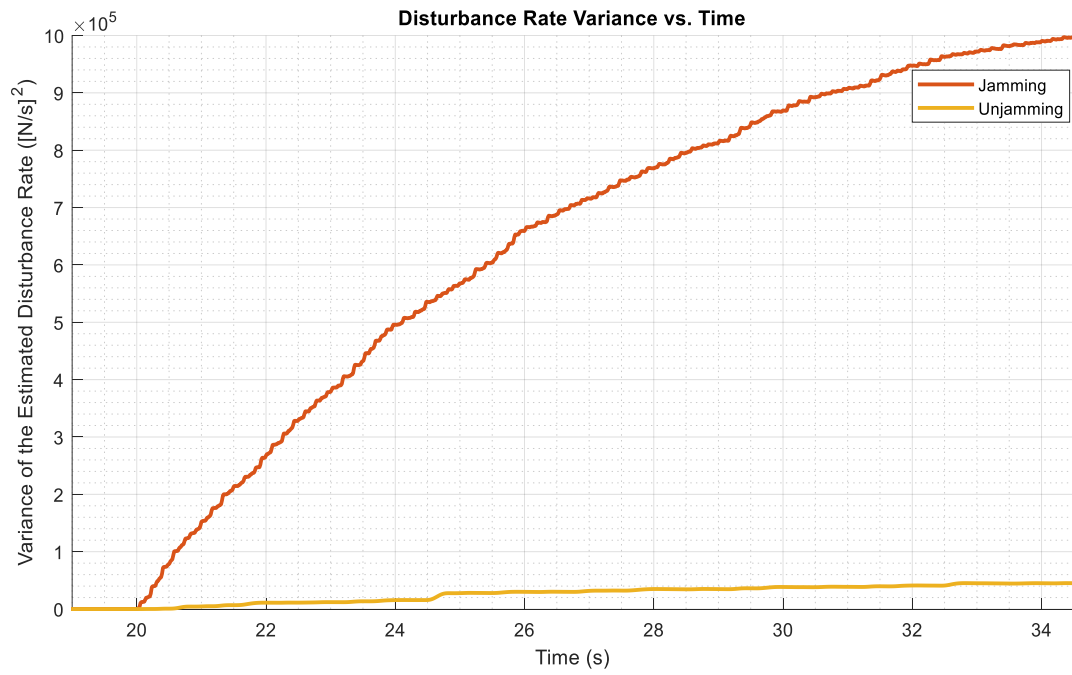
Figure A.16. Variance of the Estimated Disturbance
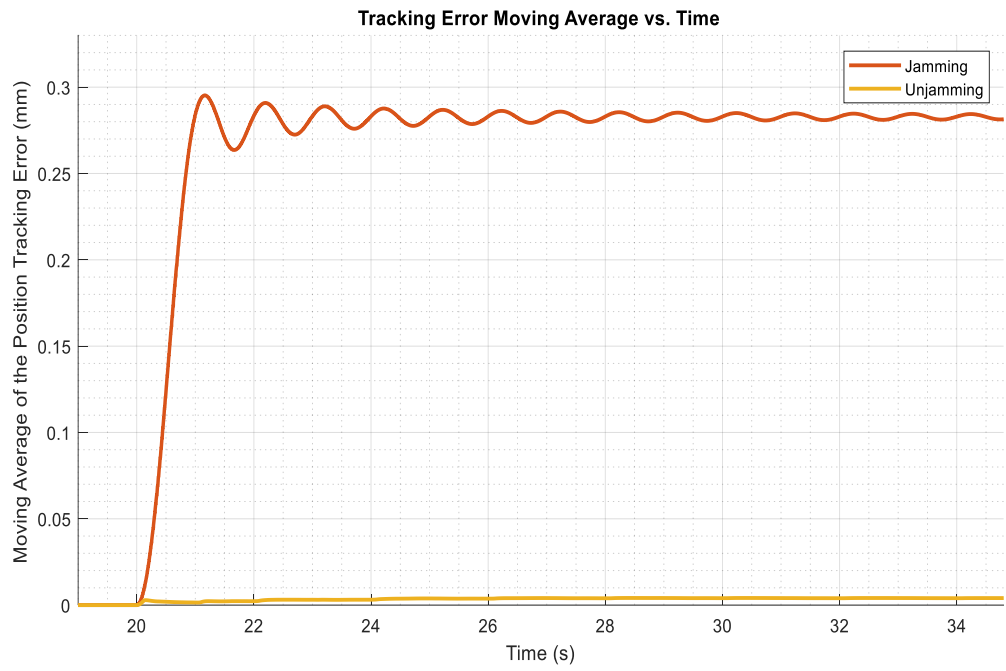
Figure A.17. Moving Average of the Position Tracking Error
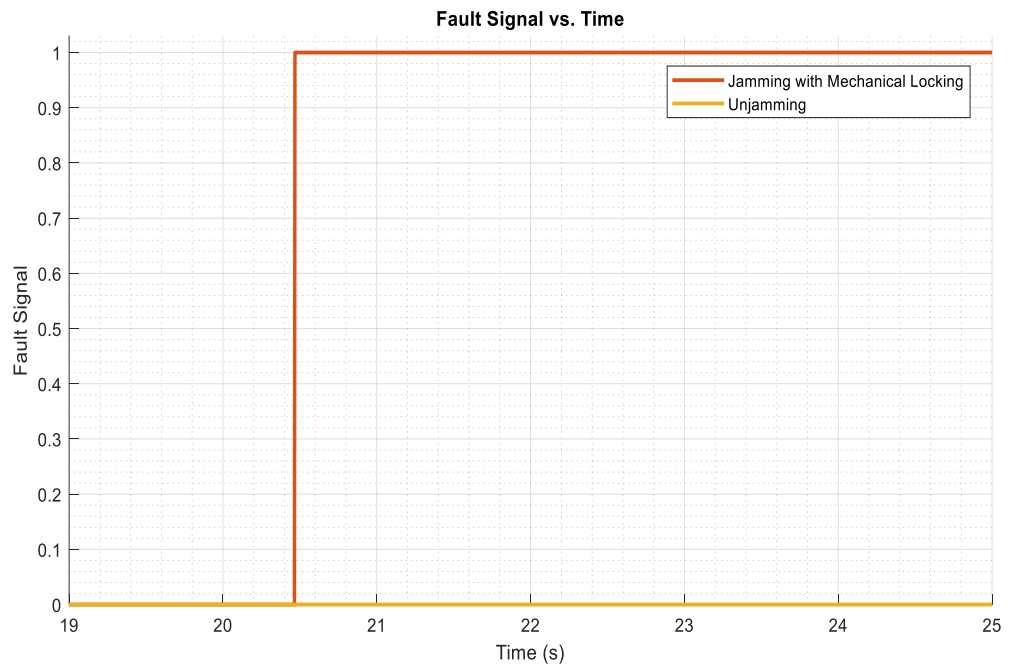
Figure A.18. Generated Fault Signal

117

Test Cases 7 and 8:
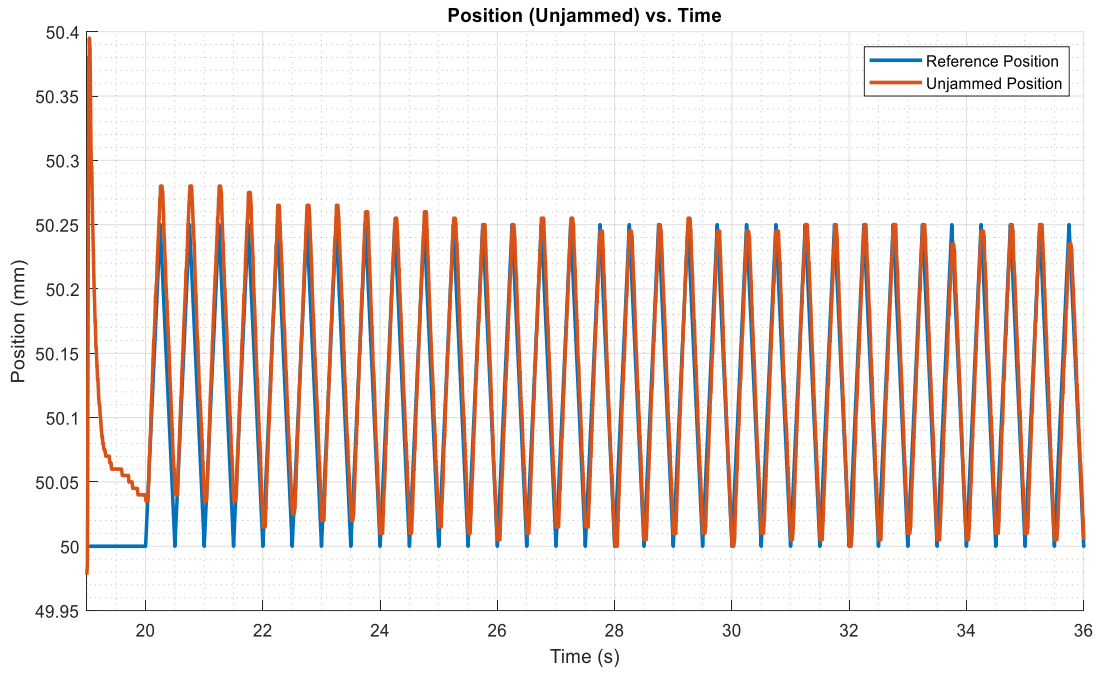
Figure A.19. EHA Position Response under the Unjammed Case
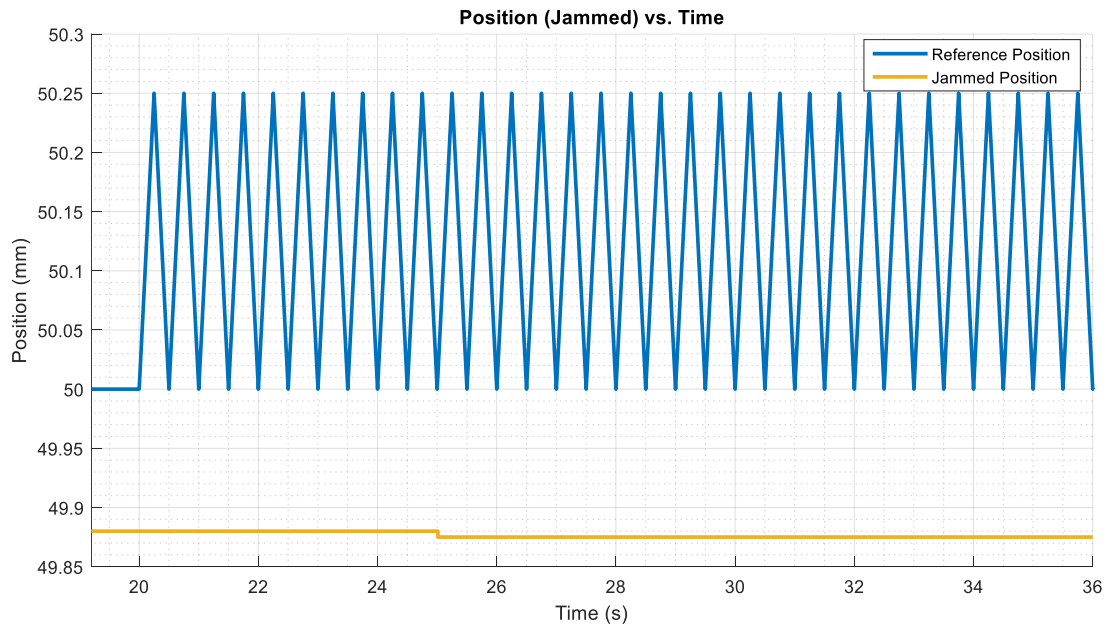
Figure A.20. EHA Position Response under the Jammed Case
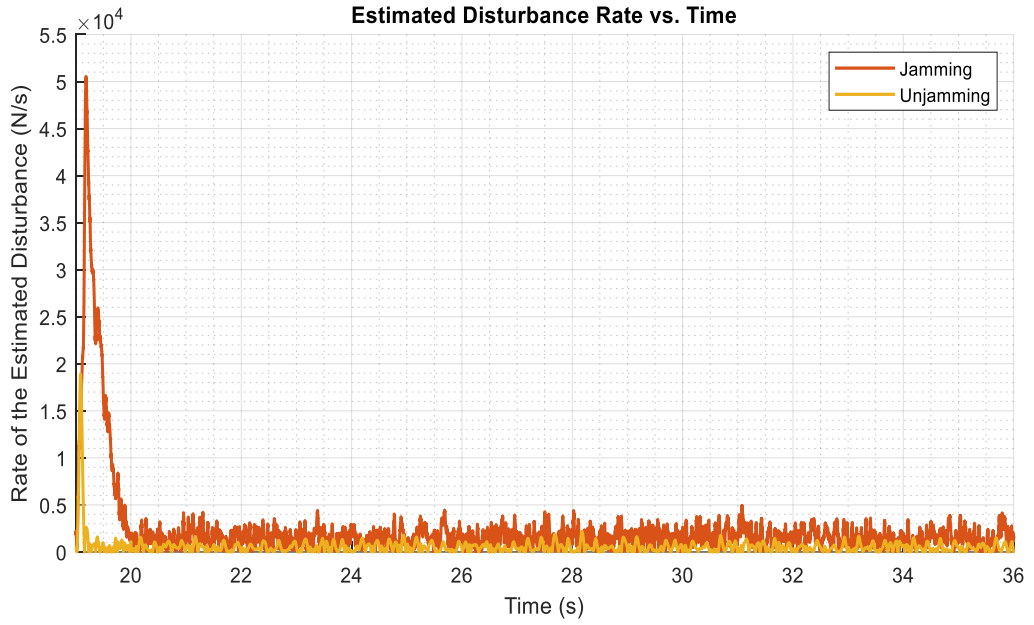
Figure A.21. Rate of the Estimated Disturbance

Figure A.22. Variance of the Estimated Disturbance

119
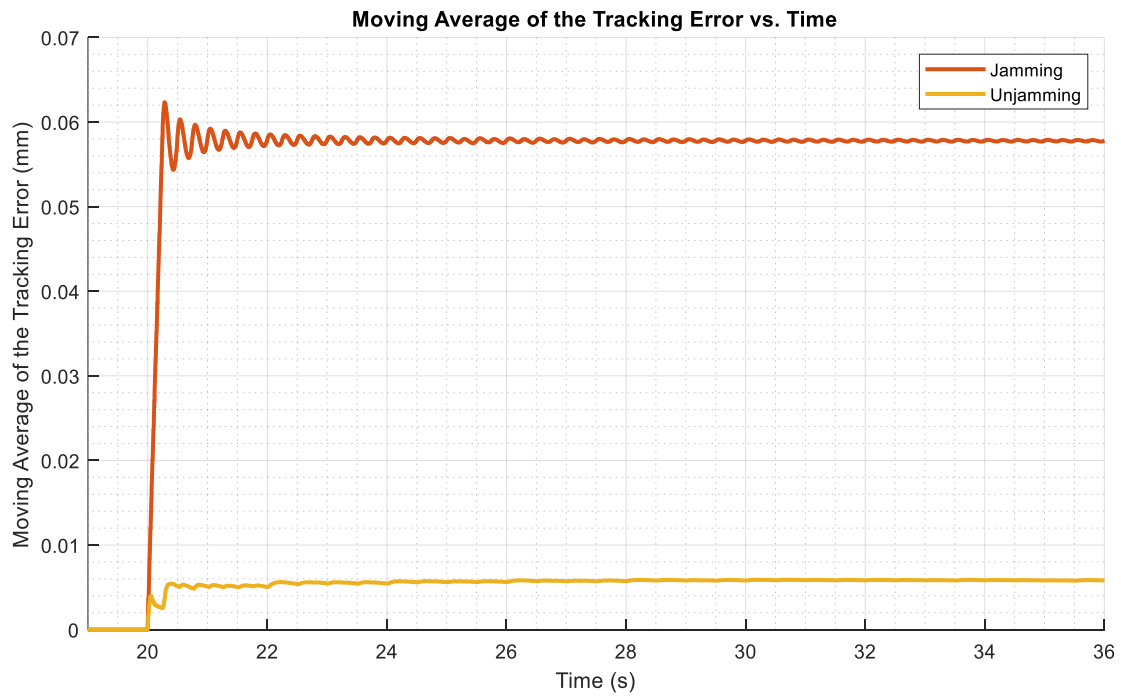
Figure A.23. Moving Average of the Position Tracking Error
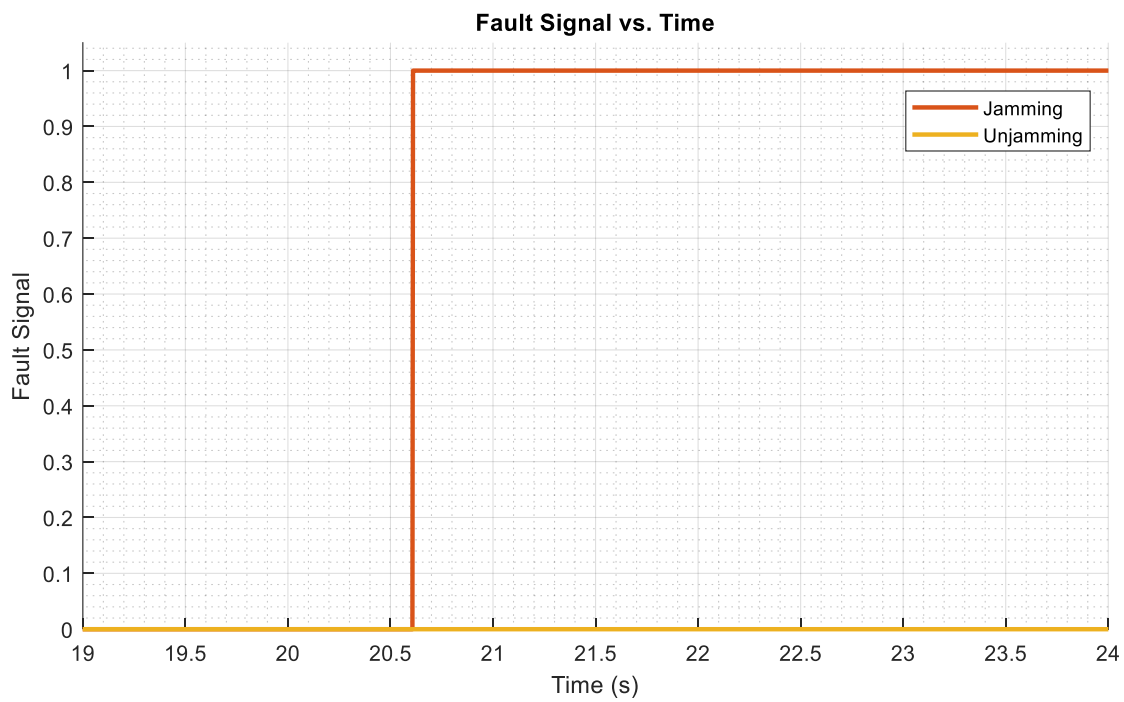
Figure A.24. Generated Fault Signal

Test Cases 11 and 12:
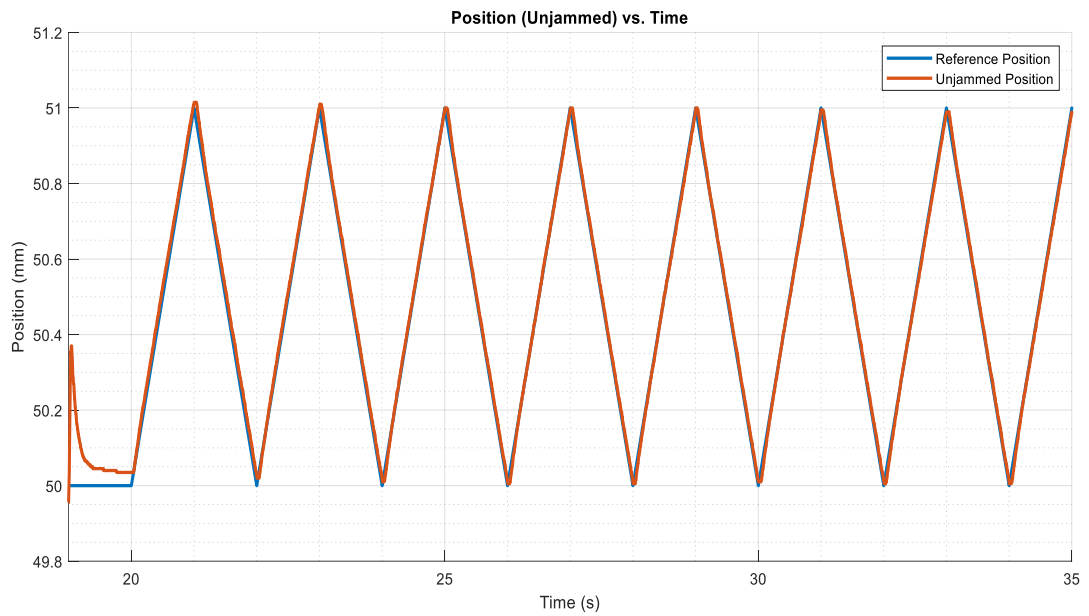
Figure A.25. EHA Position Response under the Unjammed Case
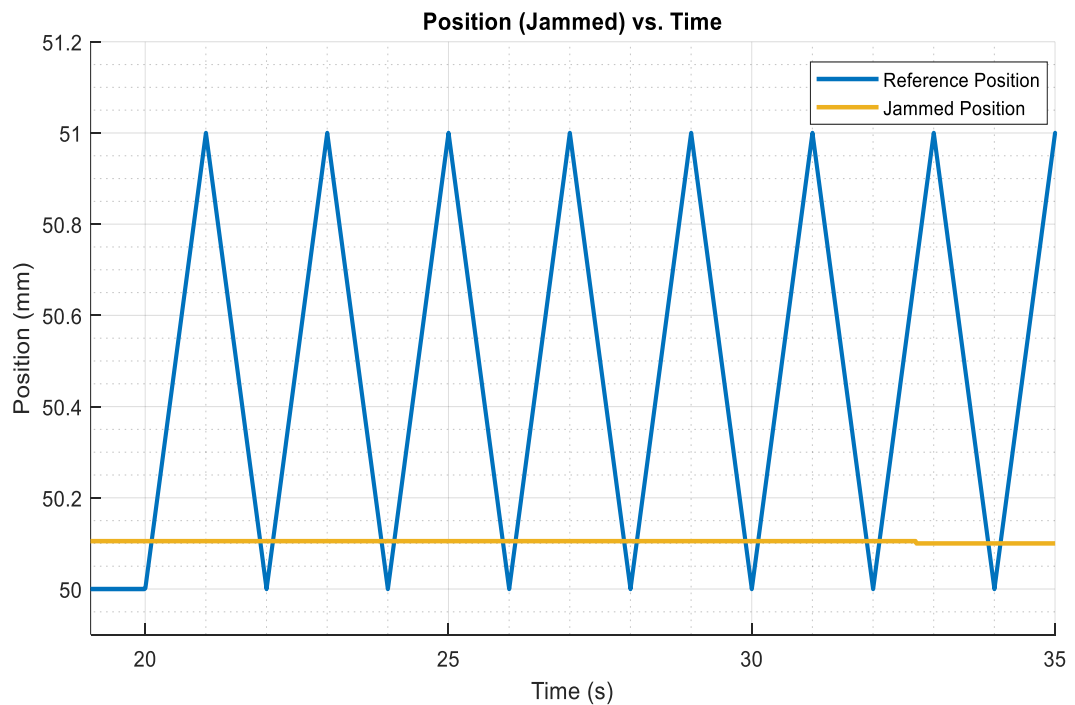
Figure A.26. EHA Position Response under the Jammed Case
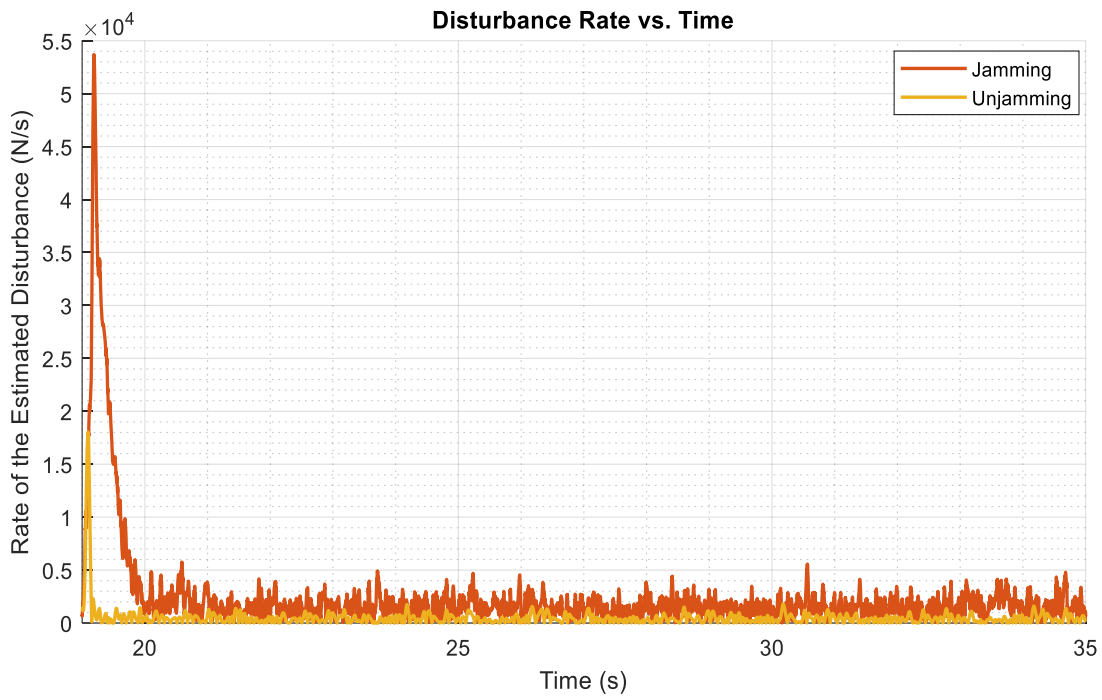
Figure A.27. Rate of the Estimated Disturbance
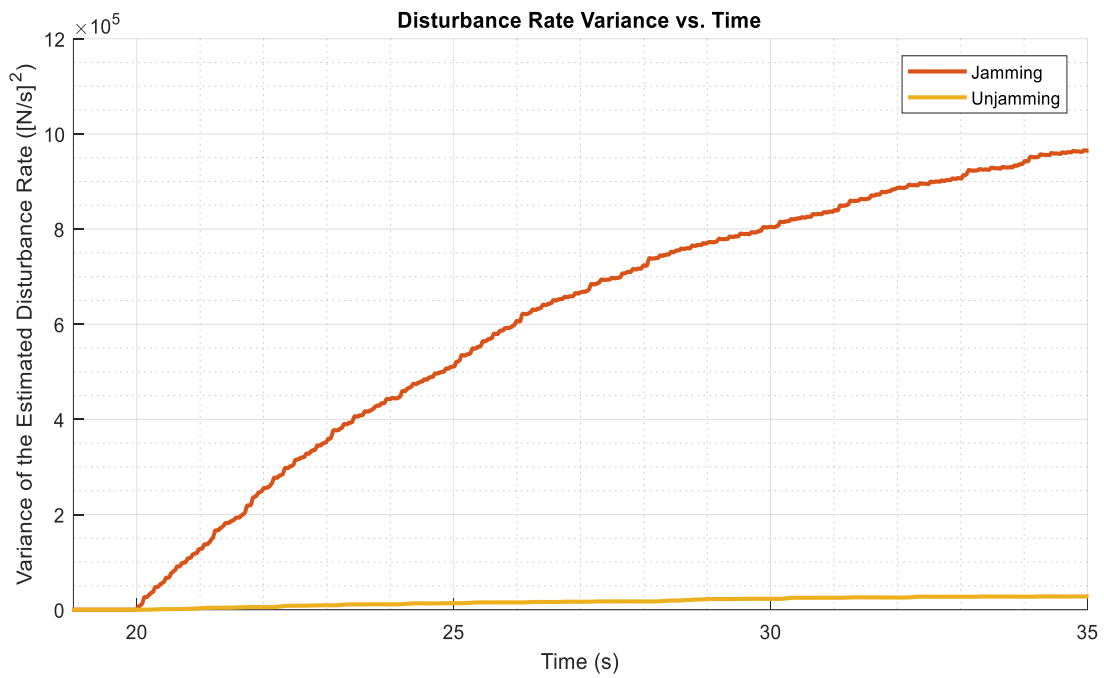
Figure A.28. Variance of the Estimated Disturbance Rate
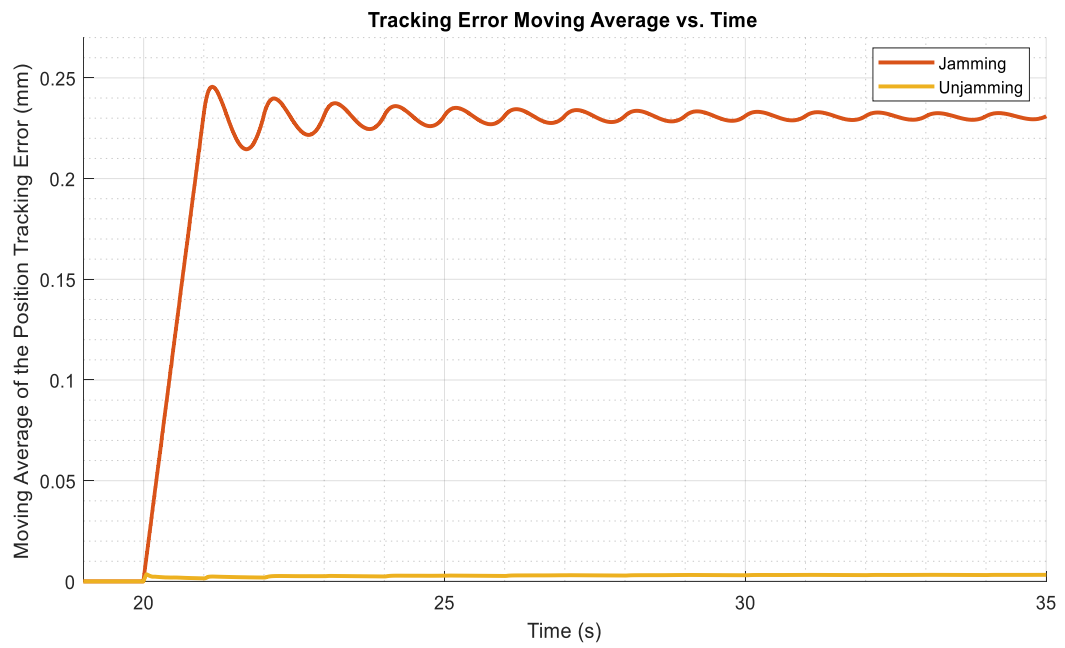
Figure A.29. Moving Average of the Position Tracking Error
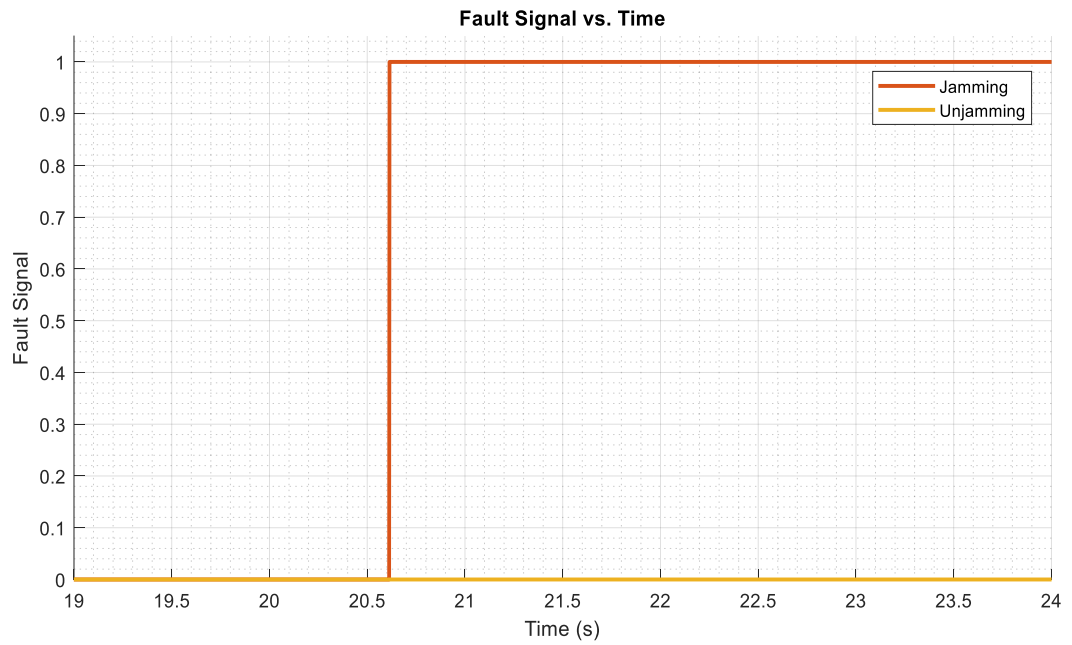
Figure A.30. Generated Fault Signal